DESIGN, FABRICATION, PROGRAMMING, AND EVALUATION OF AN ANKLE FOOT SIMULATOR

by

Jonathan James Miller

A thesis submitted to the faculty of
The University of Utah
in partial fulfillment of the requirements for degree of

Master of Science

Department of Mechanical Engineering

The University of Utah

August 2016

The University of Utah Graduate School

STATEMENT OF THESIS APPROVAL

The thesis of **Jonathan James Miller**

has been approved by the following supervisory committee members:

Andrew S. Merryweather	,Co-Chair	**Mar 21 2016**
		Date Approved
Mark Andrew Minor	,Co-Chair	**Mar 17 2016**
		Date Approved
John M. Hollerbach	, Member	
		Date Approved

and , by **Timothy A. Ameel** Chair/Dean of the Department/College/School of **Mechanical Engineering**

and by David B. Kieda, Dean of The Graduate School.

ABSTRACT

Parkinson Disease (PD) is a progressive and chronic movement disorder that affects an individual's ability to walk and move naturally. Research shows that training using virtual reality can offer improvements over traditional therapy and decrease the effects of some PD symptoms.

In an effort to address the need for such therapeutic intervention, a Virtual Reality (VR) rehabilitation simulator was developed using 3D graphical displays in concert with haptic Smart Shoes. The system creates challenging virtual terrain to safely train participants in situations that demand greater balance and neuromuscular control. As part of this effort, an Ankle Foot Simulator (AFS) was created to mimic human gait, including ankle and foot response to a variety of terrain features. This thesis describes the development and testing of a novel AFS robot designed to mimic human gait and evaluate Smart Shoe behavior and response to perturbations.

The major design requirement for the AFS robot is to reproduce natural gait dynamics by: 1) matching complex trajectories of the ankle, 2) generating Ground Reaction Forces (GRF) during normal walking gait, and 3) mimicking foot/ankle dynamics such as ankle roll over. This thesis focuses on the design and control of the AFS to achieve sufficient Range of Motion (ROM) to mimic human gait, including extreme ankle rollover, while providing appropriately fast

dynamics, sufficient load capacity, and high repeatability. Design aspects of the AFS include 1) forward and inverse kinematic derivations of the ankle mechanism, 2) derivations of feedforward components of the control algorithms, and 3) mapping ankle mechanism actuator forces to ankle moments.

The AFS robot tracks ankle position and orientation data to within 5.5 mm and 5.5 degrees. The AFS is also able to reproduce GRFs, including dorsal/plantar flexion and inversion/eversion ankle moments with an r^2 value of 0.82 or more. The AFS also demonstrates passive ankle stiffness. To improve performance of the AFS, an iterative learning controller is suggested for future work.

I would like to dedicate this thesis to my family.

TABLE OF CONTENTS

LIST OF TABLES

ACKNOWLEDGMENTS

A special thanks to Ken Openshaw, who designed the frame for the AFS, and SME Steel for donating the materials and welding the frame of the AFS.

CHAPTER I

INTRODUCTION

Motivation

Parkinson Disease (PD) is a progressive and chronic neuromuscular disorder that affects the individual's ability to walk and move, resulting in bradykinesia, or slowness of movement, and rigidity, a stiffness of the limbs and trunk. Due to these symptoms, people with PD are twice as likely to fall as are their peers without PD; falls may result in potentially serious injuries [1]. Currently, nearly one million people in the United States are living with PD. Research shows that participating in regular exercise can decrease some of the symptoms of PD. Particularly important are exercises that challenge the individual to "change tempo, activity, or direction," as well as "activities that require balance and preparatory adjustments" [2].

In an effort to address the need for dynamic therapeutic interventions, an interdisciplinary team of researchers proposed the development of a Virtual Reality (VR) simulator or Treadport with real-time haptic terrain feedback to improve therapy and provide a more immersive experience to an individual exploring a virtual environment. The terrain feedback is accomplished using Smart Shoes [3] worn by individuals in the Treadport. The Treadport is

composed of 3D projectors shown on multiple screens in front of the user and on the large treadmill and capable of rendering sloped terrain with the help of an active harness system.

As part of this effort, an ankle foot simulator was designed and built to test and evaluate the performance of the haptic Smart Shoes. This thesis discusses the design, control, and evaluation of the Ankle Foot Simulator (AFS) robot that systematically and reliably reproduces human gait. The gait trajectories are measured in a laboratory with force plates and a motion capture system [4].

Challenges

In order to meet the demands of the "smart shoe project," a robot was needed that could mimic the motion of human gait, including Ground Reaction Forces (GRF). Many challenges existed in meeting this goal, including accurately modeling normal human gait patterns, the ability to fully represent the ankle Range Of Motion (ROM) required to mimic those patterns, and the ability to tolerate the ankle loading requirements during gait.

To define human gait, motion capture data were recorded in concert with force plate data. Design requirements—such as kinetics, speed, acceleration and range of motion—were defined.

Collected data show that the robot needs to support a load of around 900 N. The robot also needs to match the anatomical speeds of the human ankle, which peak at around 2 m/s and accelerate at around 15 m/s^2 in the direction of travel. The robot also needs to have an ankle mechanism that has sufficient ROM to

mimic the foot and ankle during healthy normal gait. This ankle also needs to support the GRFs generated during gait and be able to actuate, generating ankle moments. The derivation of closed-form solutions for the forward and inverse kinematics of the ankle mechanism need to be solved. Also, part of the ankle design is the requirement that it fit inside a shoe and have room for a 6 Degree Of Freedom (DOF) load cell to measure internal ankle moments. Controlling the AFS robot to both track position and force was a challenge along with synergizing all of the DOF, which include natural passive ankle responses to changes in terrain or smart shoe.

Approach

A parallel robot using a three-tiered gantry system along with an ankle mechanism was considered because of the loading requirements (see Figure 1).

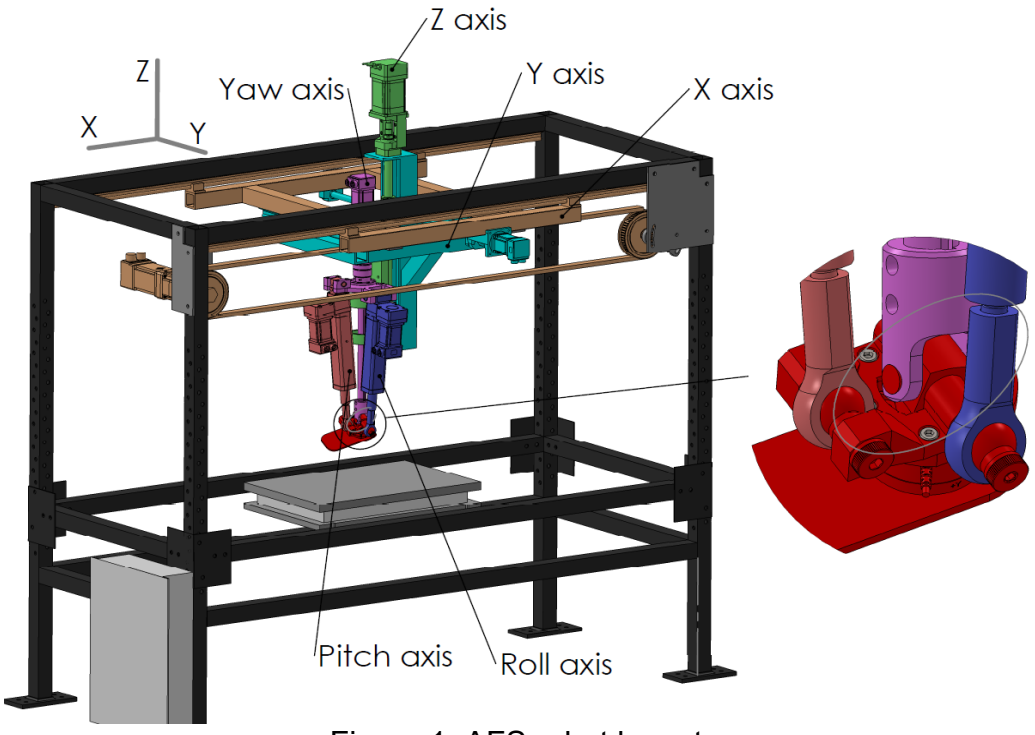

Figure 1: AFS robot layout.

To drive the gantry, ball screws were considered due to their precision and high driving force. For the axis responsible for the motion in the direction of travel, this was not an option because a ball screw would be too long between supports, causing harmonics at operational speeds. To achieve the speed and acceleration required for this axis, a belt and pulley system was used in conjunction with a gear box. The selection of the gear ratio allowed an impedance-matching approach to be used. Impedance matching is used to maximize the power transfer from the motor to the gantry and provides a nice balance between torque and speed.

Designing an ankle mechanism that 1) would allow room for a load cell to be placed between the ankle and the bottom of the foot, 2) provides sufficient load-bearing capacity, 3) is actuated, and 4) has the ROM required to replicate natural gait was challenging. To solve the load cell design space problem, a load cell with sufficient load capacity and acceptable form factor was chosen. The ankle was built around the load cell, and to ensure sufficient ROM, the ankle joint was checked for interference between parts in extreme configurations. The final design consists of a U-joint with linear actuators acting orthogonal from one another for orientation.

Kinematics for the ankle mechanism were found using a variety of geometrically based techniques. To solve the inverse kinematics of the ankle mechanism, rotation matrices and simple spatial translations were used to find the location of the AFS's ball joints, given a desired orientation. The Roll and Pitch actuator lengths were calculated using the Pythagorean Theorem.

The approach used to solve the forward kinematics included using the intersecting points of geometric shapes. For the Roll axis, the geometry of the ankle mechanism simplifies to an intersection of two circles; the Pitch axis simplifies to the intersection of two spheres and reduces to an intersection of two circles.

Control of both position and force was accomplished by using an admittance multiloop controller. The inner loop is responsible for position and uses a Proportional Derivative (PD) controller. The outer loop is responsible for force and uses a Proportional Integral (PI) controller. The outer force loop perturbs the desired target position of the inner loop to achieve a desired force. Natural ankle dynamics are achieved by multiplying orientation error by a passive stiffness coefficient, the result of which is then added to the desired ankle moment of the respected axis.

Related Work

Many groups have built AFSs, each more advanced than the previous generation. In early studies, Jones [5] used levers attached to tendons to actuate a cadaveric foot and used bathroom scales to measure the resulting weight distribution of the foot. Thordarson [6] used an instron during testing because it could maintain a constant load. Sharkey [7] used a bar and slot method to generate a gait profile. Modern Robotic Gait Simulators (RGS), like the one from Aubin [8], used a Stewart-like platform that has 6 Degrees Of Freedom (DOF). One drawback of using a Stewart-like platform is the limited

ROM. The design by Aubin can only model ankle Roll and Yaw of +/-15 degrees, whereas the AFS can model up to +/-25 degrees of Roll and almost 100 degrees of Yaw. The limited ROM of Aubin is sufficient to study healthy normal gait patterns, but anything more aggressive, such as a full ankle rollover event, cannot be observed with their setup as described in the literature. Aubin might be able to mount their shank and foot at an angle of 15 degrees and thus try to use all +/- 15 degrees to test ankle rollover, however, whether or not this attempt was ever made is unknown.

Most RGS, use cadaveric feet with a tibia attached to a robot's end-effector. Cable and pulley systems are used to attach ankle tendons to linear actuators and control the motion of the foot. Drawbacks of using cadaveric feet are that they degrade quickly during testing and are only usable for 2-5 days, and, at most, approximately 100 tests, before another foot must be attached [8]. Additionally, most foot donors are elderly and their bones are prone to breaking under anatomical loading conditions. However, using cadaveric feet enables the study of simulated muscle activation and anatomic structures of the foot. The uses of a robotic ankle and foot does not have the drawbacks of breaking or degrading over time.

Traditionally, gait simulators that use a robotic foot and ankle, such as the one developed by Hung-Jen Lai [9], are limited in their capability. Their gait simulator is for general motion and only focused on the major DOF associated with gait, while neglecting other DOFs [10]. While major gait events can be observed, fewer DOFs limit the fidelity of the simulation.

Most robotic ankle joint designs are centered on two rotational joints that are both orthogonal and coincident to each other using a universal joint as in LOLA [11] and WABIAN-2RIII [12] [13]. Other designs such as NAO [14] use a shell/scaffolding approach where motors and gear train are housed within the ankle to achieve the same joint configuration. Actuating the ankle joint is accomplished using connecting rods attached to linear actuators [11] [12]. Ankles of both LOLA and WABIAN-2RIII are actuated by two linear actuators located posterior to the center of the ankle joint. The ankle joint actuators of the AFS robot designed for our work are located lateral and posterior to the ankle joint.

The aim of this thesis was to replicate human gait, including the GRF and passive ankle dynamics in all planes of motion, with the robustness and repeatability of a robotic ankle.

Contributions

Contributions to this project consist of the design, manufacturing, building, programming, testing, and evaluating of the AFS robot. An itemized list of key contributions is provided:

- Design, manufacturing, assembly, and analysis of the Ankle Foot Simulator, including all electrical and mechanical systems
- Kinematic analysis of ankle mechanism
- Design of the complete control system
- Signal processing of the load cell

- Robot control algorithm and code
- Robot system support program

Thesis Organization

This thesis is organized in the following manner. First, the system requirements are found in Chapter 2, as are the design specifications. Next is the gantry and ankle design in Chapters 3 and 4, where designs are discussed and selected along with a presentation of the mechanical features of the chosen design. Following the ankle design is a discussion of the robot controller and supporting program structure in Chapter 5. Next is the forward and inverse kinematic derivation of the AFS ankle mechanism in Chapter 6, followed by the evaluation and conclusion in Chapters 7 and 8, respectively.

CHAPTER II

SYSTEM REQUIREMENTS

System requirements of the AFS were determined by studying the motion of the ankle and GRFs involved during the contact phase of healthy normal walking gait. Information such as ROM, maximum ground reaction forces, internal ankle moments, and ankle velocities and accelerations were used to define system requirements.

Performance Specifications

Gait kinematics and GRFs were collected by MaryEllen Hunt [4] using the motion capture system in the Ergonomics and Safety Lab at the University of Utah. Maximum forces, moments, velocities and acceleration at the ankle along with ROM are shown in Table 1 and were used to determine the performance required of the AFS in order to reproduce normal gait.

Trajectory Specifications

Trajectory data were collected using a motion capture system in the Ergonomic and Safety lab at the University of Utah [4]. This motion capture

Table 1: System requirements

Axis	X	Y	Z	Pitch	Roll	Yaw
Force [N] / Moments [Nm]	100	30	560	37	8	7
Velocity [m/s] / [rad/s]	2	0.5	0.75	8.7	1.2	0.9
Acceleration [m/s^2] / [rad/s^2]	15	5	6	82	26	21
Range of Motion [m] [rad]	0.25	0.032	0.092	1.45	0.018	0.21

system uses reflective markers placed on participants on anatomical landmarks that aid in modeling skeletal kinematics. Participants walked along an elevated walkway that is described in [4]. A pair of 400 mm X 600 mm force plates (Bertec Inc, Ohio) embedded in the walkway collected GRFs in concert with the motion capture system. Based on the collected data, ankle position and orientation with respect to a global coordinate frame and internal joint forces and moments were calculated.

Multiple ankle trajectories from different subjects were analyzed when determining the system requirements. Variables of interest for the design requirements of the AFS were as follows: first, ankle velocity during the contact phase with the ground; second, ground reaction forces; and third, internal torque generated at the ankle.

The motion tracking data were collected at 100 Hz and processed using Visual 3D (C-motion Inc, MD) to fill marker trajectory gaps and filter data. The data point density was increased to allow the AFS controller to have a new trajectory data point for each time step of the control loop. The motion tracking data were also prefixed with an acceleration phase to smooth the ramp up when the AFS was brought up to speed just before heel strike, and appended with a

deceleration to slow down the AFS and bring it to a stop before returning to the starting position. Figure 2 and Figure 3 show the robot's prescribed trajectory of acceleration, contact phase, and deceleration.

Space Requirements

The AFS frame size was determined in part by the need to observe the function of the AFS with motion capture cameras and for ease of access to the robot for maintenance and repair. A large and open frame box style was designed by Ken Openshaw, a member of a senior design group, and was built and donated by SME Steel. The frame is 1.8m long, 0.9m wide, and 1.5m tall (see Figure 4). The length of the frame was designed to allow the gantry to accelerate and decelerate before and after the contact phase of the trajectory. When decelerating the X axis gantry, special consideration of the gantry's kinetic energy is taken into account to allow enough room to decelerate and reduce kinetic energy during deceleration.

As a primary function of the AFS is to test the Smart Shoe, the AFS had to be designed in a way that the ankle fit a variety of shoe types and sizes without obscuring the operator's view of the shoe during the gait cycle. The ankle also had to mimic the full ROM typically seen in a healthy gait and withstand the applied forces and moments. This combination of size restriction on the ankle, ROM requirement, and load capacity resulted in challenging design constraints, which are discussed in Chapter 4, Mechanical Design Features.

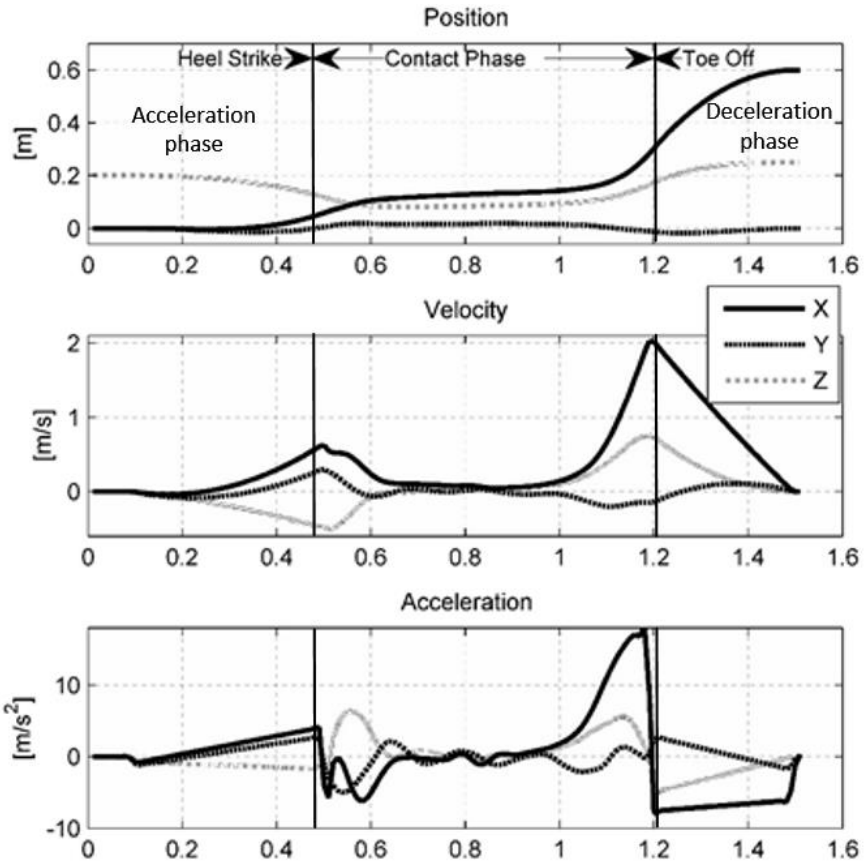

Figure 2: Ankle position, velocity, and acceleration trajectories.

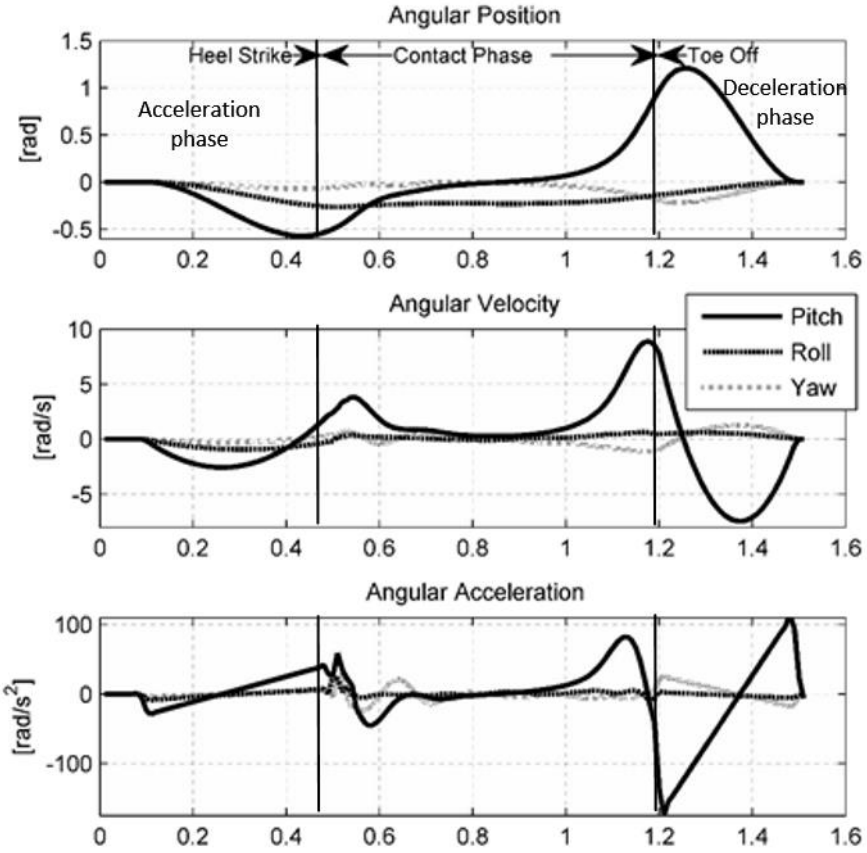

Figure 3: Ankle angular position, velocity, and acceleration trajectories.

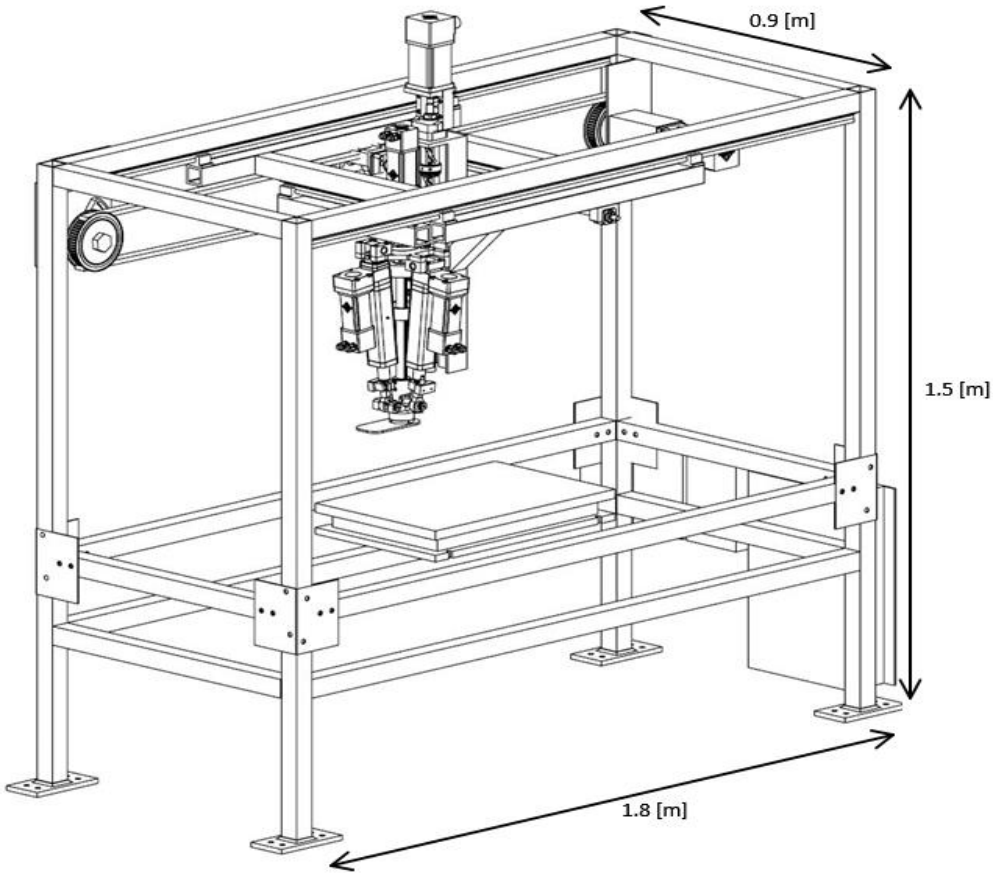

Figure 4: Cad model of the AFS robot.

Instrumentation Requirements

To validate the AFS robot, sensors were chosen to measure kinematics and kinetics of human gait. These features included position and orientation of the ankle and foot, ground reaction forces, and internal ankle moments. Position and orientation are measured using high-density encoders on the motors that control the robot. Using forward kinematics, the position and orientation of the AFS ankle can be calculated. GRFs are measured with a 6 DOF Advanced Mechanical Technology, Inc. (AMTI) force plate; the internal ankle forces and moments are measured using a 6 DOF ATI load cell.

CHAPTER III

GANTRY DESIGN

The gantry of the AFS is responsible for positioning the ankle. Figure 5 illustrates the coordinate system of the AFS and also the section of the gantry system responsible for positioning along that axis. Each axis is driven by a brushless DC motor that has a high-density encoder used to provide position feedback to the controller.

The gantry is made out of aluminum to keep the weight down but still provides adequate stiffness. The aspect ratio of different gantries was determined by both force calculations for each bearing block and by potential binding due to cogging effects. The cogging comes from only having the transmission of power connected at one side, i.e., the belt for the X axis and a ball screw for the Y axis, see Figure 5. The linear bearings for both the X axis (peach) and Y axis (green) gantries are oriented upside down. This orientation provides the greatest support in the direction that is opposing the reactive forces generated during the contact phase of the gait cycle. Loading calculations of the linear bearings can be found in the APPENDIX. Placing the linear slides upside down and within the frame has an added bonus of using the frame as a stopping block to prevent the robot from sliding off the rails in case of a robot malfunction, drive failure, or user error.

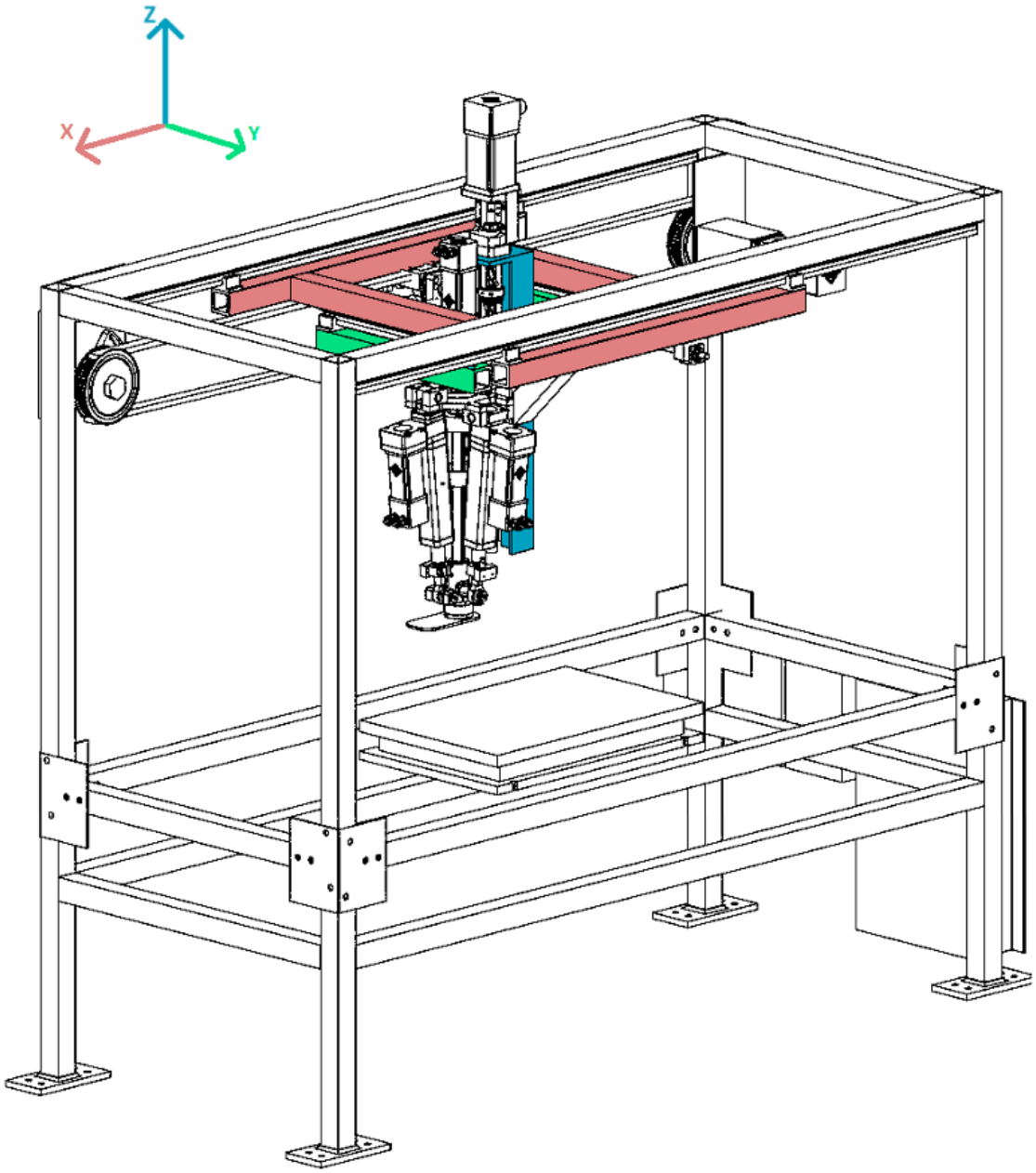

Figure 5: AFS gantry layout, X gantry (peach), Y gantry (green) and Z gantry (blue).

Design Selection

A Stewart table-like robot Aubin [8] was considered by the design team because it offers a 6 DOF high force platform; however, because of the large work space needed for the gait cycle, this idea was abandoned. A prismatic system was chosen for the gantry system due to its simple design; all but one actuator was uncoupled from the others, making controlling the robot simpler.

The gantry consists of three axes and utilizes both belt and ball screw drive trains. The speed profile of the ankle during the stance phase of the gait cycle reaches 2 m/s in the direction of travel (X axis) (see Figure 5). To achieve this speed, a synchronous belt and pulley system was used. The synchronous belt is toothed to prevent slipping and has steel tension members instead of the standard fiberglass to withstand shock loads better. A ball screw system was determined unsuitable for the X axis because of the long unsupported length of the screw that would have been required. This would have resulted in a relatively low critical rpm, where the system would lose performance, and a reduced service life of the robot. Ball screw drive trains were chosen for both the vertical (Z axis) and side-to-side motion (Y axis) of the trajectory, as they provide high rigidity and can be directly driven by the motor. High rigidity was desired to help with system repeatability.

Mechanical Design Features

The X axis is driven by a belt and pulley system to accomplish the high speed needed to recreate the gait profile. A ball screw system was chosen for the Y

and Z axis for simplicity and mechanical advantage without the need for a gear box. The option to preload the nut to eliminate backlash was also a deciding factor for choosing the ball screw system.

Actuator Selection

For the X axis, a belt drive was chosen to meet the speed requirements. Because the X axis is the most demanding in regard to both speed and acceleration, having the ability to match inertial impedance with a gear box was beneficial. The equation used to determine the gear box ratio is

$$N = \sqrt{\frac{I_m}{I_L}} \tag{1}$$

where N is the gear ratio, I_m is the inertia of the motor and gear box, I_L is the inertia of the load.

For both the Y and Z stage actuator, a ball screw design was chosen. Other actuators that were considered were linear motors, but these were rejected due to their cost.

An equation describing the motor torque required as a function of desired force and acceleration of a load for a ball screw is

$$\tau = \frac{p}{2\pi} \cdot \frac{F_L}{\eta} + \left(J_m + J_s + \frac{m_L + m_S}{\eta} \cdot \frac{p^2}{4\pi^2} \right) \cdot \frac{\pi}{180} \cdot \alpha \tag{2}$$

where p is the Pitch of the ball screw, F_L is the force of the linear actuator, η is the efficiency, J_m is inertia of motor, J_S is inertia of screw, m_L is mass of the load being pushed, m_S is mass of the screw, α is the linear acceleration in m/s^2.

Dynamic Models and Simulations

Dynamics were derived from motion capture data that included ankle position and ground reaction forces. Motor torques were calculated to replicate these dynamics based upon actuator power transmission. These calculations were trivial, as the dynamics of the AFS are uncoupled and can be calculated on an individual basis. Dynamic models of individual actuator systems were created during the design phase of the project to help in choosing adequate motors and actuators to meet design specifications. The result of such a model can be seen in Figure 6, where the rated torque speed curve of the motor is compared with the calculated torque and speed of the simulation. The motor and gear box combination were chosen using impedance matching. Impedance matching maximizes power transfer to the robot by balancing the inertia of the motor with the system through a gear box.

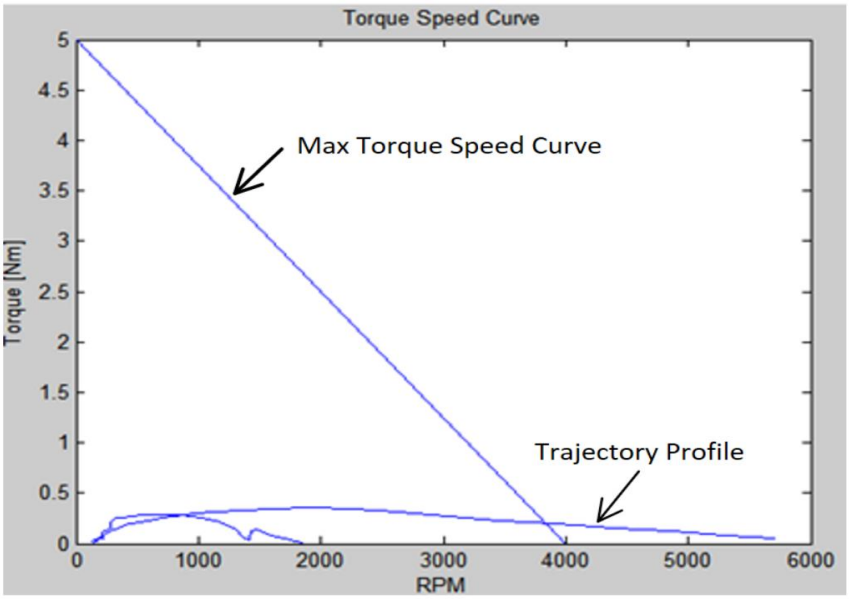

Figure 6: X axis torque speed requirements. (Line going from 5 Nm to 4000 rpm is the motor's torque speed curve.)

With this design, the robot can both accelerate fast and reach a high velocity in the short travel distance constrained by the frame. The data used in this figure are not what were originally used to design the robot, and as a result the rpm goes beyond the motors' rated 4000 rpm limit. This was deemed acceptable because the robot would be operating well below the rated torque. When decelerating the X axis gantry, special consideration of the gantry's kinetic energy was taken into account to allow enough room to decelerate. If the servo drives used to run the AFS are required to store energy above their rated capacity, during deceleration the drive will move into an overvoltage fault and cease to decelerate the gantry. This leaves the gantry to coast to the Sorbothain bumpers at the end of the rails. To fix this issue, a power resistor was installed to increase the rate of power dissipation.

Load Analysis

To meet the design feature of having a rigid robot, an analysis of the deflection of the gantry was performed using SolidWorks and can be seen in Figure 7. The forces used in this analysis were the maximum forces seen for each axis and were intended to be a worst case scenario calculation. This analysis was performed before the ankle mechanism was designed and does not include the deflections from the ankle. The result is approximately 1 mm of deflection at the bottom of the Z axis stage during full loading. If this deflection becomes a problem, an additional square linear bearing on the Z axis would significantly increase rigidity and reduce this deflection.

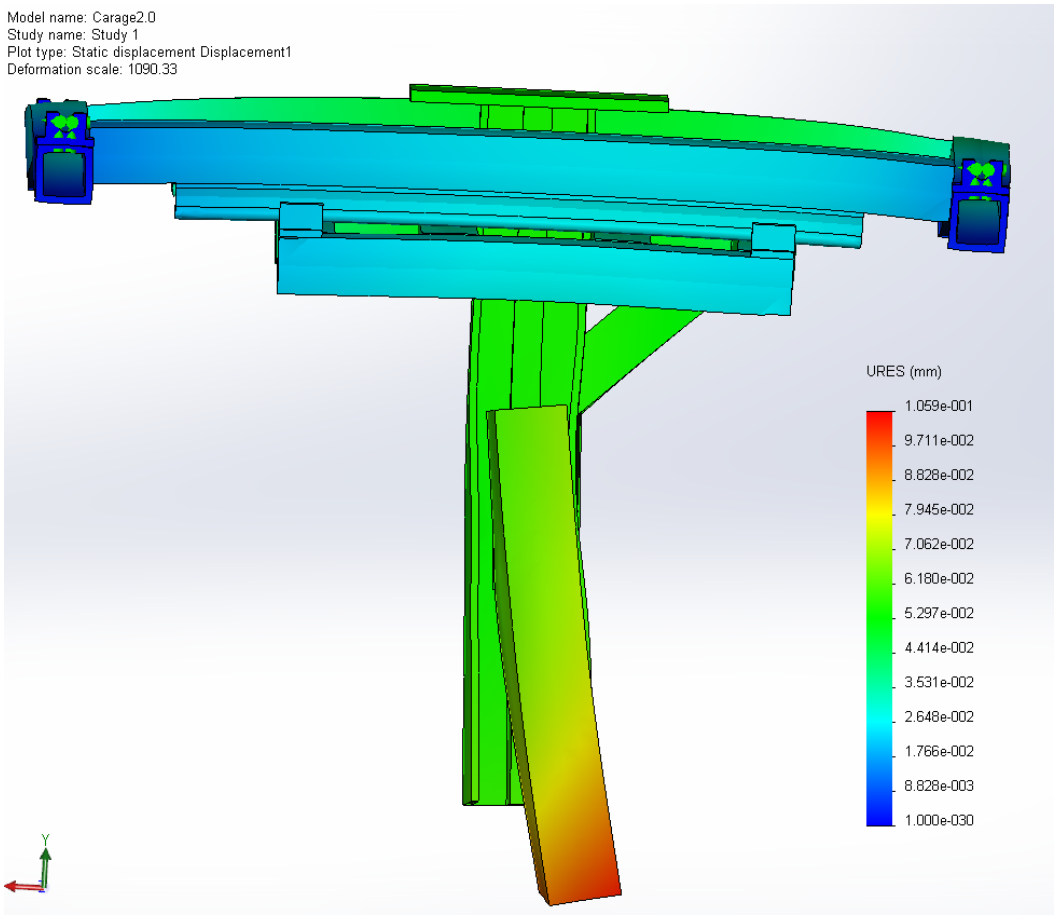

Figure 7: Deflection of the gantry during loading.

Linear Rails

One challenge of making the gantry system was ensuring that the linear rails were parallel to each other. It was decided that with the available facilities on campus, we could not accurately measure where the linear rails needed to be placed during assembly, thus, a different approach was used. The approach involved analyzing the steps of mounting and securing the linear rails to the frame to determine if we could make the rails inherently parallel. The resulting approach is illustrated in Figure 8. To make the rails parallel, a standard was made to be the distance between the rails (1-2). With this standard and rail (3-4)

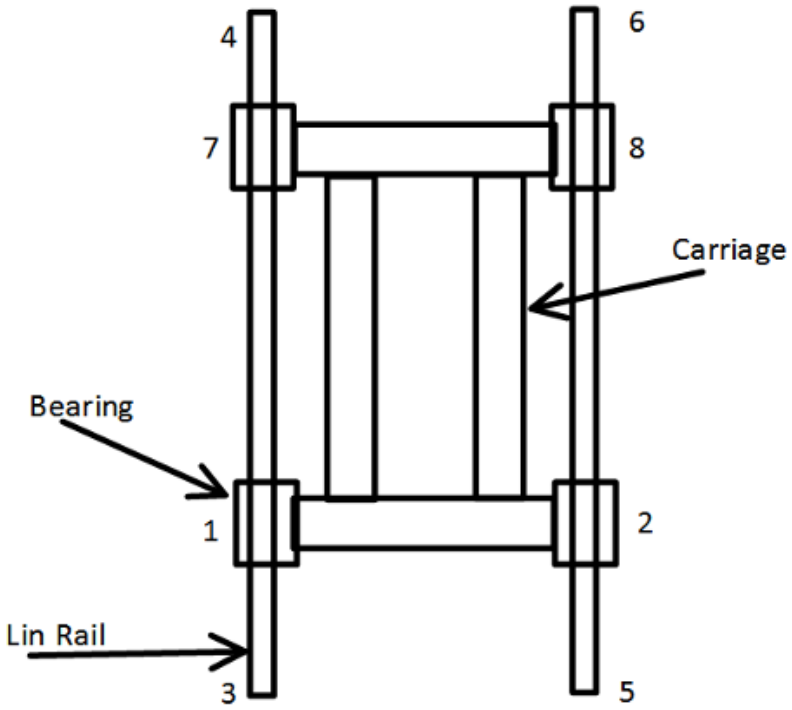

Figure 8: Fixture order of linear rails to the AFS frame.

mounted on the frame, the opposite rail (5-6) was placed and mounted, taking care that the standard used to fix the distance between the rails was close when drill holes were marked. Both rails were bolted down when the standard moved freely along the rails, indicating constant distance between the rails. Bearings 7 and 8 were then bolted to the gantry. This fixture-order resulted in parallel rails without having to measure the distance.

CHAPTER IV

ANKLE DESIGN

The AFS ankle mechanism is responsible for the orientation of the foot. Each orientation axis of the ankle is driven by a brushless DC motor that has a high-density encoder attached to provide orientation feedback to the controller. The physical design of the ankle consists of a center shaft that acts as the shank of the leg. At the bottom of the shaft is a simple u joint that acts as the ankle complex. Rigidly attached to the center shaft is a plate that acts as a point of actuation where the two linear actuators are able to manipulate the plane that the foot is attached to.

Design Selection

Ankle Alternatives

All similar robots in the literature use a simplified design of the ankle joint, and most are passive [9]. The only one that comes close to the capability of the AFS designed in this study is the Stewart Table. The Stewart Table is a very rigid 6 DOF table with a force plate attached. This force plate makes contact with a stationary foot [8].

Another design was based on the Simple Compact Wrist [15] design, as seen

in Figure 9 a. The design was fundamentally flawed, as actuating both the Pitch and Roll axes at the same time caused binding. However, this problem was resolved by adding an additional pivot joint (Figure 9 (a) feature 1) that allowed for the out-of-plain motion needed to fulfill the desired motion but without binding. The wrist design was modified in SolidWorks to analyze the kinematic relationships. It was found that the altered design would work, and the existing wrist was modified to demonstrate the principal. The modification worked so well that the final ankle design uses the same mechanism that can be seen in Figure 9 (b) feature 1.

The ordering of the DOFs from the Simple Compact Wrist to the AFS was changed to mimic the order of DOFs of the anatomical leg, with the first DOF being a Yaw pivot at the hip followed by Pitch and Roll at the ankle. This made the ankle more compact because Yaw motion is realized above the ankle (see Figure 10). Another improvement over the Utah/M.I.T wrist is the coupling of the linear actuators to the joint. In the Utah/M.I.T wrist, an axial force applied by the actuator also applies a radial force that causes a moment on the linear bearings, reducing service life. The AFS ankle mechanism avoided this moment by allowing the actuator to pivot up above and act directly on the ankle plate.

Mechanical Design Features

The center of the AFS's ankle joint consist of a u joint with actuators located along the principal axis of rotation. Both actuators connect to the ankle using heim joints oriented to allow for the greatest ROM along the plantar/dorsal

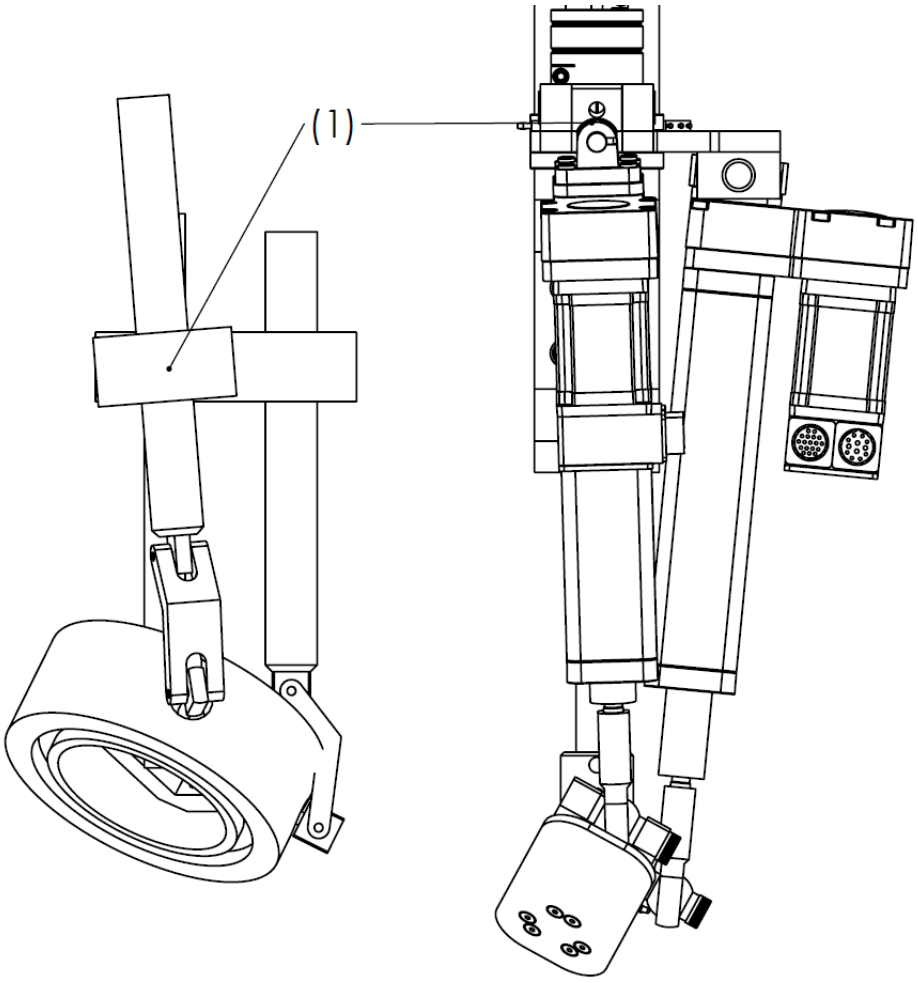

(a) (b)

Figure 9: Comparison of joint design. (a) Simple Compact Wrist showing revised design feature. (b) AFS ankle mechanism showing incorporated design feature. (1) Pivot that prevents binding due to out-of-plane motion.

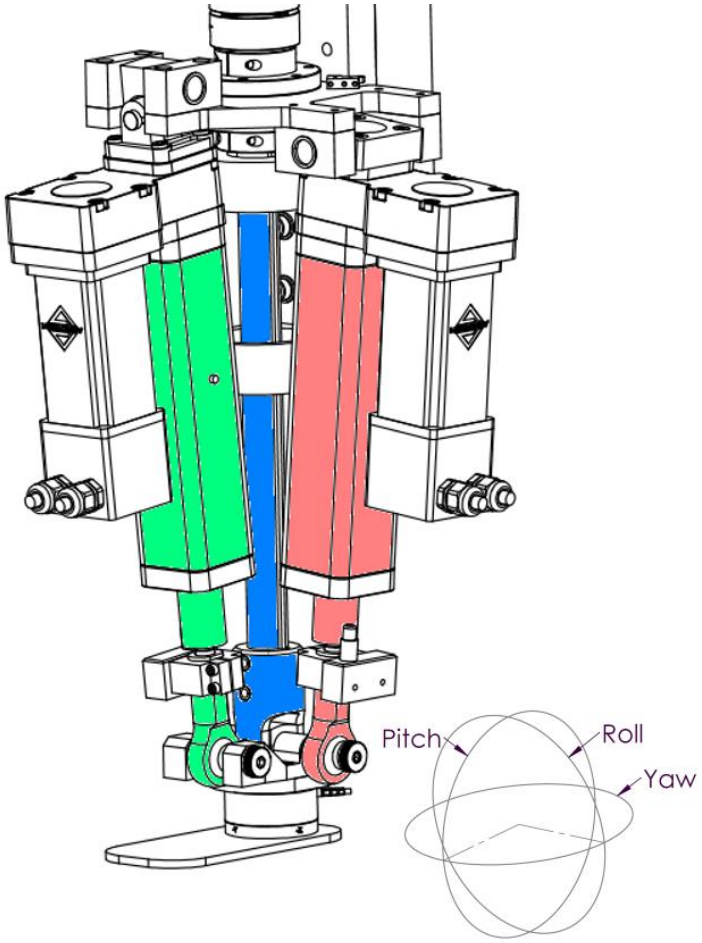

Figure 10: AFS robot ankle design. Yaw (blue), Roll (peach) and Pitch (green).

flection. One of the two actuators required an additional pivot (Figure 9 feature 1) at the connection to allow out-of-plain motion and prevent binding. This feature was missing in the Utah/M.I.T Dexterous Hand platform and was added during this project to determine if an additional pivot would fix the binding. Adding this pivot fixed the binding issue seen in the Simple Compact Wrist and was implemented in the AFS ankle design (see Figure 10). Interference checks in SolidWorks played a major part in making sure the ankle had the ROM required for normal gait. Checks were made at the maxima and minima of the

ankle joint (see Figure 11). After designing the ankle in SolidWorks, it was 3D printed to check the design. Checking the 3D-printed part was a good idea, as it turned out the CAD file of the u joint from McMaster had the yoke dimensions larger than the actual yoke, resulting in a loose yoke in the prototype. This error was fixed in the design and the part was printed again to make sure everything would fit. After the part was verified, the plans were sent to the machine shop for manufacturing. The measured ROM of the ankle mechanism is shown in Figure 12. The ROM needed for normal gait and ROM of the AFS ankle mechanism can be seen in Table 2. The ROM measurement was made by recording the encoder readings and moving the ankle along its physical limits. Angles were calculated using forward kinematics with encoder values as the input. The ankle was actuated using the readings of the load cell as an input.

For a better understanding of the AFS ankle, Figure 13 (a) provides an exploded view of the ankle structure and (b) provides a cutaway view to show

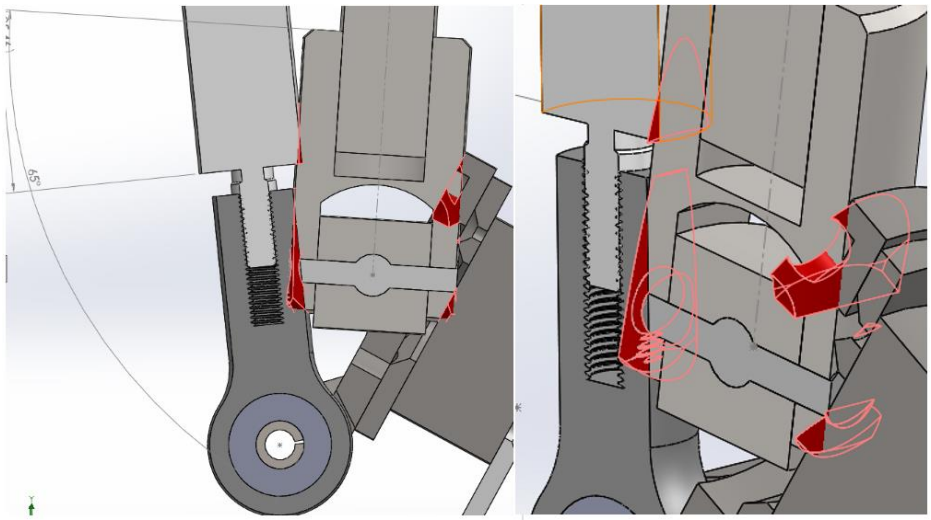

Figure 11: Ankle joint range of motion Interference check.

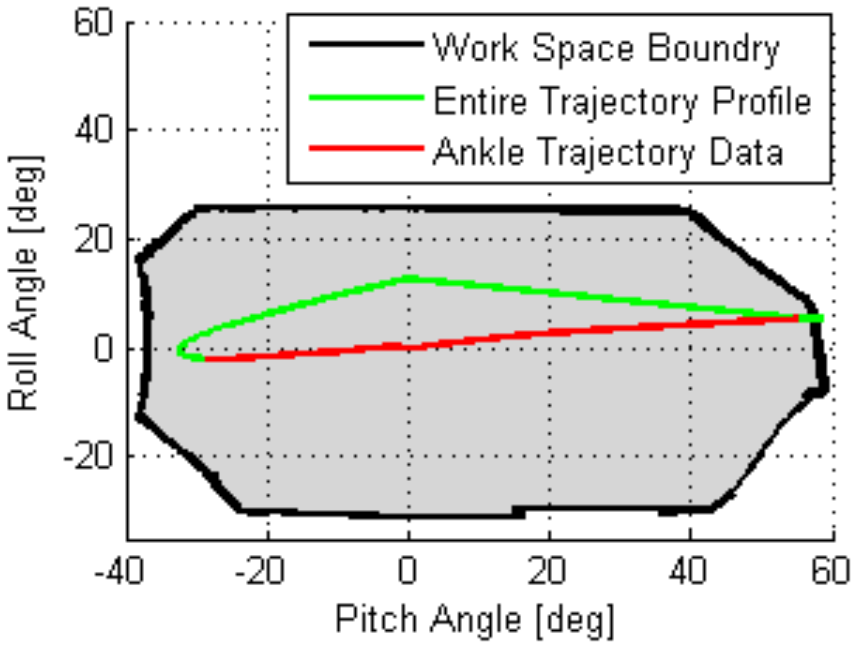

Figure 12: Ankle mechanism available work space (gray), trajectory orientation of the ankle (green), raw gait data (red).

Table 2: ROM comparison between AFS ankle mechanism and normal gait.

	Normal Gait	AFS
Pitch	-28° to 56°	-35.6° to 58°
Roll	-2° to 5°	-30° to 24°
Yaw	-5° to 7°	-6° to 99°

the interactions of the different components. Each ball joint (1) and (7) is fastened to the ankle plate (2) by shoulder bolts (8) and (9) and is where the linear actuators attach. The Roll ball joint rests on a drill bushing (6). The ankle plate is supported by half of a universal joint (3) (4) (5), with (2) and (8) comprising the other half. The yoke (5) attaches to the Yaw shaft, which is not shown.

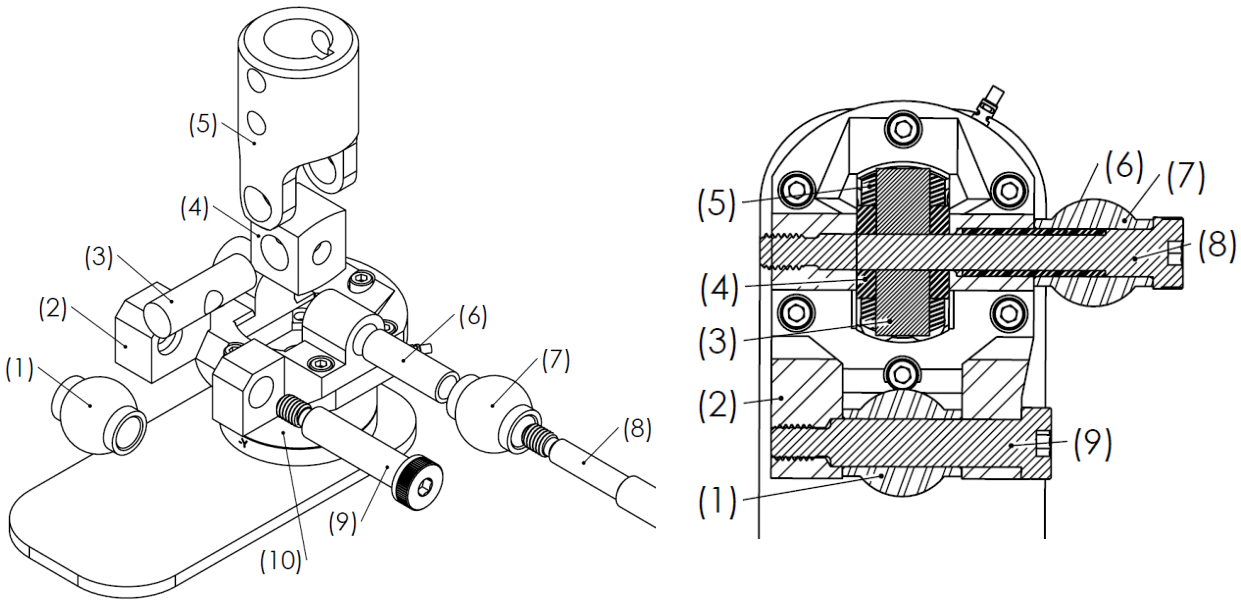

(a) (b)

Figure 13: View of the internals of the AFS ankle mechanism design. (a) Exploded view of the ankle design. (b) Section view of the ankle design. 1) Pitch ball joint, 2) Ankle plate, 3) Cross shaft, 4) Cross block, 5) Yoke, 6) Bushing, 7) Roll ball joint, 8-9) Shoulder bolts, 10) Load cell.

Actuator Selection

To actuate the ankle, a ball-screw-driven system, similar in fashion to the ones used in the Utah/MIT dexterous hand, was designed. Due to the iterative design process, off the shelf linear actuators were chosen because of their robust design and self-containment, making them an easy feature to match specification. These linear actuators articulate the ankle in both the Pitch and Roll DOF.

Equations (3) and (4) describe the motor torque needed to generate a linear force F_L, as well as the motor torque needed to accelerate a mass m_L where p is the pitch of the ball screw, η is the efficiency of the ball screw, and $J_m$is the inertia

of the motor. In determining force requirements at the ankle, dynamic geometric relationships have to be taken

$$\tau_{force} = \frac{p}{2\pi} \cdot \frac{F_L}{\eta} \tag{3}$$

$$\tau_{inertia} = \left(J_m + J_s + \frac{m_L + m_s}{\eta} \cdot \frac{p^2}{4\pi^2}\right) \cdot \frac{\pi}{30} \cdot \alpha \tag{4}$$

into consideration. Dynamic relationships for the ankle mechanism are the line of action angles from the linear actuators to the ankle plate, as seen in Figure 14; the line of action angle changes, depending on the orientation of the ankle. Describing the change in force to generate the desired moment can be accomplished using (5), where F_{total} is the required actuator force to generate the desired moment *M* based on the line of action angle with the ankle plate θ.

$$F_{total} = \frac{M \cdot r}{\sin(\theta)} \tag{5}$$

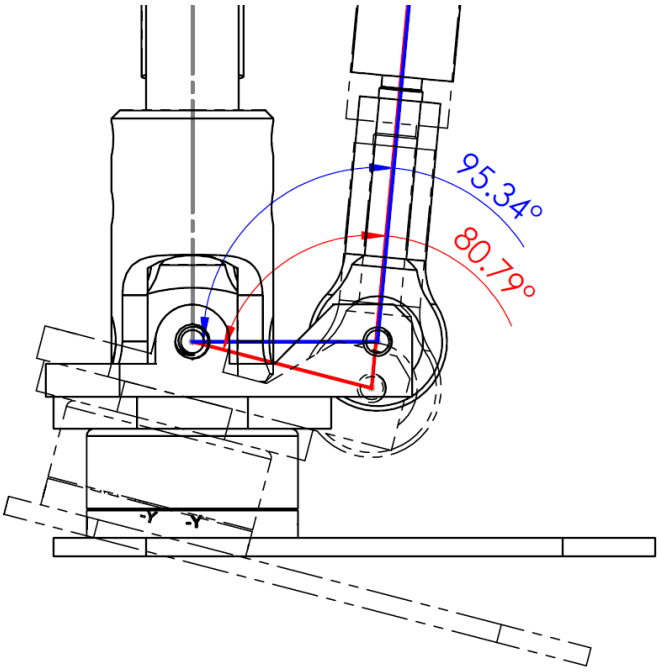

Figure 14: Cad model of ankle showing change in actuator line of action.

The distance from the center of rotation to the line of action is *r*. With this new definition of force requirements based upon orientation of the ankle, the appropriate linear actuator and motor were selected. The maximum expected dynamic loading of the ankle dictated the class of actuator needed. Next was the motor and Pitch of the linear actuator selection, making sure that the resulting combination kept the motor operating under the continuous torque speed curve for the majority of the operation. While (5) is correct and was used to choose an appropriate motor and linear actuator, a more complete and elegant solution to this problem that includes moment coupling between actuators can be found in Controls, Ankle Moment Feedforward Calculations equations (11)- (13).

Load Analysis

Designing an ankle that is compact, has sufficient ROM, and is able to withstand the forces generated due to geometry was a challenge. Stress analyses were performed during the design process to determine if the AFS ankle design would fail under load. The result for the final design of the ankle plate can be seen in Figure 15, which depicts the Roll moment acting on the heim joint. This analysis consists of the ankle plate, bushing, and heim joint with the Roll bolt missing, as this is used for pressing the heim joint against the ankle plate and not load bearing. The result is a factor of safety of 6.47, which was determined sufficient for this project.

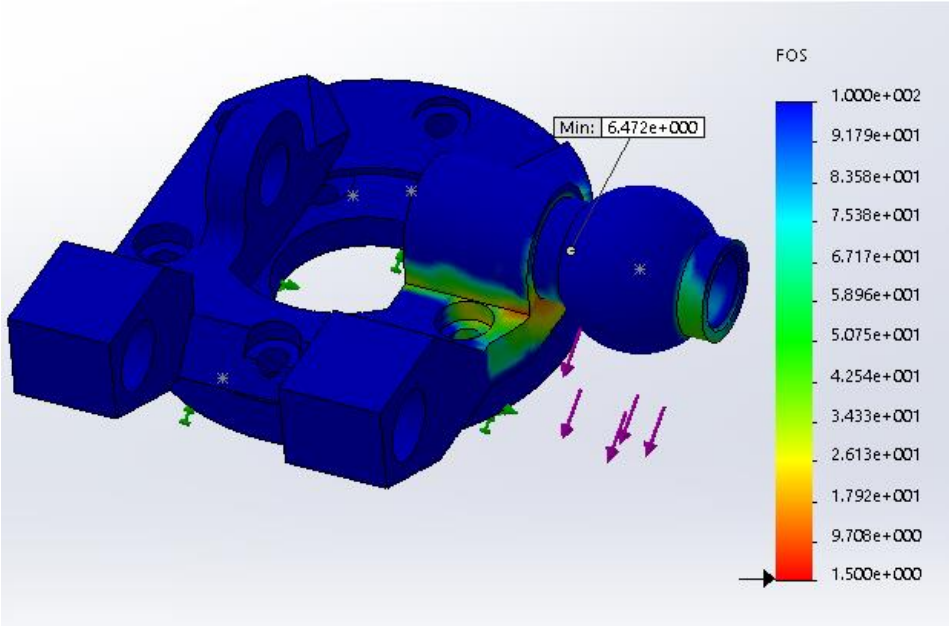

Figure 15: Stress analysis of the AFS ankle plate design due to ankle Roll over.

CHAPTER V

CONTROLS

An admittance multiloop trajectory and force controller is used to control the AFS robot, Figure 16. The inner loop is responsible for following the prescribed trajectory, while the outer loop is responsible for modifying the inner trajectory in order to achieve the desired ground reaction forces.

The majority of the trajectory is known beforehand, minus small changes to satisfy the desired contact forces. The control loop utilizes feedforward compensation of the expected dynamics to predict required torques for the motors. The feedforward aspect of the controller uses the predicted

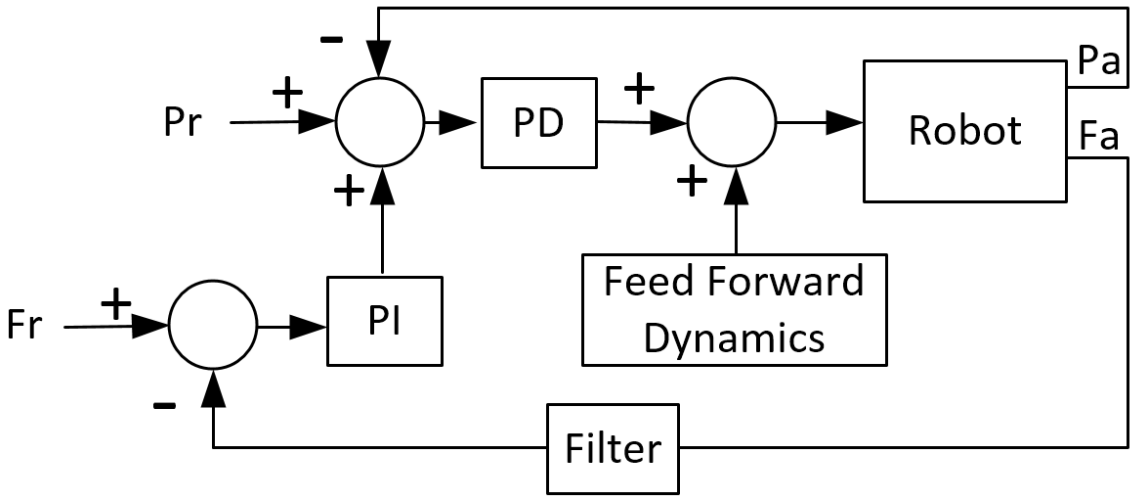

Figure 16: Block diagram of the AFS controller.

trajectory instead of the trajectory generated from the force error, because the noise from the load cell or force plate would propagate into the trajectory, and thereby cause chatter in the computed torques.

The PI's integrator in the force loop accumulates error during the run. This error results in a residual position offset after a run. The system needs to reset this error to zero before the next run or the residual position offset will invalidate the run. Resetting the residual error to zero would cause the position command signal to the robot to be discontinuous. To eliminate any potential discontinuities due to residual error alleviation, the signals from the force loop's PI pass through a transfer function where the error is set to zero. The transfer function is designed to program the change in error with some virtual mass and damping, allowing for a smooth transition between the two states.

Safety Features

Limit Switches

Limit switches are placed on all DOF to allow initialization of the position estimates of the motor encoders. If, after calibration, a limit switch is triggered, the robot will shut down to prevent catastrophic failure. I/O pins on the D-Space used for limit switches have a pull-down resistor attached to them. All switches are normally closed, allowing the +5V to be read by the I/O pins. When a switch is triggered it opens the circuit and stops the +5V signal. If there is a problem with the wiring (disconnected wire), the D-Space reads the signal as a limit switch trip and will take appropriate action, depending on the state of the AFS.

Watchdog

There are many watchdogs monitoring the AFS to keep it running safely. The first safety feature consists of checking the min and max position of the desired trajectory with the available work space of the AFS robot. If the desired trajectory is outside the bounds of the AFS's work space, the system will not run. The second safety feature is after the system is calibrated, if a limit switch is hit, the system will shut down. Third is a velocity check loop that monitors the velocity of the robot. If the robot exceeded the velocity limit, the system shuts down. Last is the Emergency Stop that, when pressed, shuts down the robot.

Instrumentation

Position and orientation are calculated using forward and inverse kinematics, and are measured using high-density encoders on the brushless DC motors of the AFS. Precision snap action limit switches are used for calibrating the work space. The hall effect limit switches provided by Thomson Linear have a repeatability of 0.2 mm and a hysteresis of 1.5 mm. This was unacceptable and physical snap action limit switches were used instead that have a repeatability of 0.013 mm. GRFs and internal moments of the ankle are measured using a force plate and load cell, respectively, and are shown in Figure 17.

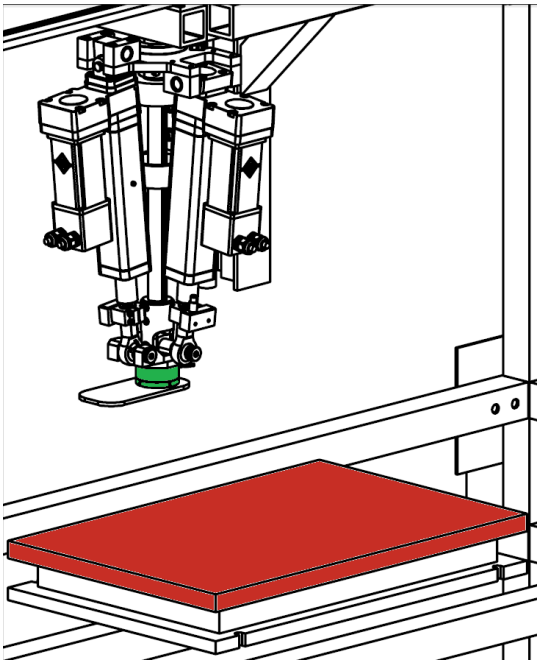

Figure 17: Cad model showing locations of the force plate (red) and load cell (green).

AFS Dynamics

Gantry Dynamics

The motor torque equations for the gantry's X, Y, and Z axes can be seen in equations (6), (7), and (8), respectively.

$$\tau_{mX} = \left(J_m + J_{p1} + \frac{J_{p2}}{\eta} + \frac{m_L + m_b}{\eta} \cdot \frac{r_p^2}{2}\right) \cdot \frac{\pi}{30} \cdot \alpha + r_p \cdot \frac{F_L + F_f(V)}{\eta} \tag{6}$$

$$\tau_{mY} = \left(J_m + J_s + \frac{m_L + m_s}{\eta} \cdot \frac{p^2}{4\pi^2}\right) \cdot \frac{\pi}{30} \cdot \alpha + \frac{p}{2\pi} \cdot \frac{F_L + F_f(V)}{\eta} \tag{7}$$

$$\tau_{mZ} = \left(J_m + J_s + \frac{m_L + m_s}{\eta} \cdot \frac{p^2}{4\pi^2}\right) \cdot \frac{\pi}{30} \cdot \alpha g + \frac{p}{2\pi} \cdot \frac{F_L + F_f(V)}{\eta} \tag{8}$$

where J_m is the motor's inertia [kgm^2], J_p is the inertia of the pulley [kgm^2], η is the efficiency, m_L is the mass of the load [kg], m_b is the mass of the belt [kg], r_p is the radius of the pulley [m], α is the motor's angular acceleration [rad/s^2], F_L is the load

force [N], F_f is the friction force [N], p is the Pitch of the ball screw [m], N is the gear ratio.

Feedforward dynamic or computed torque control is used in the controller to precalculate expected motor torques and push this information to the amplifiers. This includes torques resulting from acceleration, viscus friction, and static friction. With these models calculating the expected torques, the PD and PI controllers can focus on just correcting errors in the models instead of driving the entire robot from rest to motion. These calculations use the desired trajectory and force data to avoid noisy signals. The increase in position tracking performance is documented in Table 3, where the robot was run at 1/3 speed with and without the feedforward compensation.

Motor current prediction from the feedforward compensation and actual can be seen in Figure 18. In this test, the robot was running at anatomically correct speeds without contact. All motors perform within design ranges except for the X and Y axis (Figure 18 a and b respectively). The X axis shows actual current draw of 225%, when was determined acceptable as the motor is running at low speeds. The X axis has room to be overdriven to achieve the desired performance because the

Table 3: Tracking error reduced with the use of feedforward compensation.

	% Decrease
X	65.71
Y	71.15
Z	85.24
Pitch	45.00
Roll	38.10
Yaw	38.18

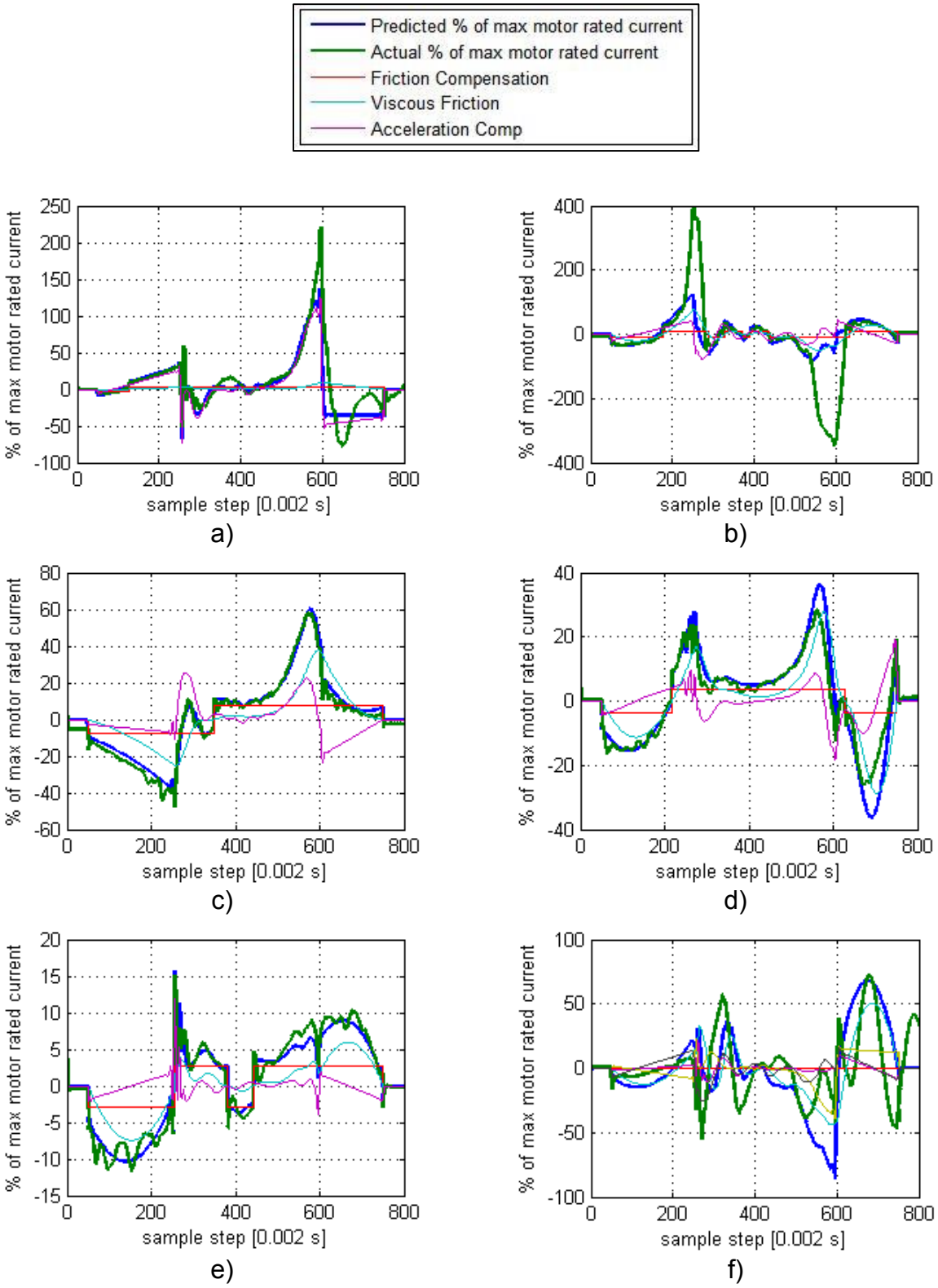

Figure 18: Feed-forward torque compensation of X axis (a), Y axis (b), Z axis (c), Pitch axis (d), Roll axis (e) and Yaw axis (f).

servo amplifier has not yet reached its limit. The Y axis, however, cannot be overdriven because the amplifier is already at its limit. The Y axis has fallen short of performance specifications because more friction is present in the ball screw drive than what the design allows. This problem is discussed in more detail in the Future Work section.

Ankle Dynamics

The ankle's Roll and Pitch motor torque equations combine equations (3) and (4), resulting in equation (9). The equation for the Yaw axis is described in equation (10).

$$\tau_{mPitch/Roll} = \left(J_m + J_s + \frac{m_L + m_s}{\eta} \cdot \frac{p^2}{4\pi^2}\right) \cdot \frac{\pi}{30} \cdot \alpha + \frac{p}{2\pi} \cdot \frac{F_L(\theta) + F_f}{\eta} \tag{9}$$

$$\tau_{mYaw} = \left(J_m + J_g + \frac{J_L}{N^2 \cdot \eta}\right) \cdot \frac{\pi}{30} \cdot \alpha + \frac{M_L + M_f}{N \cdot \eta} \tag{10}$$

where τ_m is the motor torque, J_m is the motor's inertia, J_s is the inertia of actuator, J_g is the inertia of the gear box, m_L is the mass of the load, m_s is the mass of the linear actuator piston, η is the efficiency of the motor and linear actuator, p is the Pitch of the linear actuator, α is the angular acceleration of the motor, F_L is the actuator force required to produce the desired moment and is a function of θ, F_f is the force to overcome friction, M_L ankle Yaw moment, and M_f is the moment due to friction.

Ankle Moment Feedforward Calculations

The mapping between motor torque and ankle moment is nonlinear and is a function of ankle orientation. This is because the angle of actuation changes with the orientation. Solving the required actuator force to produce a desired ankle moment about the Pitch axis is

$$F_{pitch} = \frac{M_{pitch\_d}}{r \cdot \left[\overrightarrow{V_1} \times \overrightarrow{V_2}\right]_j} \tag{11}$$

where F_{pitch} is the force of the Pitch actuator, M_{pitch_d} is the desired Pitch ankle moment, r is the distance O0 to O3, $\overrightarrow{V_1}$ is the vector from O0 to O3, and $\overrightarrow{V_2}$ is the vector from O4 to O3 (see Figure 19). The force from the Pitch actuator (A) results in out-of-plane moments that need to be solved for and taken into consideration when calculating the Roll actuator (B) force. Solving for the moments resulting from the Pitch,

$$\bar{M}_{pitch\,result} = r \cdot F_{pitch} \cdot \left[\overrightarrow{V_1} \times \overrightarrow{V_2}\right] \tag{12}$$

combining the resultant moment in the Roll plane due to the Pitch actuator with the desired Roll moment, we can solve for the Roll actuator force,

$$F_{roll} = \frac{\left(M_{roll\_d} + \left[\bar{M}_{pitch\,result}\right]_i\right)}{r \cdot \left[\overrightarrow{V_3} \times \overrightarrow{V_4}\right]_i} \tag{13}$$

where $\overrightarrow{V_3}$ is the vector from O0 to O1 and $\overrightarrow{V_4}$ is the vector from O2 to O1. An additional moment is also generated about the Yaw axis due to the Pitch actuator but is constrained by the u joint and does not need to be taken into consideration. The dynamic response of the ankle plays an important role in the performance of the AFS robot. The AFS should exhibit passive ankle stiffness as well as

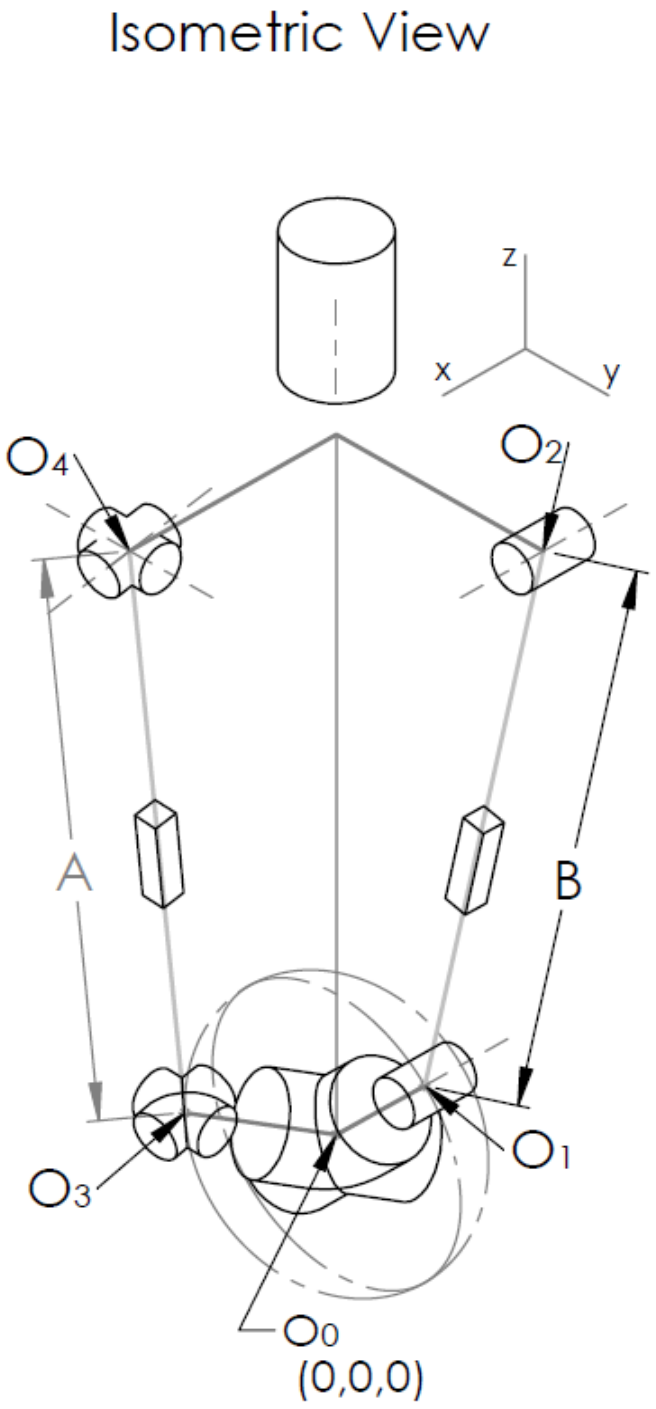

Figure 19: Geometric layout of ankle mechanism.

respond appropriately. The ankle stiffness model defined by Roy [16] serves as a basis for this work. Passive ankle stiffness values found in the literature are positive Pitch motion (plantar) 18 N-m/rad, negative Pitch motion (dorsi) 30 N-m/rad, positive Roll (inversion) 20 N-m/rad, negative Roll (eversion) 28 N-m/rad. Using equation (5) and (14) and solving for the actuator force, equation (15) can be derived. Replacing θ with θ_{error} and defining M as a function of θ_{error} as in equation (16), we can calculate the motor torque required to give the desired ankle stiffness.

$$\tau_{motor} = \frac{p}{2 \cdot \pi} \cdot \frac{F_{actuator}}{\eta} \tag{14}$$

$$\tau_{motor} = \frac{M \cdot r \cdot p}{\eta \cdot 2\pi \cdot \sin(\theta)} \tag{15}$$

$$M(\theta_{error}) = K \cdot \theta_{error} \tag{16}$$

where p is the Pitch of the linear actuator, $F_{actuator}$ is the linear force of the actuator, η is the efficiency of the linear actuator, M is the desired moment, r is the lever arm that the linear actuator acts on, K is the ankle stiffness, θ_{error} is the error between the reference ankle orientation and the actual orientation. Implementation of this controller can be seen in Figure 20.

In the case of an unwanted ankle Rollover, the Y axis becomes coupled to the Roll axis, as is shown in Figure 21. The ankle rotates about a fixed point where the bottom of the shoe contacts the force plate. The distance between the force plate and the center of the ankle is described as radius r. This lateral motion in the Y axis is described in equation (17) and is used to augment the Y axis trajectory to reflect a more anatomically correct ankle Roll over.

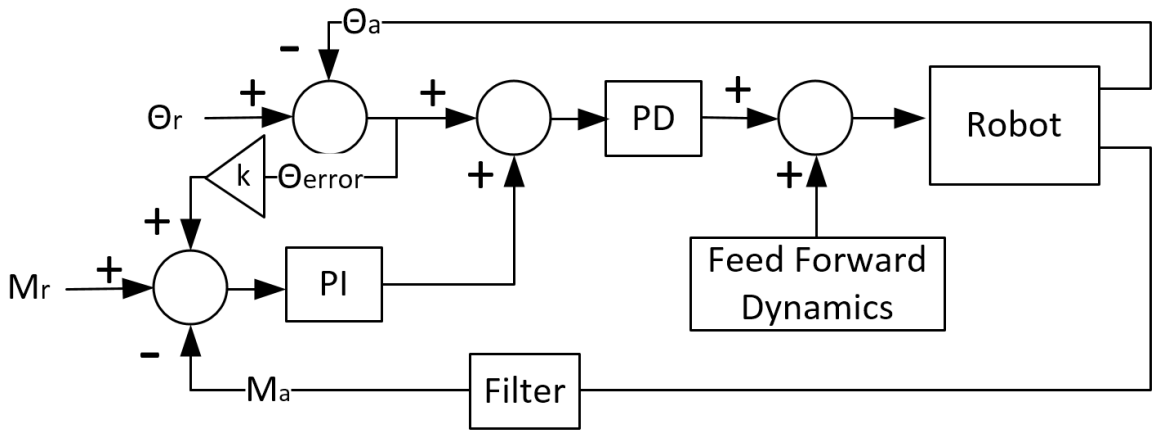

Figure 20: Passive ankle stiffness controller.

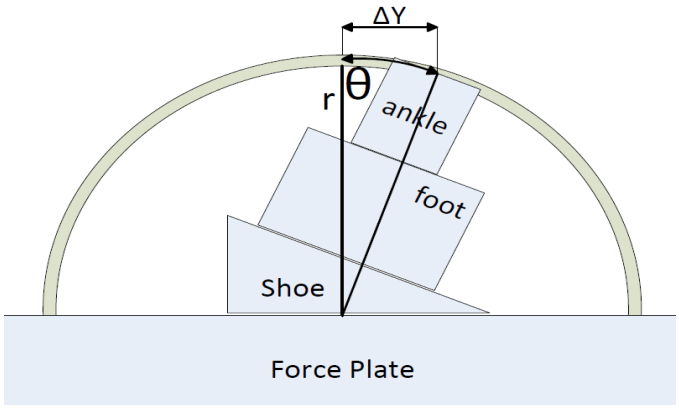

Figure 21: Displacement in the Y axis due to ankle rollover.

$$\Delta Y = r \cdot \sin(\Delta\theta) \tag{17}$$

where r is the radius of the instantaneous center of rotation, $\Delta\theta$ is the error between the desired and actual ankle orientation.

Trajectory

Finding a suitable way to load the trajectory data into the AFS was difficult. If the data consisted of too many points, it would not load and would result in an error. Once the data were loaded onto the D-space, a function was used to

crosscheck the current time with the time stamp on the data and match what set of values should be sent to the controller. This process was not reliable and caused problems because slight variations in the controller's loop time would push out a data set ether too early or hold onto a set for an extra loop cycle, depending on whether the loop cycle was faster or slower than expected. It was decided that a simpler march approach through the data would be desirable, eliminating problems with slight variations in loop times. Once the data were loaded into D-Space, a function would iteratively step through the data one-by-one for each time step, pushing these data sets to the controller. This method proved to be the most reliable way to tell the robot where it should be at a given time, but as a result, the time step of the data needs to match the control loop frequency. If there is a mismatch in the data's time step and the controller's loop frequency, the robot will run faster or slower, depending on the discrepancy of the time step.

CHAPTER VI

FORWARD AND INVERSE KINEMATICS

As a 6 DOF robot, the end effector of the AFS can be both placed and oriented within the robot's work space. The positioning of the AFS end effector is straightforward, as each position axis on the robot corresponds to the axis of the collected data.

Inverse Kinematics

Inverse kinematics is the process of taking a desired position and orientation of a robot's end-effector and computing the required joint angles or actuator lengths to achieve that position and orientation. From gait data collected in the lab using a motion capture system, the desired position and orientation of the AFS's ankle is known.

Solving for the AFS end effector position is accomplished using the end-effector Jacobian derived in this section, where the desired position is multiplied by a scalar composed of encoder resolution and gear train. Multiplying by a scalar is possible because the AFS's position axes are orthogonal to each other and parallel with the axes of collected gait data.

To solve the inverse kinematics of the ankle orientation, rotation matrices are

used to find the location of the ball-joints that actuate the ankle O_1 and O_3 (see Figure 22 Isometric View). Because the locations of the ball-joints are known for a desired orientation, and the location where the actuators are fixed at O_2 and O_4, the Pythagorean Theorem can be used to find the distance between and subsequently the lengths of the Roll (B) and Pitch (A) linear actuators.

Forward Kinematics

Forward kinematics is the process of computing position and orientation of a robot's end-effector based on specified joint parameters. Like the inverse kinematics, the forward kinematics for positioning of the AFS robot use linear relationships. While the orientation of the AFS ankle mechanism is more complex and requires further discussion.

Roll Axis

For the Roll axis, the geometry of the ankle mechanism simplifies to an intersection of two circles (see Figure 23). The radius R of the Roll-actuator circle is determined by the actuator's length. The radius of the ankle circle r is fixed as the distance from the center of the u joint O_0 to the ball joint O_1. The distance between the centers of the two circles is d. The equations of the two circles are

$$x^2 + y^2 = r^2 \tag{18}$$

$$(x - d)^2 + y^2 = R^2 \tag{19}$$

Solving for y and equating (18) and (19) to each other results in

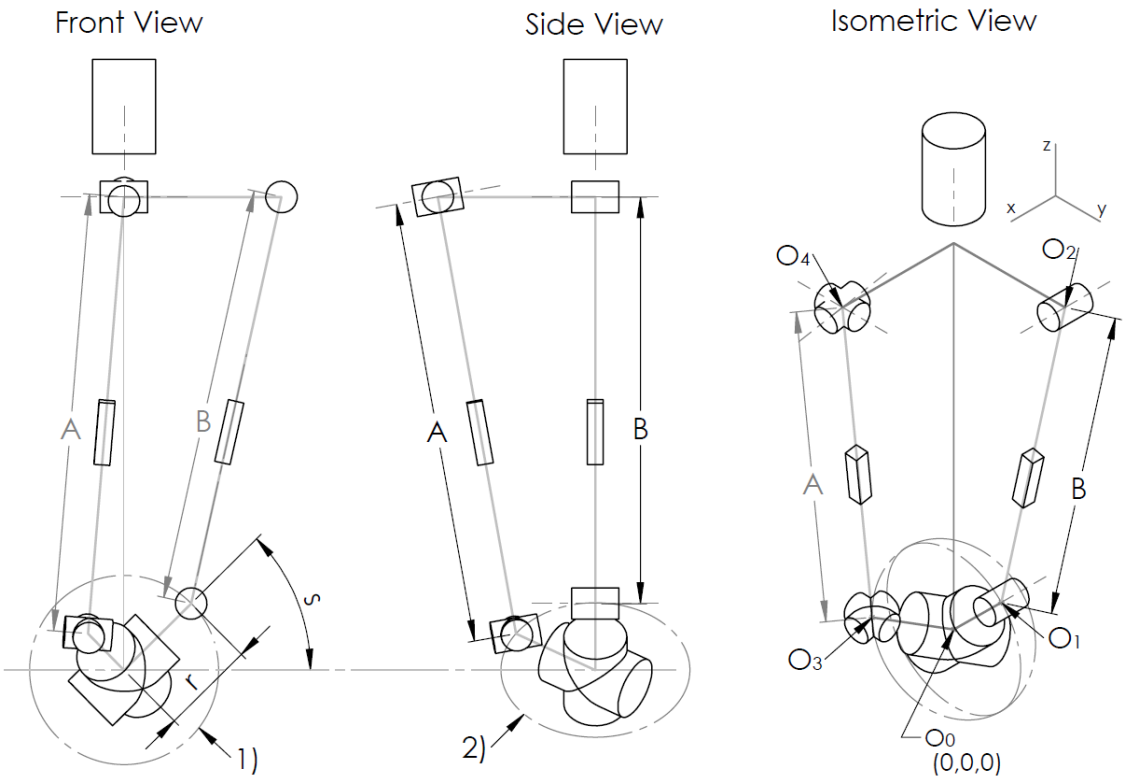

Figure 22: Kinematic representation of ankle mechanism. (A) Pitch actuator, (B) Roll actuator, (r) distance from center of u joint to actuator ball joint, (s) Roll angle, (1) path of Roll actuator ball joint, (2) path of Pitch actuator ball joint, (O_0) ankle origin, (O_1) origin of Roll ankle ball joint, (O_2) origin of Roll actuator, (O_3) origin of Pitch ball joint, (O_4) origin of Pitch actuator.

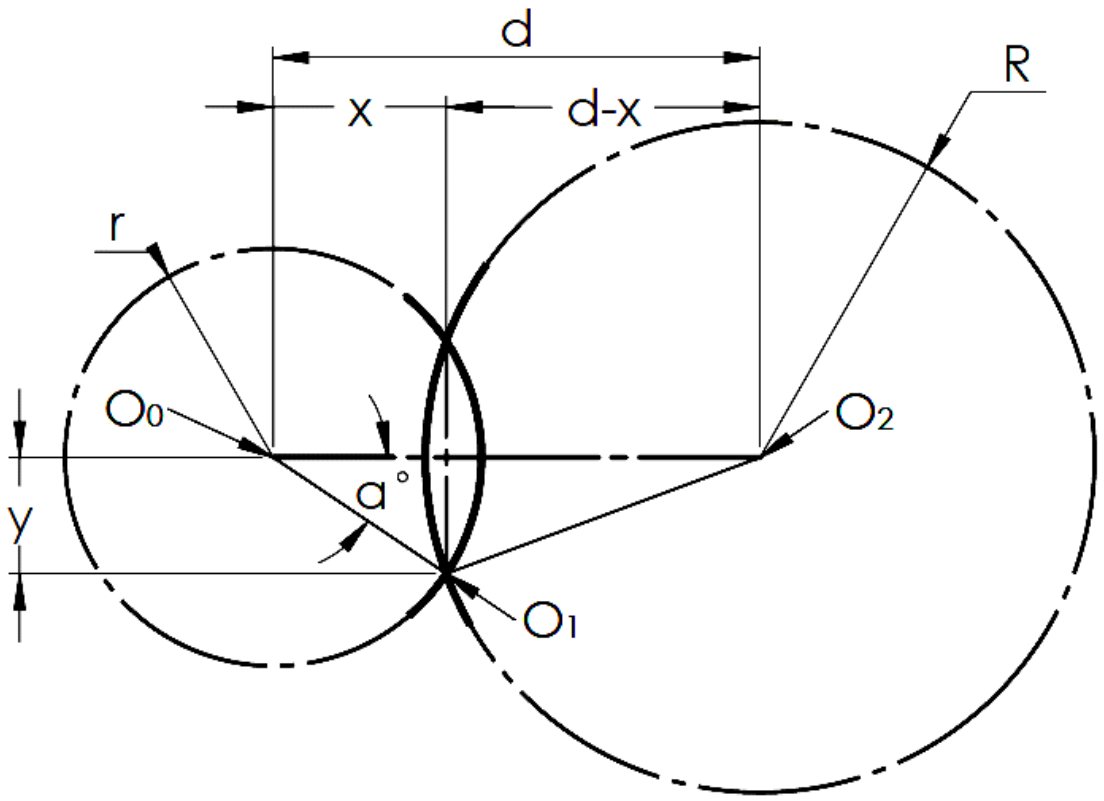

Figure 23: Roll axis geometric simplification for forward kinematics.

$$(x-d)^2 + (r^2 - x^2) = R^2 \tag{20}$$

which is then solved for x,

$$x = \frac{d^2 - R^2 + r^2}{2d} \tag{21}$$

and angle $a°$ is then calculated as

$$a° = \cos^{-1}\left(\frac{x}{r}\right) \tag{22}$$

The reference frame of Figure 23 is then rotated to account for the offset in frames and added to angle $a°$. The difference is because segment (d) does not line up with the ankle coordinate system and, as a result, nether will $a°$. This offset is the angle between the vertical Z axis and the line intersecting points O0

and O2 (see Figure 22 Isometric View).

Pitch Axis

For the Pitch Axis, the geometry of the ankle mechanism simplifies to an intersection of two spheres and reduces to the intersection of two circles (see Figure 24). The radius of the circle is the distance between the centers of the ankle u joint O_0 and the Pitch actuator ball joint O_3 (see Figure 22). The sphere geometry is defined by the length of the Pitch actuator segment A (see Figure 22).

Solving for the resulting circle that is the byproduct of two spheres intersecting can be described using 3D versions of equations (18) and (19),

$$x^2 + y^2 + z^2 = R^2 \tag{23}$$

$$(x - d)^2 + y^2 + z^2 = r^2 \tag{24}$$

Canceling common factors $y^2 + z^2$ yields equation

$$(x - d)^2 + (R^2 - x^2) = r^2 \tag{25}$$

Solving for X gives

$$x = \frac{d^2 - r^2 + R^2}{2d} \tag{26}$$

Plugging (26) into (24) results in an equation describing the intersection circle (see (b) Figure 24) of the two spheres:

$$\left(\frac{d^2 - r^2 + R^2}{2d}\right)^2 + y^2 + z^2 = R^2 \tag{27}$$

which is a circle with radius

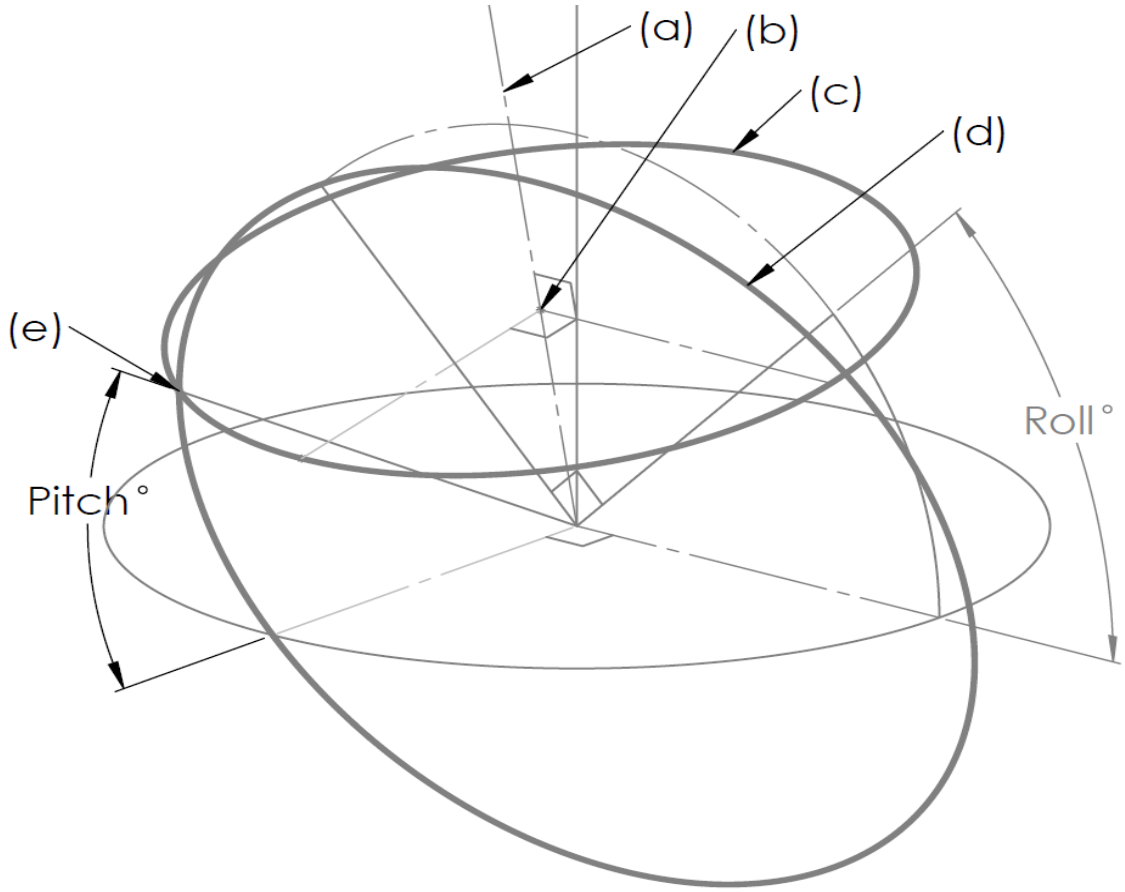

Figure 24: Geometric representation of the ankle joint. (a) vector between the centers of two spheres, (b) center of the resulting circle of the intersection, (c) intersection circle of two spheres, (d) Pitch circle, (e) intersection point between Pitch circle and sphere intersection circle and is the location of the Pitch ball joint.

$$a = \frac{1}{2d}\sqrt{4d^2R^2 - (d^2 - r^2 + R^2)^2} \tag{28}$$

Writing this circle as a parametric equation gives:

$$x = -a \cdot \sin(\rho) \cdot \cos(\gamma) + X_{offset} \tag{29}$$

$$y = a \cdot \sin(\gamma) \tag{30}$$

$$z = -a \cdot \cos(\rho) \cdot \cos(\gamma) + Z_{offset} \tag{31}$$

where ρ aligns the vector between the two spheres with the ankle coordinate frame and γ defines any point on the circle. This circle is the first constraint and

is one of two circles used to solve the forward kinematics of the Pitch actuator. The next circle describes the possible position of the Pitch ball joint, which is a function of the Roll angle β (see Figure 25). Like γ, θ defines any point on the circle, the location of the Pitch ball joint O_3.

$$x = r * \sin(\theta) \tag{32}$$

$$y = r * \sin(\beta) * \cos(\theta) \tag{33}$$

$$z = r * \cos(\beta) * \cos(\theta) \tag{34}$$

Equating (30) with (33) we can solve for γ:

$$\gamma = \sin^{-1}\left(\frac{r \cdot \cos(\theta) \cdot \sin(\beta)}{a}\right) \tag{35}$$

Substituting (35) into (29) and setting equal to (32), we can solve for the Pitch angle θ:

$$\theta = \sin^{-1}\left(\frac{X_{offset} + \#1}{r - r \cdot \sin(\beta)^2 \cdot \sin(\rho)^2}\right) \tag{36}$$

$$\begin{aligned}\#1 = \sin(\rho)(a^2 - a^2 \sin(\rho)^2 \sin(\rho)^2 + r^2 \sin(\beta)^4 \sin(\rho)^2 - r^2 \sin(\beta)^2 \\ + X_{offset}^2 \sin(\beta)^2\ )^{1/2}\end{aligned} \tag{37}$$

The forward kinematics of the ankle are used to calculate ankle orientation based on actuator length. This is important for calculating ankle stiffness that is a function of desired orientation and actual orientation. Also, the mapping between actuator length and ankle orientation, along with motor torque and ankle moment, is nonlinear and is a function of the ankle orientation. With the forward kinematics, the nonlinear ankle mechanism can be accurately modeled and controlled with the help of feedforward terms.

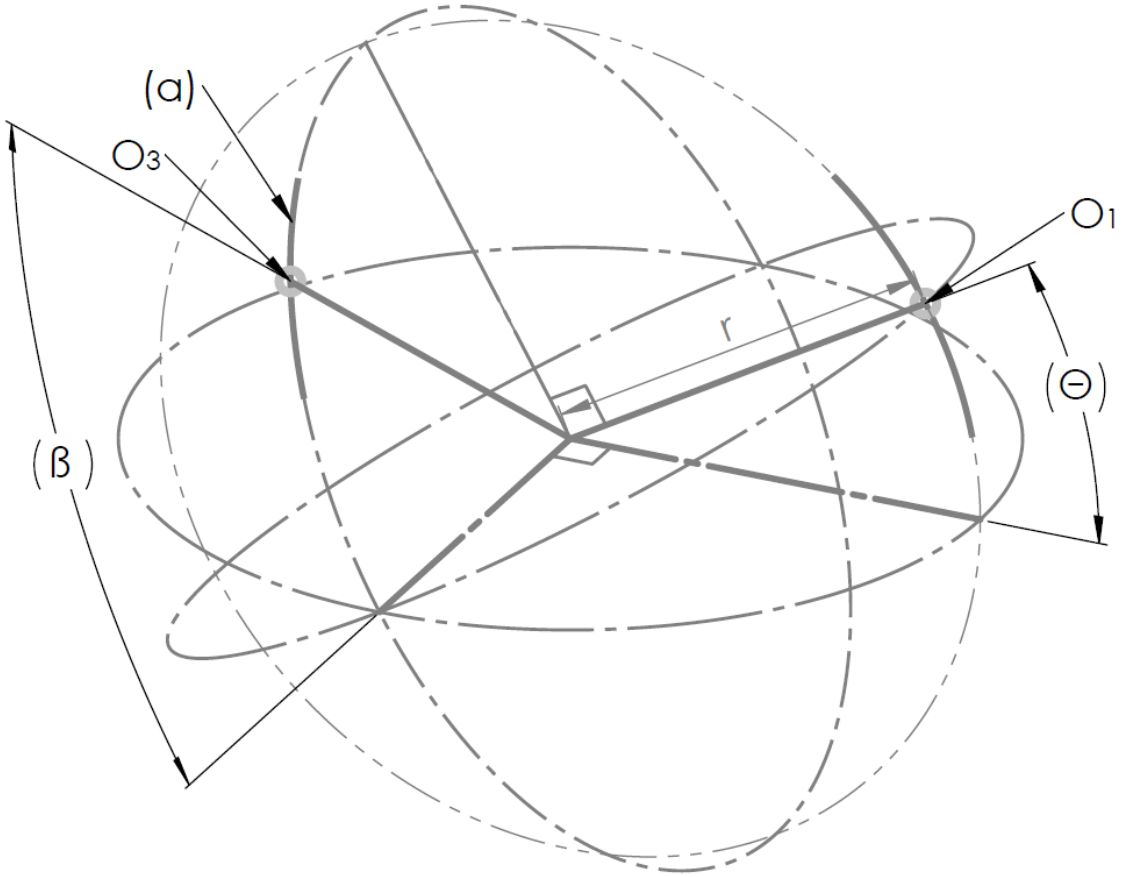

Figure 25: Geometric relationship of Pitch axis with Roll angle. 0_1 is the Roll ball joint location, 0_3 is the Pitch ball joint location, θ is the Roll angle, β is the Pitch angle, and line segment (a) is the path that the Pitch ball joint moves through based on the Roll angle.

Jacobian Formulation

The robot Jacobian relates joint positions to the linear and angular positions of the end-effector. In the case of the AFS robot, this process is fairly straightforward, as all but one of the axes are decoupled. Equation (38) is the Jacobian used for the AFS

$$\begin{bmatrix} Pos_X \\ Pos_Y \\ Pos_Z \\ \theta_{Roll} \\ \theta_{Pitch} \\ \theta_{Yaw} \end{bmatrix} = \begin{bmatrix} \pi D_p/(1000*20) & 0 & 0 & 0 & 0 & 0 \\ 0 & P_Y/2000 & 0 & 0 & 0 & 0 \\ 0 & 0 & P_Z/2000 & 0 & 0 & 0 \\ 0 & 0 & 0 & \#2 & 0 & 0 \\ 0 & 0 & 0 & (\#3 &) & 0 \\ 0 & 0 & 0 & 0 & 0 & 2\pi/(2000*10) \end{bmatrix} \cdot \begin{bmatrix} q_X \\ q_Y \\ q_Z \\ q_{Roll} \\ q_{Pitch} \\ q_{Yaw} \end{bmatrix} \quad (38)$$

where $Pos_{X,Y,Z}$ are the Cartesian coordinates of the end-effector, $\theta_{Roll,Pitch,Yaw}$ are the orientation of the end-effector, $q_{X,Y,Z,Roll,Pitch,Yaw}$ are the joint encoder counts, Dp is the X axis pulley diameter [m], Py is the Pitch of the Y axis ball screw [m], Pz is the Pitch of the Z axis ball screw [m]. #2 is Equation (39),

$$\#2 = sin^{-1}\left(d - \frac{\left(\frac{d^2 - r^2 + \left(R - q_{Roll} \cdot \frac{0.19685}{2000}\right)^2}{2d} \right)}{r} \right) - offset \quad (39)$$

where *d* is the distance between the centers of the u joint and the pivot of the Roll actuator [m], *R* is the zero-angle length of the actuator [m], *r* is the length between the center of the u joint to the Roll heim joint [m], and the *offset* is to correct for the difference in coordinate frames of reference [rad]. This offset is the angle between the vertical Z axis and the vector between points O0 and O4, see Figure 22 Isometric View. Pitch angle (#3) in equation (39) is calculated using equations (36) and (37) and is a function of both the Pitch and Roll actuator lengths (Figure 22 feature A and B, respectively).

CHAPTER VII

EVALUATION

The goal of the AFS robot is to reproduce gait data at a physiologically correct speed in a repeatable manner while also balancing response to uneven terrain in a fashion similar to a human ankle. These gait data include ankle/foot trajectory, ground reaction forces, and internal ankle moments. In order to consider the AFS project a success, adequate performance must be documented in four areas:

1. Motion Tracking: This test will determine how well the AFS robot can track a trajectory.
2. Force and Moment: This test will determine the performance of the Force controller given step inputs.
3. Combined Force and Trajectory: This test will determine how well the AFS robot can reproduce ground reaction forces during gait that is run at anatomically correct speeds and forces.
4. Passive Ankle Stiffness: This test will determine the response and performance of the passive ankle stiffness model.

Methods and Procedures

First, Motion Tracking and repeatability is tested by having the AFS run full-speed gait profiles without the end effector contacting the environment. The position of the end effector is measured using high-density encoders on the motors of the AFS robot (38). Position and orientation tracking errors between the desired trajectory and the resultant trajectory are calculated using forward kinematics with motor encoder counts as the input and positon and orientation as the output. The maximum error from the desired trajectory and the r^2 value is used to determine accuracy of the robot. Standard deviation of error from the mean, and Root Mean Square Error (RMSE) are used to determine repeatability.

Second, Force and Moment step response tests were conducted to determine the force controller's performance. This test used Faded Glory Men's Canvas Lace Oxford Casual Shoe, size 11, from Walmart (Figure 26). The shoe was positioned just above the force plate before a step input was given. All tests where accompanied with a force in the Z direction. The metrics used to quantitatively assess the controller's performance are percent overshoot and rise time. Settling time was not chosen as a performance metric because the robot trajectory is dynamic.

Third, combined position and force tests were performed at anatomically correct speeds and GRFs. Position and force tracking error were measured. The same PD and PI gains used in the previous tests were used for this test. This test was performed with the same shoe and foot used in the other force test. A total of five runs were performed to determine the repeatability and variability in

Figure 26: Test set up with shoe.

the AFS controller. The maximum error, r^2, RMSE, and mean standard deviation are calculated to determine performance.

Fourth, the passive ankle stiffness controller is tested to determine how well it matches literature data. Passive ankle stiffness was tested by placing the foot and shoe on an uneven surface and loaded in the Z direction. Ankle moments along with ankle Roll angle were measured. The combination of the two determine the performance of the passive ankle stiffness controller and model.

Motion Tracking

Anatomically correct speed tests were performed to determine how well the AFS robot tracks a given trajectory, and the repeatability of the resulting trajectory. A data set of 10 runs was used in this evaluation. Deviation of the X

axis with respect to the mean trajectory of all 10 runs can be seen in Figure 27. The X axis deviates from the mean a maximum of 1 mm. The standard deviation from the mean trajectory can be seen in Figure 28 and shows a maximum standard deviation of +- 0.4 mm. These results show that the X axis has a 95% confidence interval of 0.25 mm. Results for all axes are in Table 4.

To determine how well the robot tracks a trajectory, the r^2 was calculated between the desired trajectory and the mean of all 10 runs. The results are tabulated in Table 4. The only axis that shows any performance issues is the Yaw axis and possibly the Y axis. When designing the Yaw axis, the dynamics of both the X and Y axis were not taken into consideration. This causes the Yaw axis to experience moments from the off-axis center of mass that were not

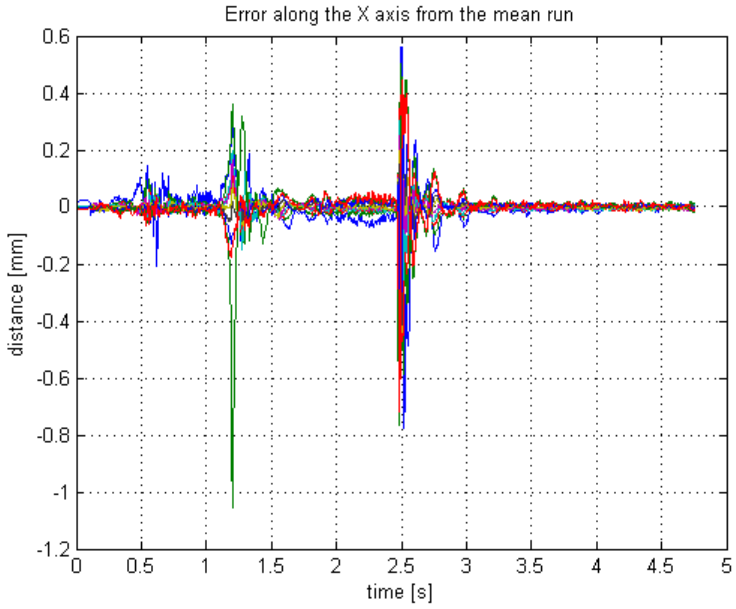

Figure 27: X axis error from the mean.

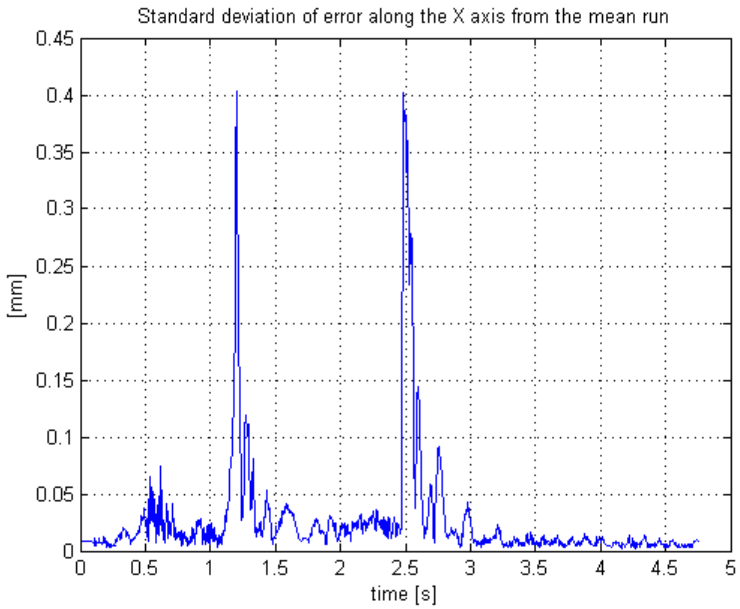

Figure 28: X axis standard deviation from the mean.

Table 4: Motion tracking and repeatability results.

Axis	RMSE	mean STDev [mm][deg]	r^2	max mean error [mm][deg]
X	4.81E-05	0.0262	0.999986	5.48
Y	6.27E-05	0.0279	0.991704	3.73
Z	5.04E-05	0.0492	0.999995	2.17
Pitch	0.0038	0.0037	0.999901	2.22
Roll	0.0024	0.0027	0.999936	0.39
Yaw	0.0311	0.0232	0.800669	5.56

planned for in the control. The current draw of the Yaw axis, as seen in Figure 18 (f), only reaches 80% of the maximum for the axis. This indicates that a more accurate feedforward dynamic model of the axis or increased PD gains will improve performance.

Another problem seen during the motion tracking test is drive-current saturation for the Y axis. As seen in Figure 29, the motor is oversaturated during part of the trajectory and thus is unable to keep up with the trajectory. The majority of the tracking error in the Y axis is from this current saturation, as seen

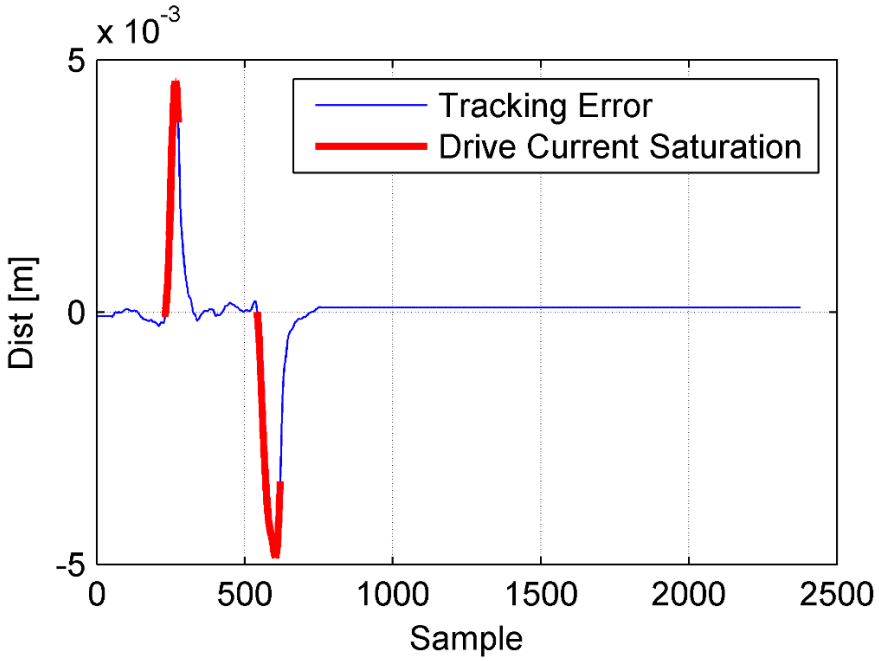

Figure 29: Y axis error and drive over saturation indicated in red.

in the figure. When the drive's current is saturated, the error increases exponentially until the dynamics of the trajectory slow down enough to allow the drive to catch up.

To determine the repeatability, Root Mean Square Error (RMSE) was calculated using the error of individual runs with respect to the mean resulting trajectory. Or in other words, how much any single run deviated from the mean resulting trajectory. The mean of the RMSE values was taken of all 10 runs and tabulated in Table 4. Standard deviations were also calculated with respect to the mean resulting trajectory and are found in Figure 30. It is noteworthy that a PD controller with feedforward-computed torque was used. Introducing an integrator would reduce steady state error. However, as the trajectory is dynamic, the integrator was deemed unnecessary and would cause problems when switching states from calibrating to system control.

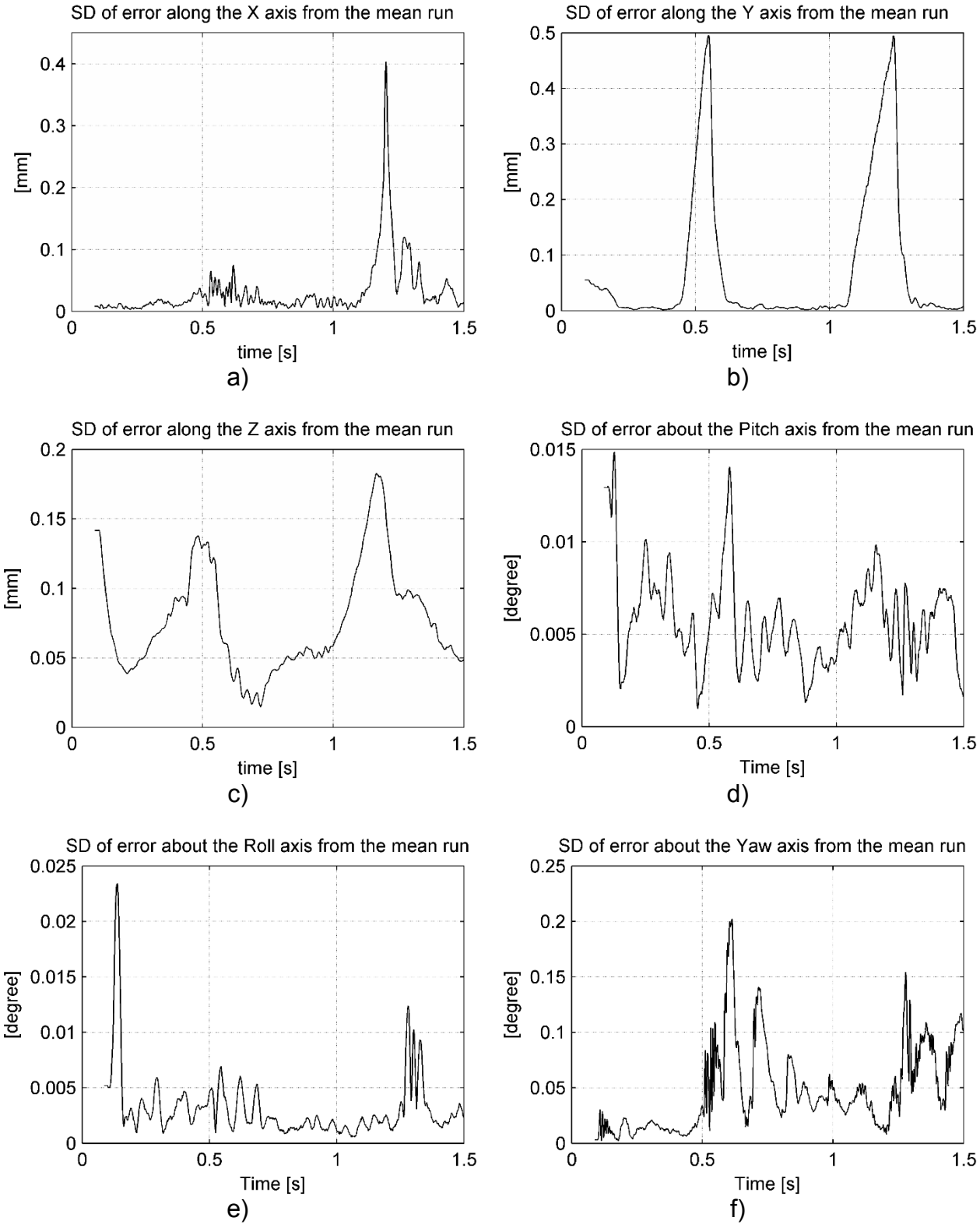

Figure 30: Position tracking standard deviation from the mean. X axis (a), Y axis (b), Z axis (c), Pitch axis (d), Roll axis (e), and Yaw axis (f).

Force and Moment Controller Performance

The performance of the AFS's force control loop shown in Figure 16 can be seen in Figure 31, where the individual axes were given a force/moment step input. The magnitude of the step input is equal to the maximum force/moment seen in the gait data. The desired performance of the force/moment controller is less than 10% overshoot and a settling time of less than 0.2 seconds. Tabulated results of the step response of the force controller can be found in Table 5. The step response of the force controller performs adequately with fast rise time and minimal to no overshoot.

The performance of the force controller following reference GRF can be seen in Figure 32 and in Table 6. During this test, the reference position of each individual axis was held constant. For all but the Z axis the system was preloaded along the Z axis to eliminate slipping of the shoe against the force plate.

Combined Force and Trajectory Response

Results from the anatomically correct speed and force tests can be seen in Table 7 and Figure 33. The AFS robot is able to generate ground reaction forces comparable to those seen in healthy gait, but performance is lacking when compared to the standards presented earlier. The Z, Pitch, and Roll axes have a r^2 value of greater than 0.8, indicating good tracking while X, Y, and Yaw have values of less than 0.3, indicating poor tracking. Possible explanations of the decrease in performance may be due to coupling between axes that effect the

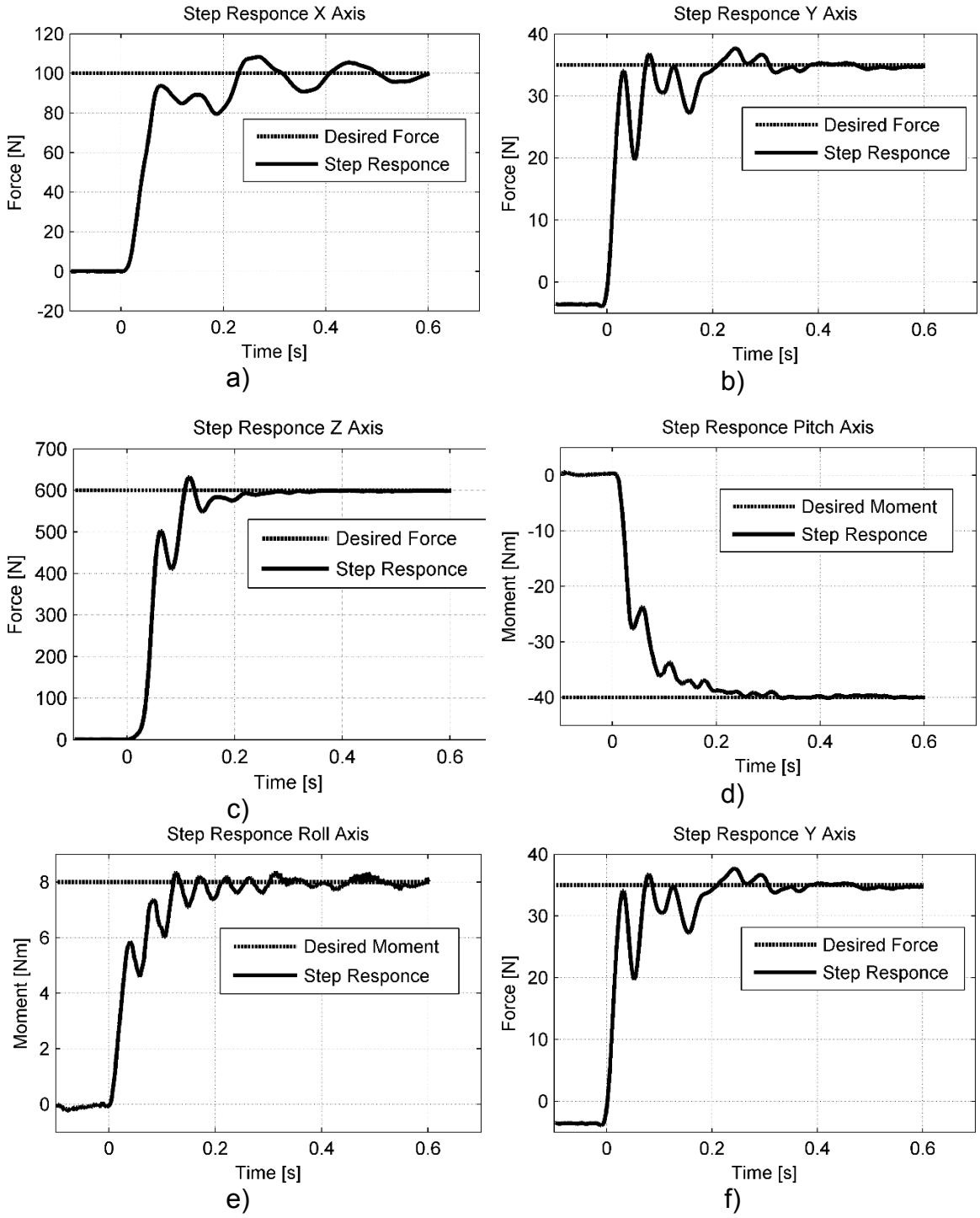

Figure 31: Force and moment step response of the AFS robot. X axis (a), Y axis (b), Z axis (c), Pitch axis (d), Roll axis (e), and Yaw axis (f).

Table 5: Force and moment step response results.

Axis	Rise time [s]	% Overshoot	Settling time [s]
X	0.0424	8.3	0.21
Y	0.0369	7.1	0.18
Z	0.0424	5.5	0.15
Pitch	0.024	0.0	0.12
Roll	0.0258	3.8	0.15
Yaw	0.0406	3.6	0.13

same force or moment. One example is the X and Pitch axis. During toe off the Pitch axis is responsible for generating a negative force in the X axis. As seen in Figure 32 (a) and (d) indicate that the Pitch axis is generating sufficient moment. One possible cause of this is having a passive forefoot or having the forefoot and midfoot joint in the wrong location.

Altered trajectory due to force loop compensation can be seen in Figure 34. The change in the desired trajectory comes from the force controller overriding the trajectory to achieve the desired force.

Passive Ankle Stiffness Response

The testing of the ankle stiffness controller discussed in equation (16) of Chapter 5 is composed of a desired Roll moment of 0.01 Nm. In the presence of an obstacle, the ankle will roll over to achieve the desired moment. The rollover angle is multiplied by an ankle stiffness K and added to the desired moment. Results of this test can be seen in Figure 35. This figure shows the result of two tests. The first test is with an ankle stiffness value of K = 0 [Nm/deg] and a desired ankle Roll angle of zero. In this test, the

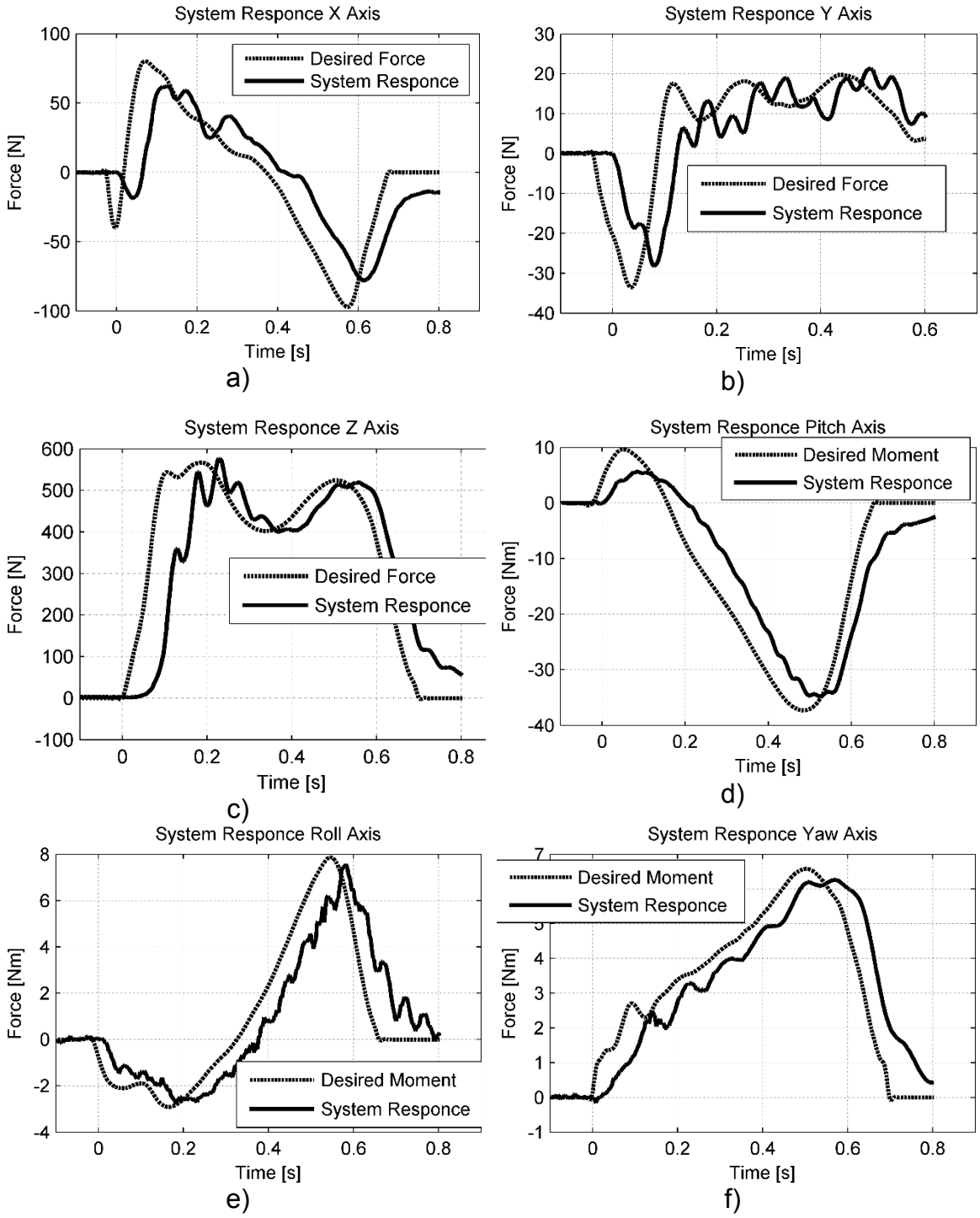

Figure 32: Force and moment GRF system response of the AFS robot. X axis (a), Y axis (b), Z axis (c), Pitch axis (d), Roll axis, (e) and Yaw axis (f).

Table 6: Force and moment GRF tracking of the AFS.

Axis	r^2	Max Error	% Max Error
X [N]	0.6155	86.3	88.7
Y [N]	0.4651	31.6	94.0
Z [N]	0.4444	439.8	77.6
Pitch [Nm]	0.8368	11.2	30.0
Roll [Nm]	0.8143	3.8	49.0
Yaw [Nm]	0.7201	2.5	37.6

Table 7: Performance and repeatability of the force controller

Axis	RMSE	Mean STDev	r^2	Max Error
X [N]	1.52	1.59	0.001	200
Y [N]	0.798	1.17	0.0153	120
Z [N]	1.56	2.28	0.9384	284
Pitch [Nm]	0.118	0.099	0.8216	17
Roll [Nm]	0.105	0.135	0.8691	3
Yaw [Nm]	0.0865	0.094	0.2945	12

force/moment controller tries to achieve the desired ankle Roll moment of 0.01 Nm and in turn modifies the ankle's Roll angle to approximately 15 degrees. The second test is with an ankle stiffness value of K = 0.525 [Nm/deg] and a desired ankle Roll angle of zero. In this test, when the force/moment controller modifies the ankle's Roll angle, it also modifies the desired moment using K. As seen in Figure 35, the resulting ankle Roll angle is 5 degrees and the desired moment is 2.5 Nm. The results of the passive ankle stiffness controller are great. The AFS robot is able to change ankle stiffness based on a perturbed ankle orientation. The perturbed ankle orientation may come from uneven terrain (Figure 36) or from the smart shoe. This is only implemented in the Roll axis but could easily be applied to the Pitch axis.

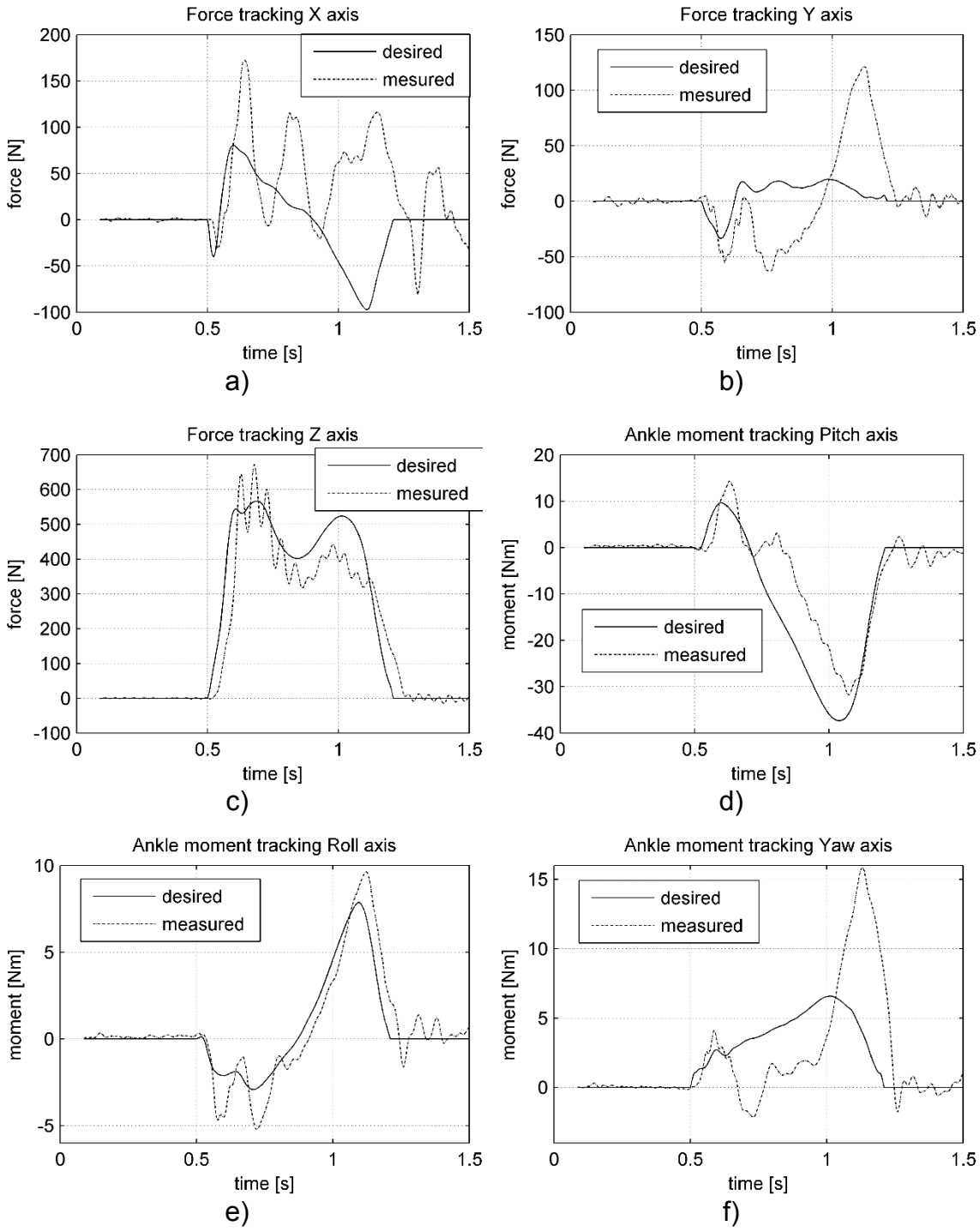

Figure 33: Force and moment tracking of the AFS robot during anatomically correct speeds and GRFs. X axis (a), Y axis (b), Z axis (c), Pitch axis (d), Roll axis (e), and Yaw axis (f).

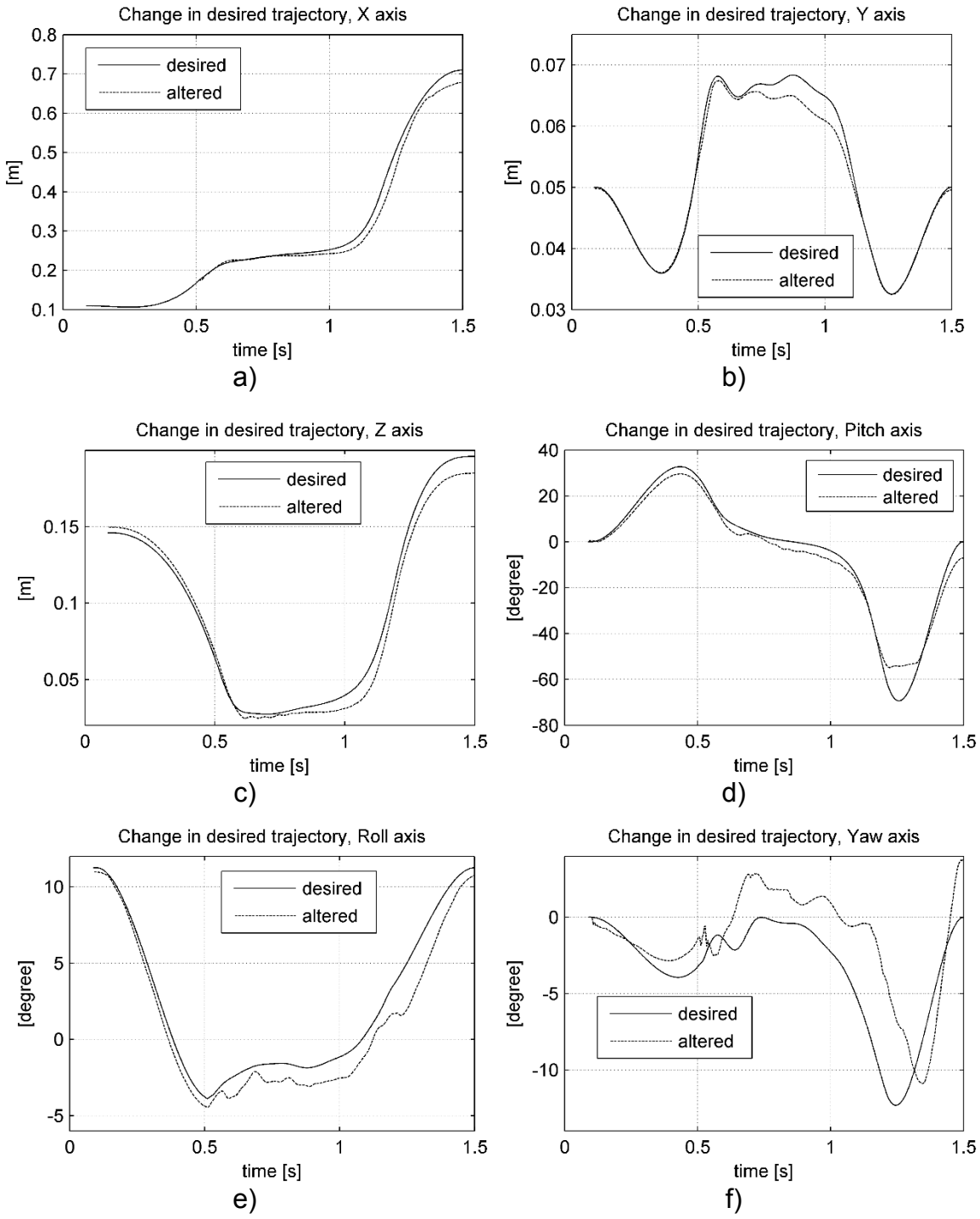

Figure 34: Altered trajectory due to force controller. X axis (a), Y axis (b), Z axis (c), Pitch axis (d), Roll axis (e), and Yaw axis (f).

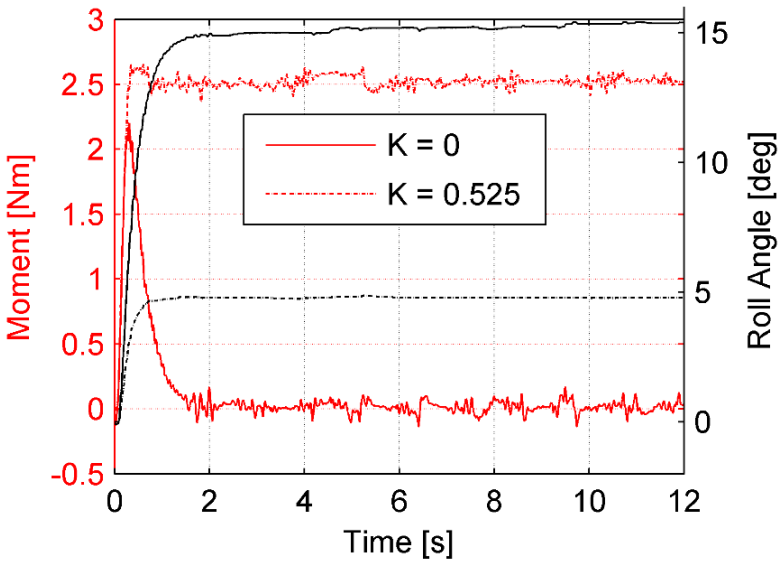

Figure 35: Passive ankle stiffness response K=[Nm/deg].

Figure 36: Ankle stiffness test setup.

CHAPTER VIII

CONCLUSION

The purpose of this project was to develop a robot that can replicate human gait. The AFS has demonstrated that it can replicate human gait, along with tracking a prescribed trajectory to within 5.5 mm and demonstrates passive ankle dynamics when evaluating ankle stiffness and ankle rollover events.

Challenges of this research ranged from designing the robotic mechanism with sufficient load capacity to recreate human gait, to kinematic analysis of the robotic mechanism to control the robot. Normal walking gait trajectories were captured in a motion capture lab along with ground reaction forces. From this data set, the number of Degrees of Freedom (DOF) and their placement were determined.

Designing an ankle mechanism that has room for a load cell to be placed between the ankle and the bottom of the foot, provides sufficient load bearing capacity, is actuated, and has the ROM needed to reproduce gait was challenging. To solve the load cell design space problem, a load cell that had sufficient load capacity was chosen. The ankle was built around the load cell, and care was taken to ensure that it had sufficient ROM to reproduce gait trajectories. The final design consists of a universal joint with linear actuators

acting orthogonal from one another for orientation. Designing a drive train that produces the velocities and forces seen in the gait data was challenging. The process of impedance matching a motor and gear box combination to the inertia of a specific axis is very iterative.

The ankle design chosen introduced its own challenges when trying to control it. The AFS robot cannot be controlled by an examination of the DH parameters alone, but by an in-depth study of the mechanical kinematics of the ankle mechanism. The line of action of the actuators that orient the ankle mechanism changes depending on the orientation. The changes in actuator line of action is taken into consideration for the forward and inverse kinematics, is as mapping actuator force to ankle moments in the feedforward loop of the robot controller. The inverse kinematics for the AFS ankle mechanism is solved by defining the plain that both the ball joints and center of the ankle lie on. Once the points are defined, trigonometry is used to calculate the lengths of the linear actuators to produce the desired orientation. The forward kinematics of the AFS ankle mechanism is solved for in two parts. First the roll angle is solved for by finding the intersecting points of two circles. The pitch angle is solved for by calculating the intersecting circle of two spheres. This circle is used in connection with a circle in a plane that is constrained by the roll angle. The intersection of the two circles is the location of the point of action of the pitch linear actuator.

Safety around the AFS robot is paramount, and many steps have been taken to ensure the safety of those using the robot and the robot itself. Limit switches are used in the gantry system to first calibrate the system and also to shut down

the system if the switches are hit after calibration is done. Also a velocity limit check is used in case of a runaway situation, and will shut down if violated.

Control of the robot consists of an admittance position and force control loops. The force loop alters the desired position that is used in the position tracking loop till the desired force is achieved. To achieve natural ankle response during perturbations, a passive ankle stiffness model was used. One shortcoming of using a passive ankle stiffness model is that it does not reflect the ankle stiffness during walking or in the event of a perturbation.

The AFS is able to generate forces equal to those seen in healthy gait. The force controller performs adequately when tracking a step response and GRF profile in the absence of a desired position and orientation. When testing the combined force and position controller, less than desirable performance was seen. The X, Y, and Yaw axes have an r^2 value of less than 0.3 in achieving the desired forces, indicating poor tracking. While the Z, Pitch, and Roll axes have a r^2 value of greater than 0.8 in achieving the desired force. One possible cause for the poor performance may be due to the flexing of the frame during high-dynamic events. Ways to improve the controller and dynamic response of the AFS are discussed in the next section.

Future Work

Following testing, the Y axis experienced greater friction than anticipated. As a result, the Y axis did not achieve full dynamic motion. To address this problem, an amplifier and motor combination, similar to that used for the Pitch

and Roll axis, must be utilized.

The effect of the acceleration of the X and Y axes on the Yaw axis is significant. This effect is caused by the asymmetric design of the ankle, resulting in a center of mass that is located off the axis of rotation. This was not taken into consideration when choosing a motor and gearbox combination. To increase the performance of this axis, a high gear ratio is desired to minimize the reflected inertia of the ankle seen by the motor. Using impedance matching, a gear ratio of approximately 100 would optimize the system.

If rigidity becomes an issue, adding a second linear bearing on the Z axis will help, as this is where most of the deflection is seen.

Position and force test results for anatomically correct speeds and forces indicate that there is a discrepancy between the position data and the force data. This discrepancy may arise from differences between the subject's anatomical ankle, foot, and shoe size with the robot's ankle location, foot, and shoe size. The focus of future work should address this discrepancy. If the two systems matched up, the desired trajectory of the position loop would not be perturbed in any way by the force loop because the position loop would automatically generate the desired forces. This is not the case, so a refined position trajectory needs to be generated that will more readily generate the desired forces. An iterative learning controller would do this. It can be expected that the performance of the combined position and force tracking controller will look more like the results shown in Figure 32, instead of those seen in Figure 33, with the addition of the iterative learning controller to the existing admittance controller.

APPENDIX A

ANKLE TRAJECTORY, MOMENTS, AND GROUND REACTION FORCES DATA GATHERED USING MOTION CAPTURE

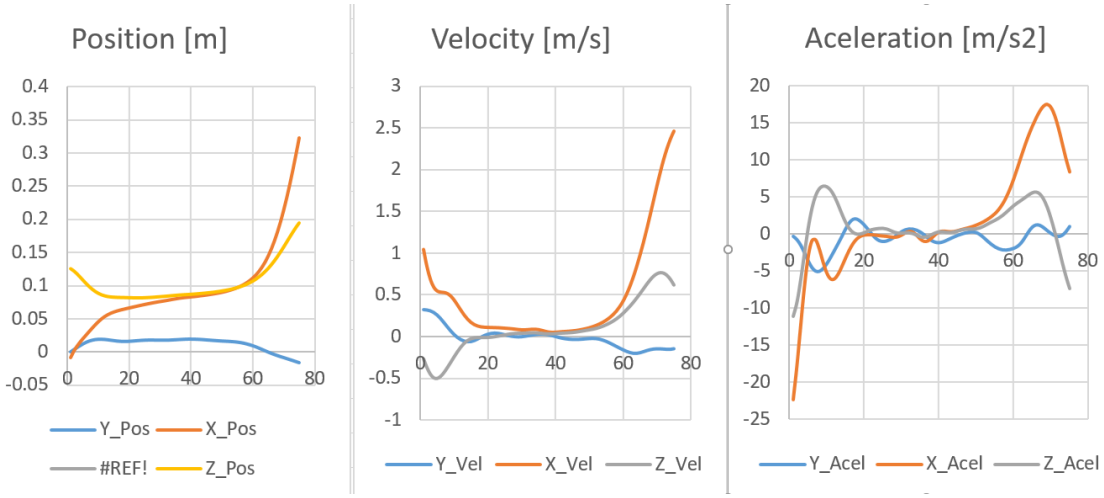

Figure 37: Cartesian coordinates of ankle position during contact phase of gait.

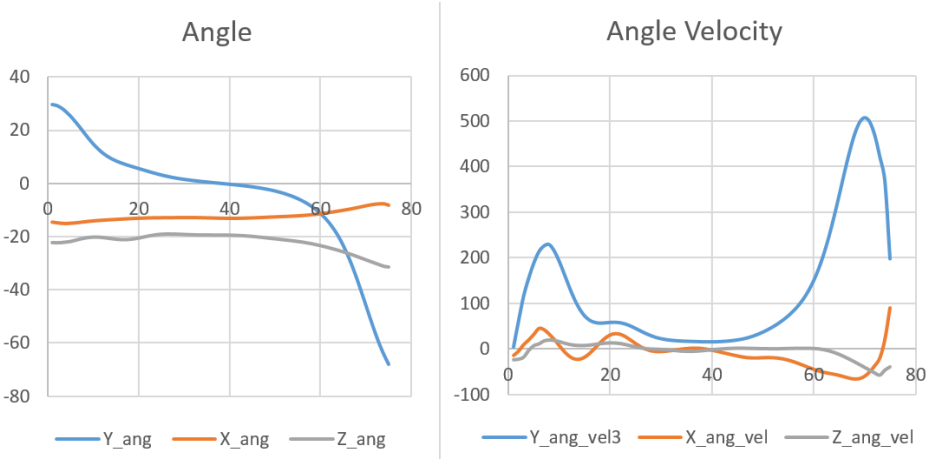

Figure 38: Ankle orientation with respect to the ground.

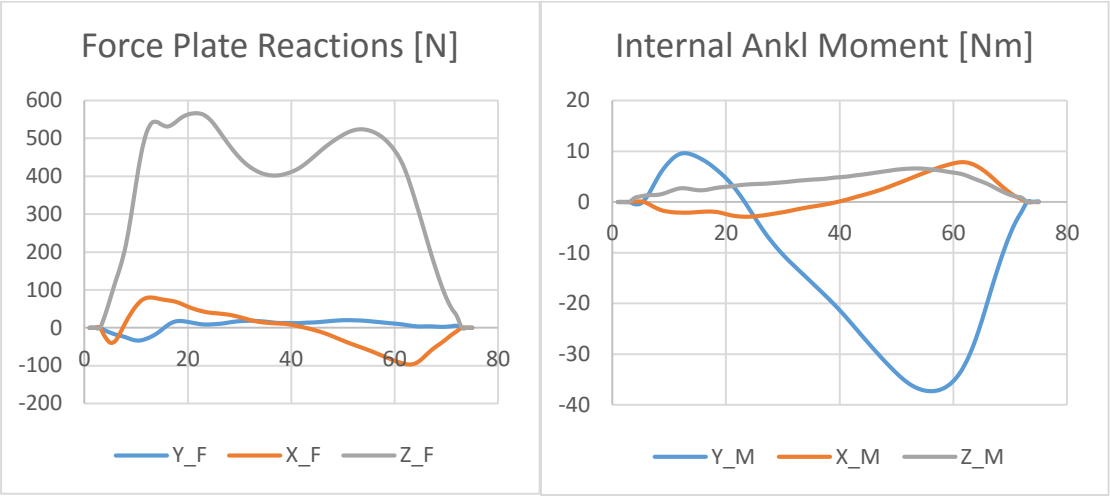

Figure 39: Ankle internal moments and GRFs.

Ankle Stiffness

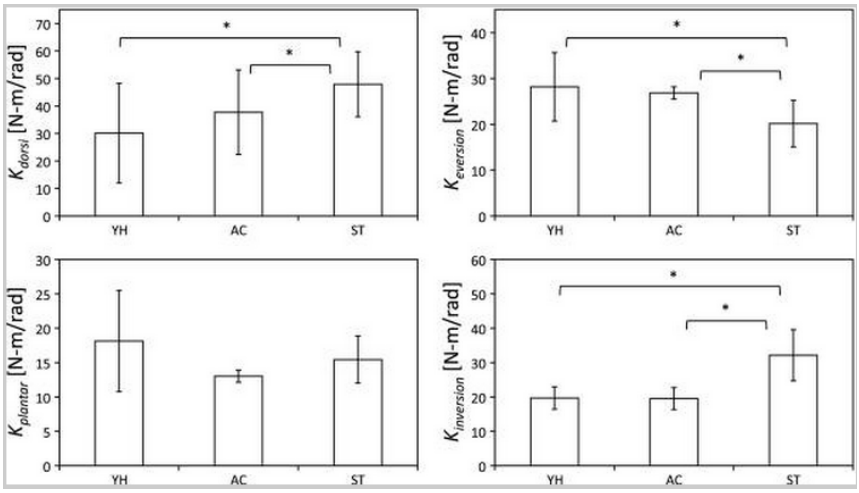

Figure 40: Passive ankle stiffness of YH, AC and ST. This figure and ankle stiffness data are from Roy [16].

Roll over
- Eversion = 0.525 Nm/deg
- Inversion = 0.35 Nm/deg

Pitch
- Dorsal = 0.525 Nm/deg
- Plantar = 0.35 Nm/deg
  - http://www.ncbi.nlm.nih.gov/pmc/articles/PMC3295205/

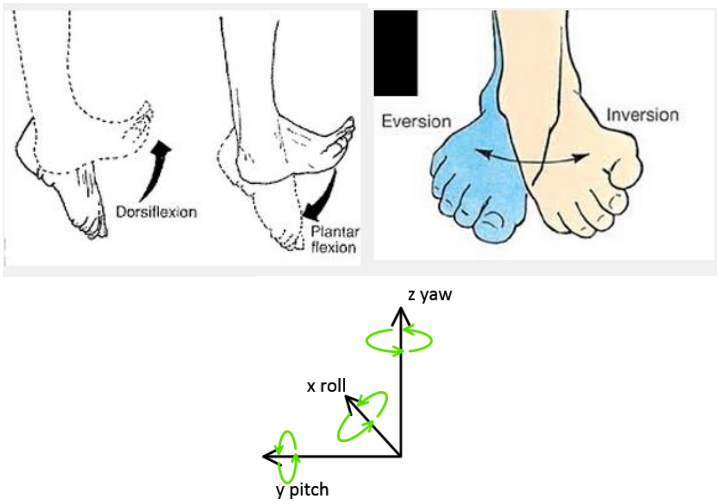

Figure 41: Nomenclature and coordinate reference.

Gantry: Linear Bearing Calculations

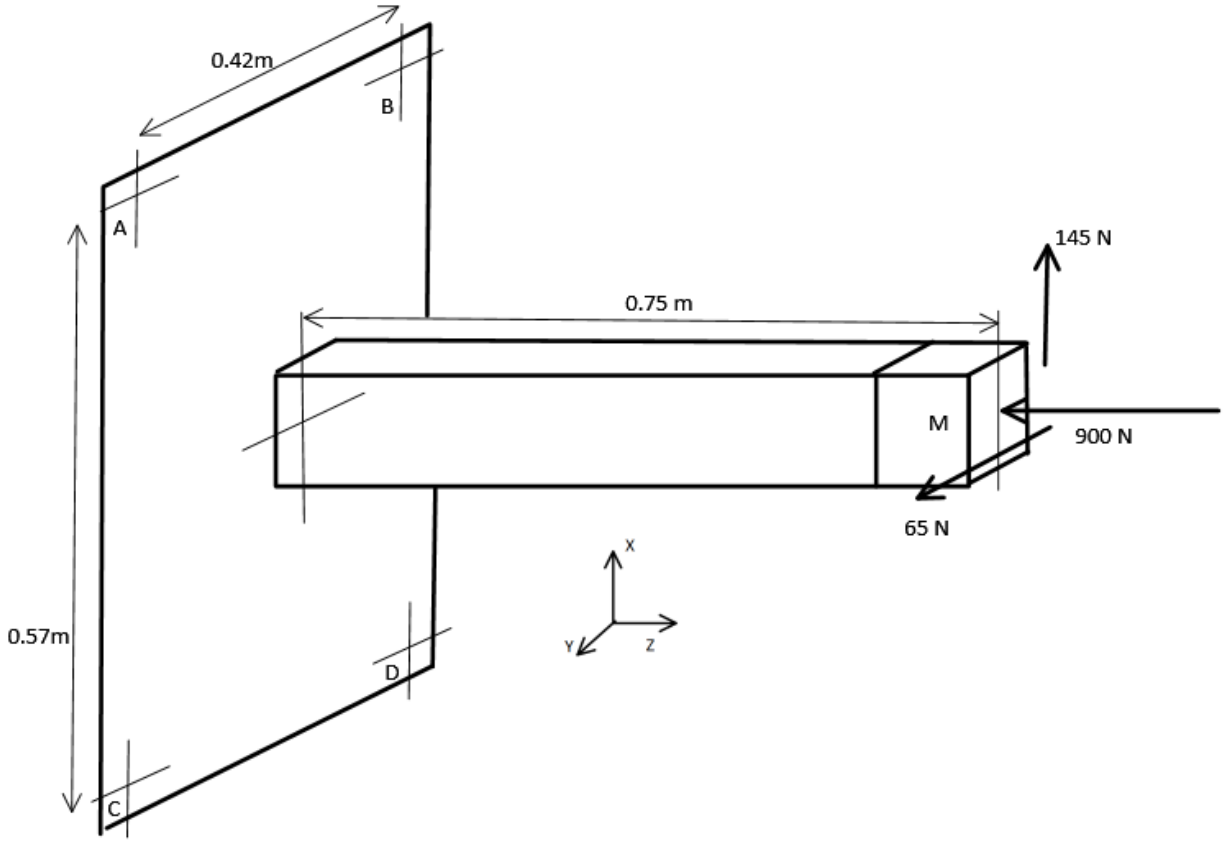

Figure 42:: Free body diagram of force calculations for linear bearings.

Table 7: Linear bearing calculation based on max GRFs.

Force N	Z	X	Y	Total
A	900/4	+ 145/4*(.75/.258)	+ 65/4*(.75/.21)	388 N
B	900/4	+ 145/4*(.75/.258)	- 65/4*(.75/.21)	272 N
C	900/4	- 145/4*(.75/.258)	+ 65/4*(.75/.21)	177 N
D	900/4	- 145/4*(.75/.258)	- 65/4*(.75/.21)	62 N

Motors Used for the AFS

Table 8: Motor model and manufacture for each axis.

Axis	Manufacture	Motor #
X	Aerotech	BM250
Y	Parker	BE232D
Z	Parker	BE343J
Pitch	Parker	BE232F
Roll	Parker	BE232F
Yaw	Parker	BE232D

Motor Specifications

Drives

The drives used on the AFS are from Copley Controls. The AFS's control computer is using a CAN BUS network setup to communicate with the drives using CME 2, a software package from Copley Controls. From CME 2 you can set up the drives (encoder counts, hall sensor commutation, motor specification, peak current), enable/disable the drives, troubleshoot any errors that may come up, and give current commands to each motor manually.

Drives used for each axis along with power rating are found in Table 10.

Table 9: Drive and amp ratting for each axis.

Axis	Drive #	Continuous/Peak Amp
X	XTL-230-40	20/40
Y	XSJ-230-06	3/6
Z	XTL-230-36	12/36
Pitch	XTL-230-36	12/36
Roll	XTL-230-36	12/36
Yaw	XSJ-230-06	3/6

Range of Motion

Table 10: ROM comparison between AFS ankle mechanism and normal gait.

	Normal Gait	AFS
Pitch	-28° to 56°	-35.6° to 58°
Roll	-2° to 5°	-30° to 24°
Yaw	-5° to 7°	-6° to 99°

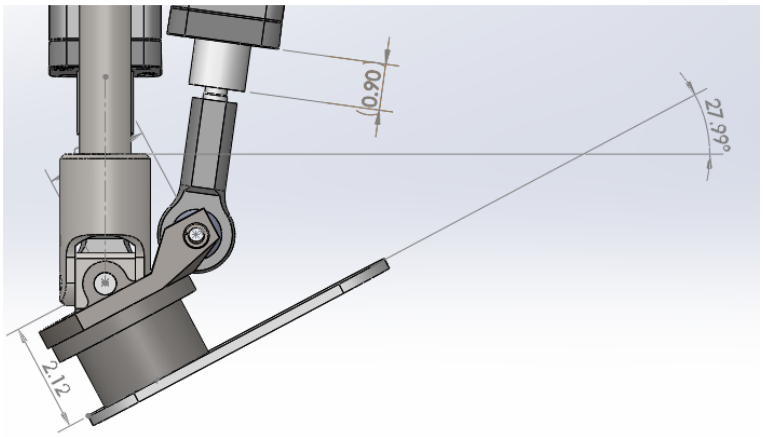

Figure 43:: Cad model of AFS ankle mechanism during heal strike.

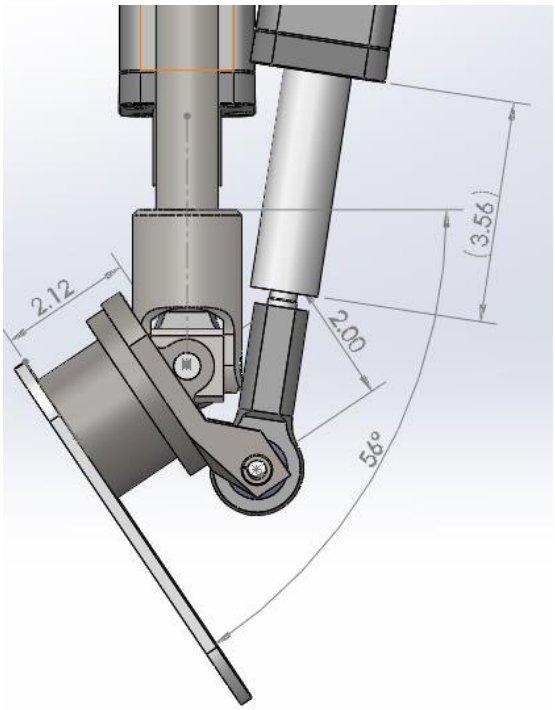

Figure 44:: Cad model of AFS ankle mechanism during toe off.

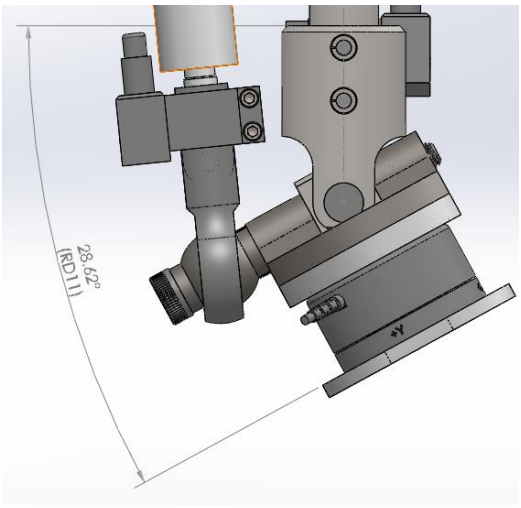

Figure 45:: Cad model of AFS ankle mechanism during rollover.

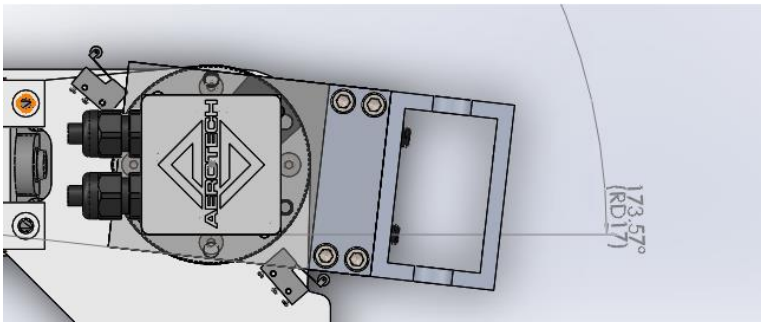

Figure 46:: Cad model of AFS ankle mechanism during extreme Yaw position.

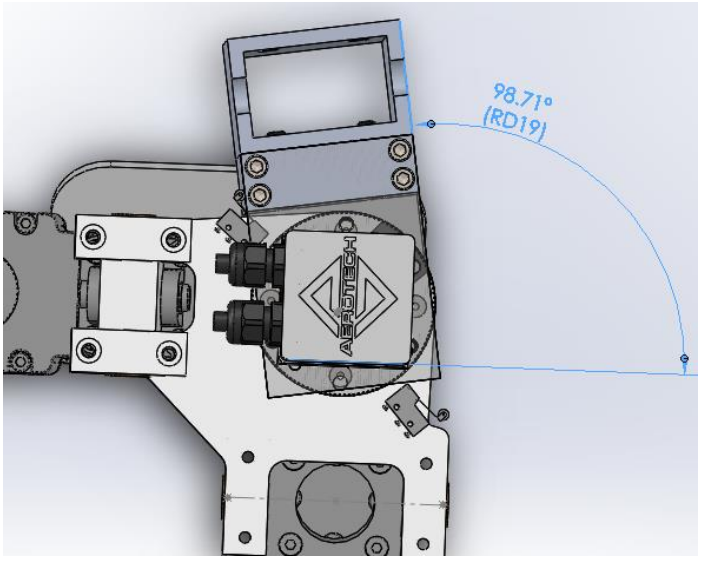

Figure 47:: Cad model of AFS ankle mechanism during extreme Yaw position.

APPENDIX B

TECHNICAL DRAWINGS

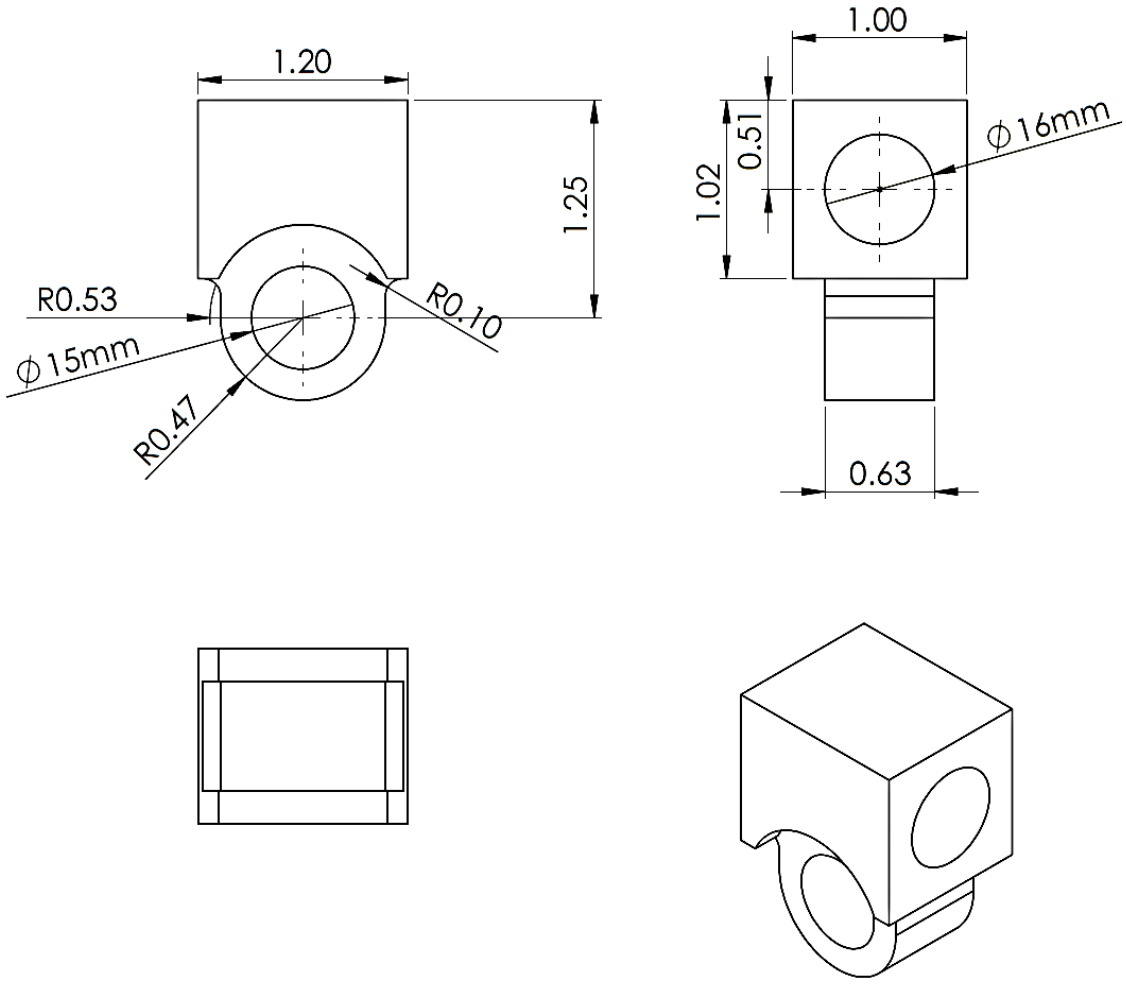

Figure 48:: Actuator mount.

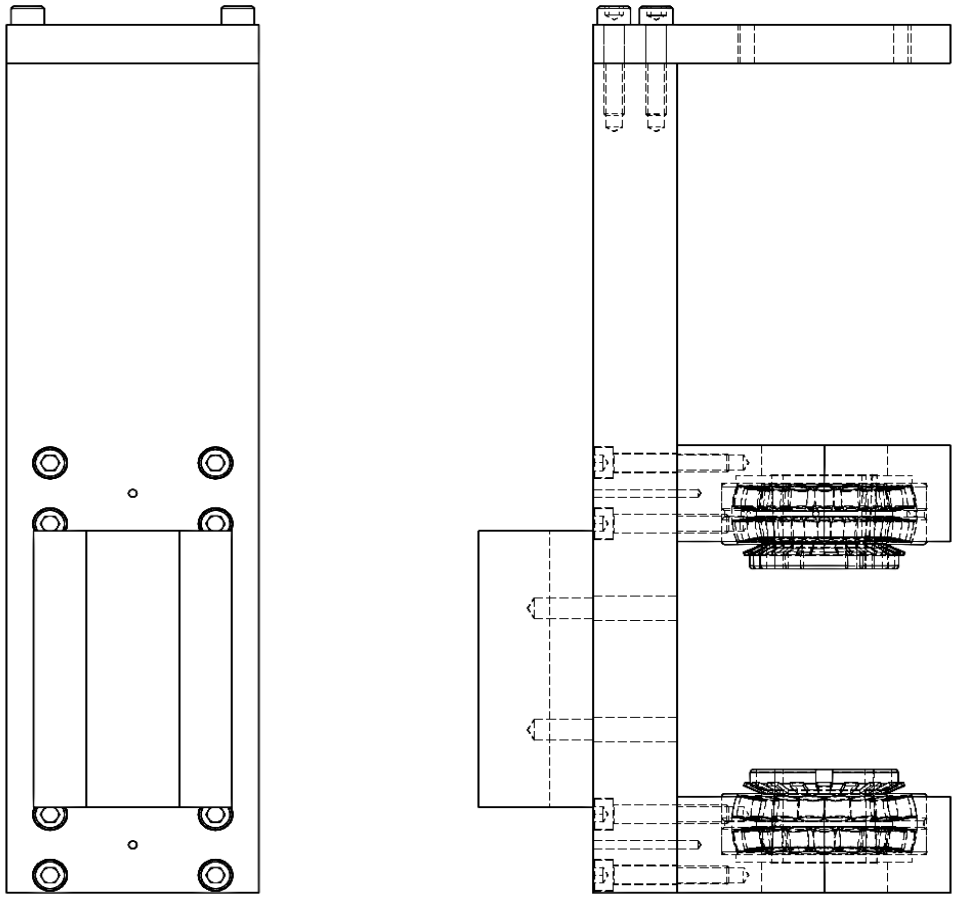

Figure 49:: Ankle mount and thrust bearing mount.

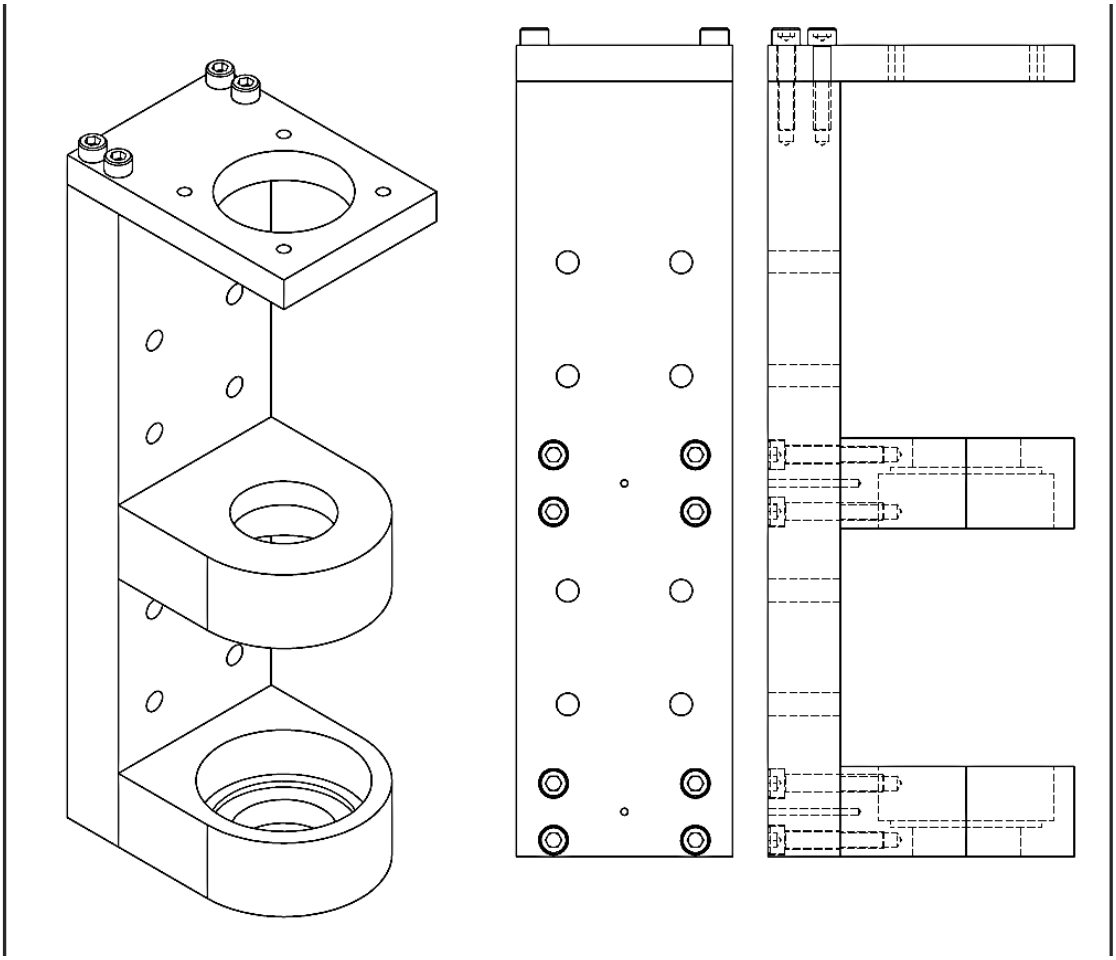

Figure 50:: Revised ankle mount.

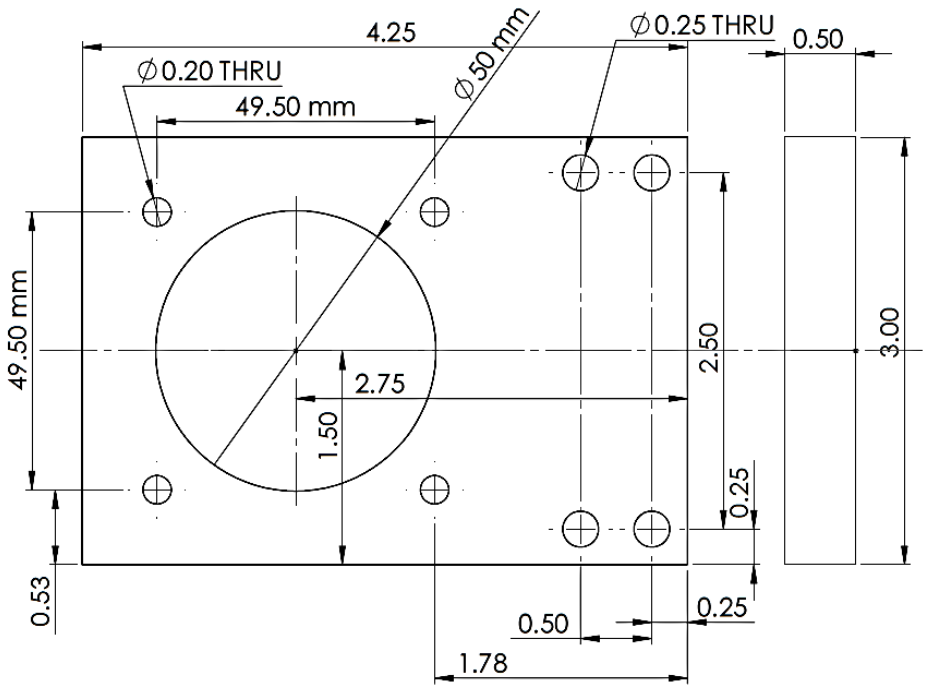

Figure 51:: Yaw motor mount.

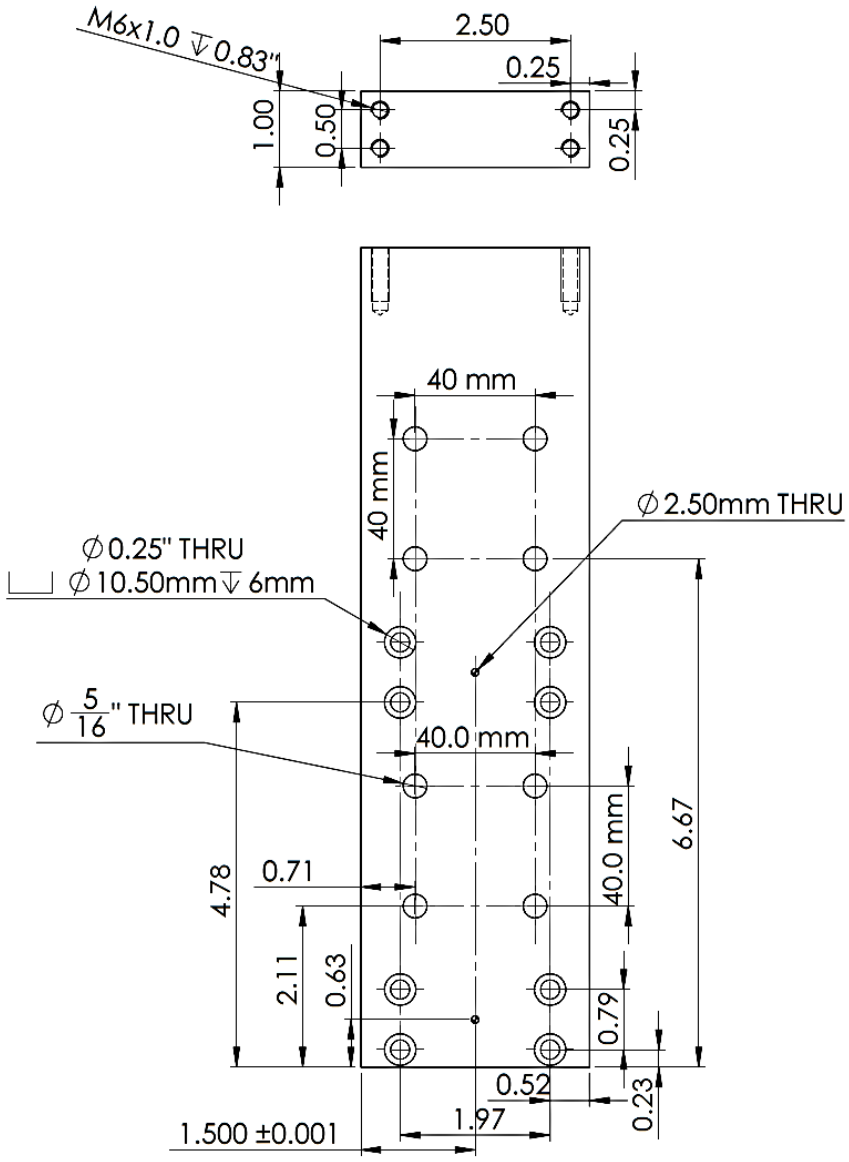

Figure 52:: Technical drawing for machining the ankle mount.

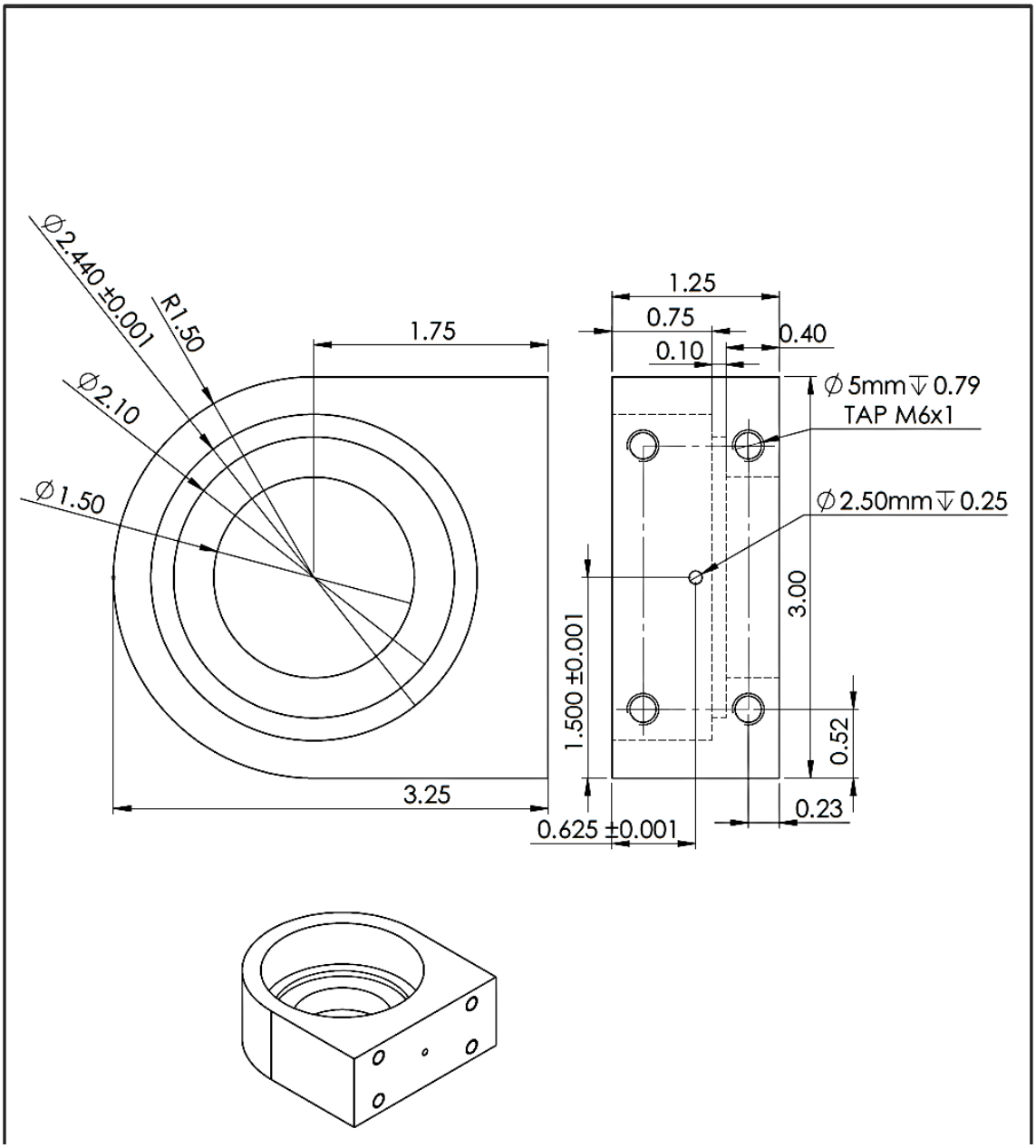

Figure 53:: Technical drawing for machining bearing blocks.

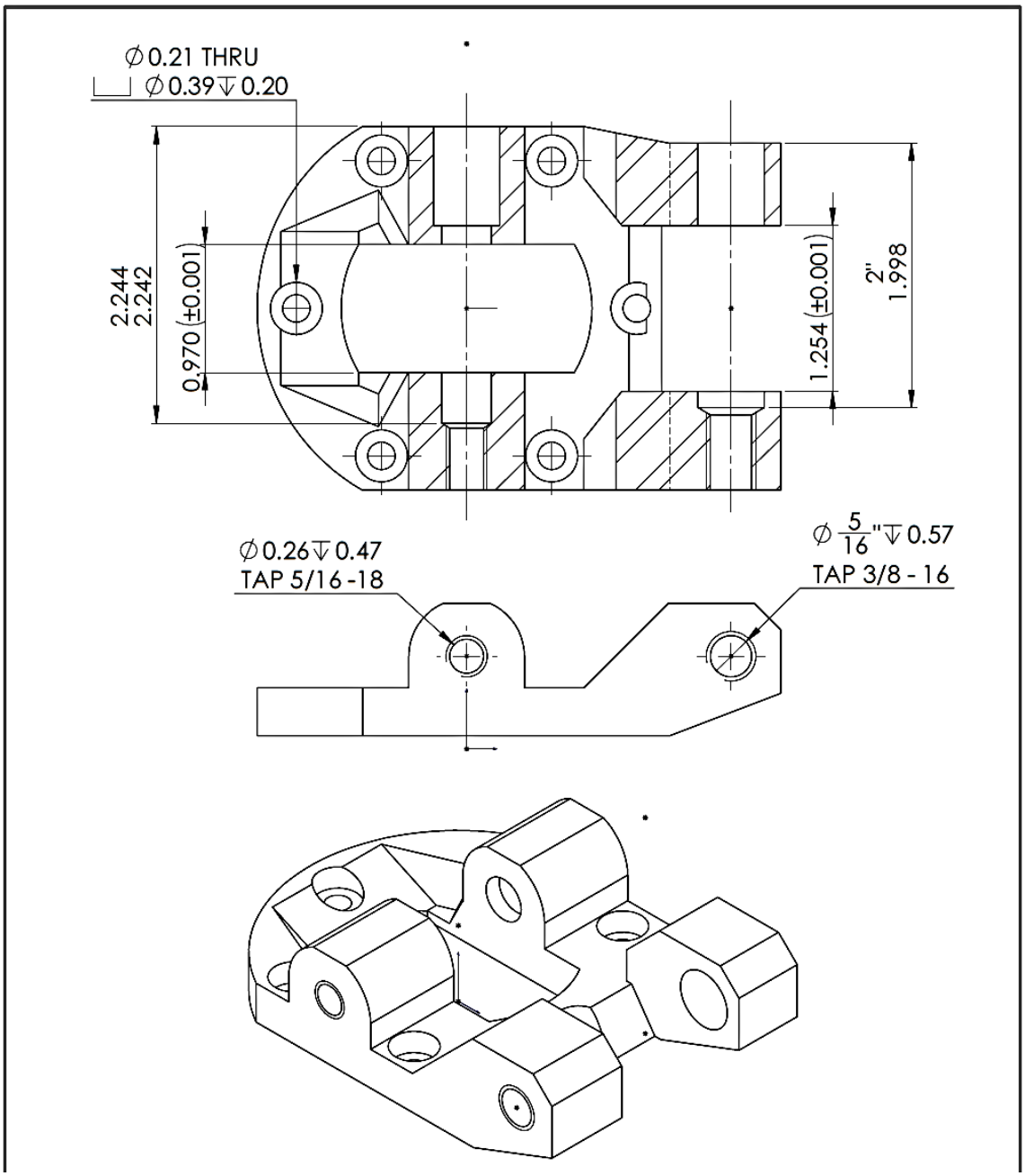

Figure 54:: Technical drawing for machining the bottom ankle plate. (1 of 3)

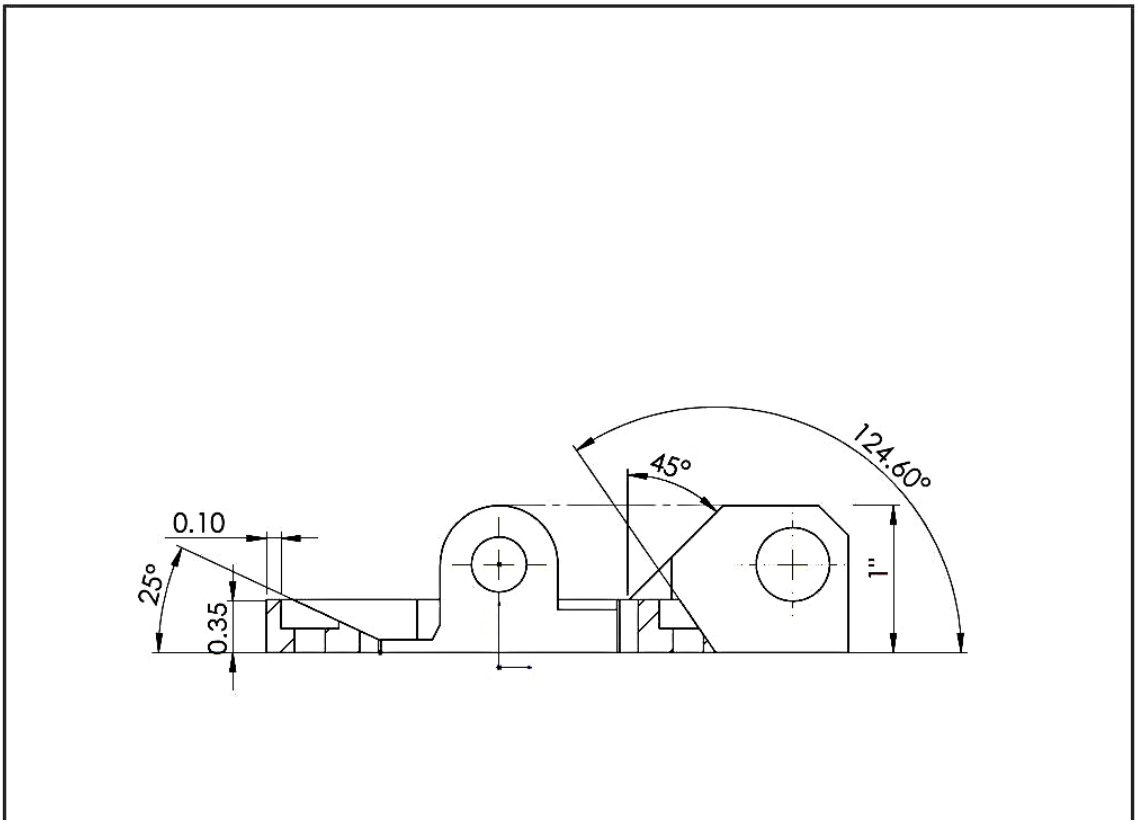

Figure 55: Technical drawing for machining the bottom ankle plate. (2 of 3)

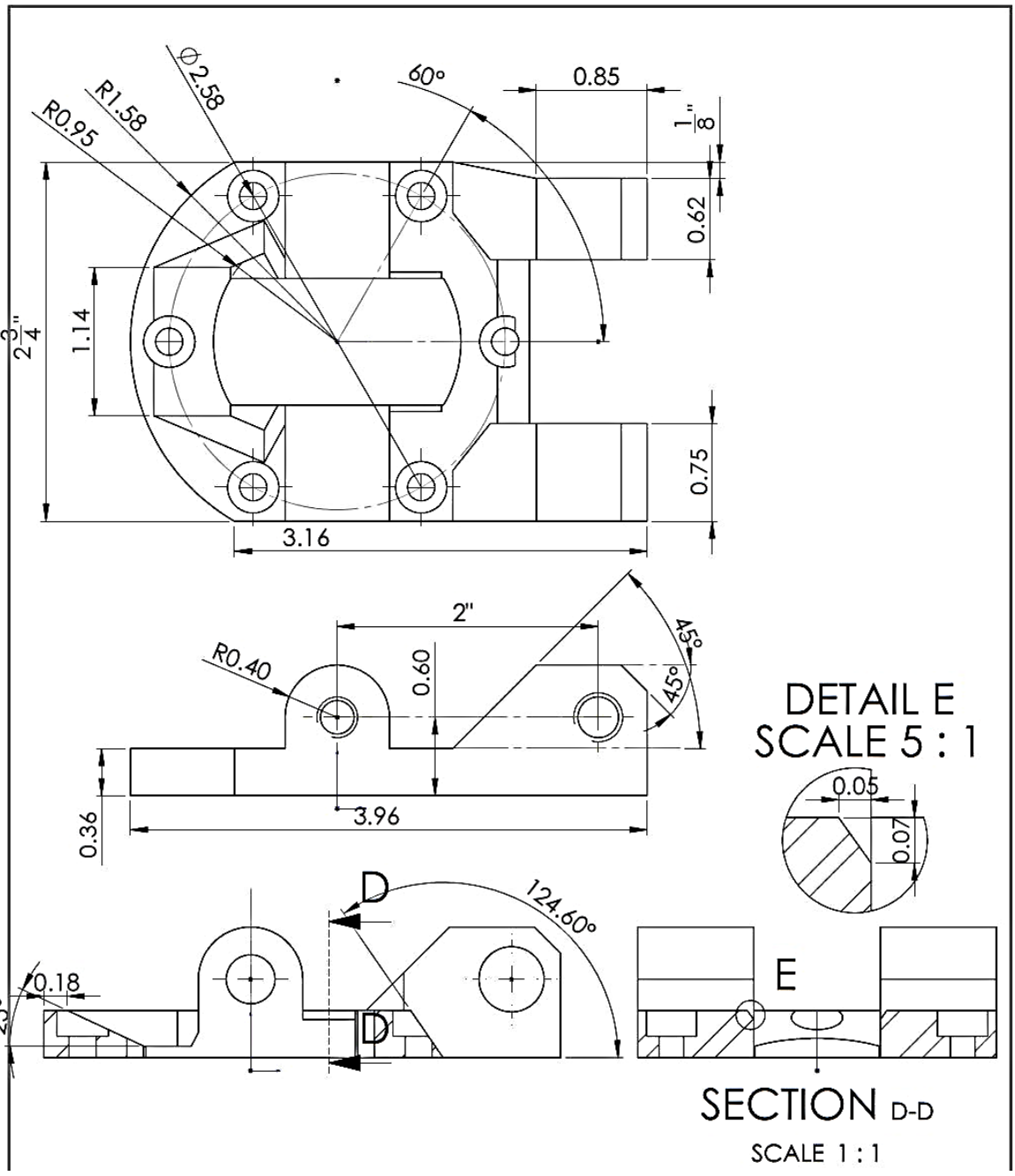

Figure 56:: Technical drawing for machining the bottom ankle plate. (3 of 3)

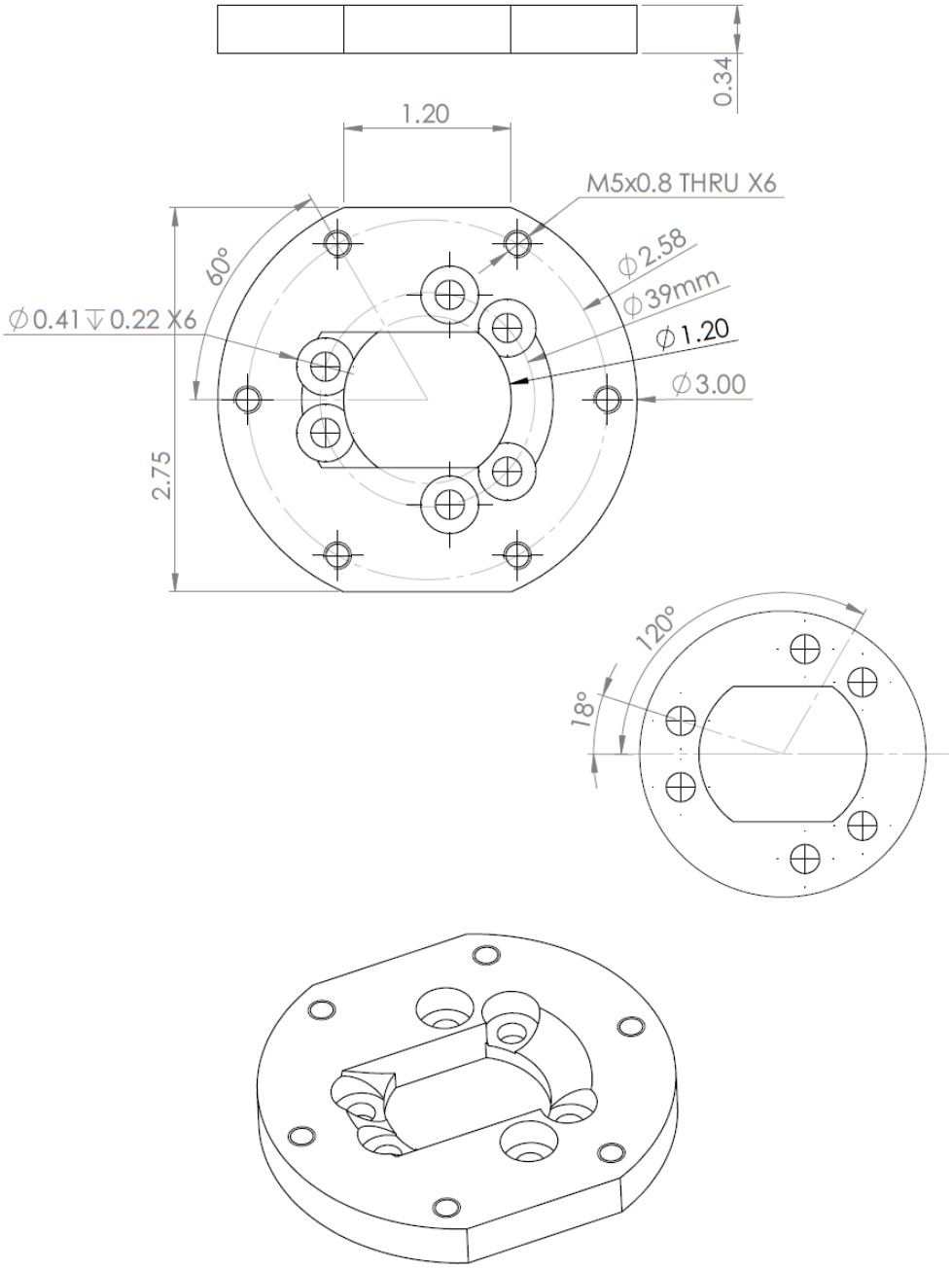

Figure 57:: Bottom mounting plate.

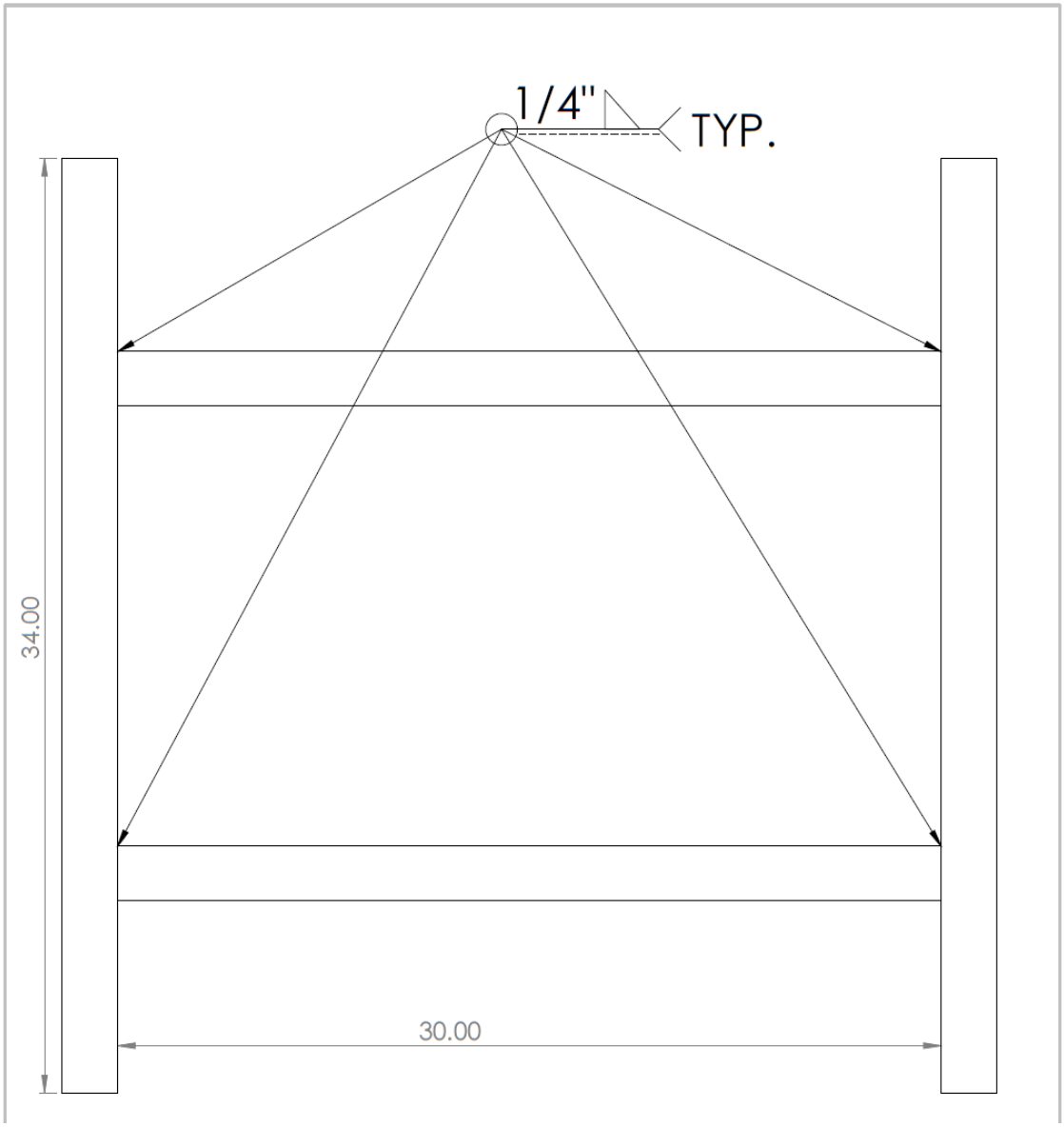

Figure 58:: X axis carriage.

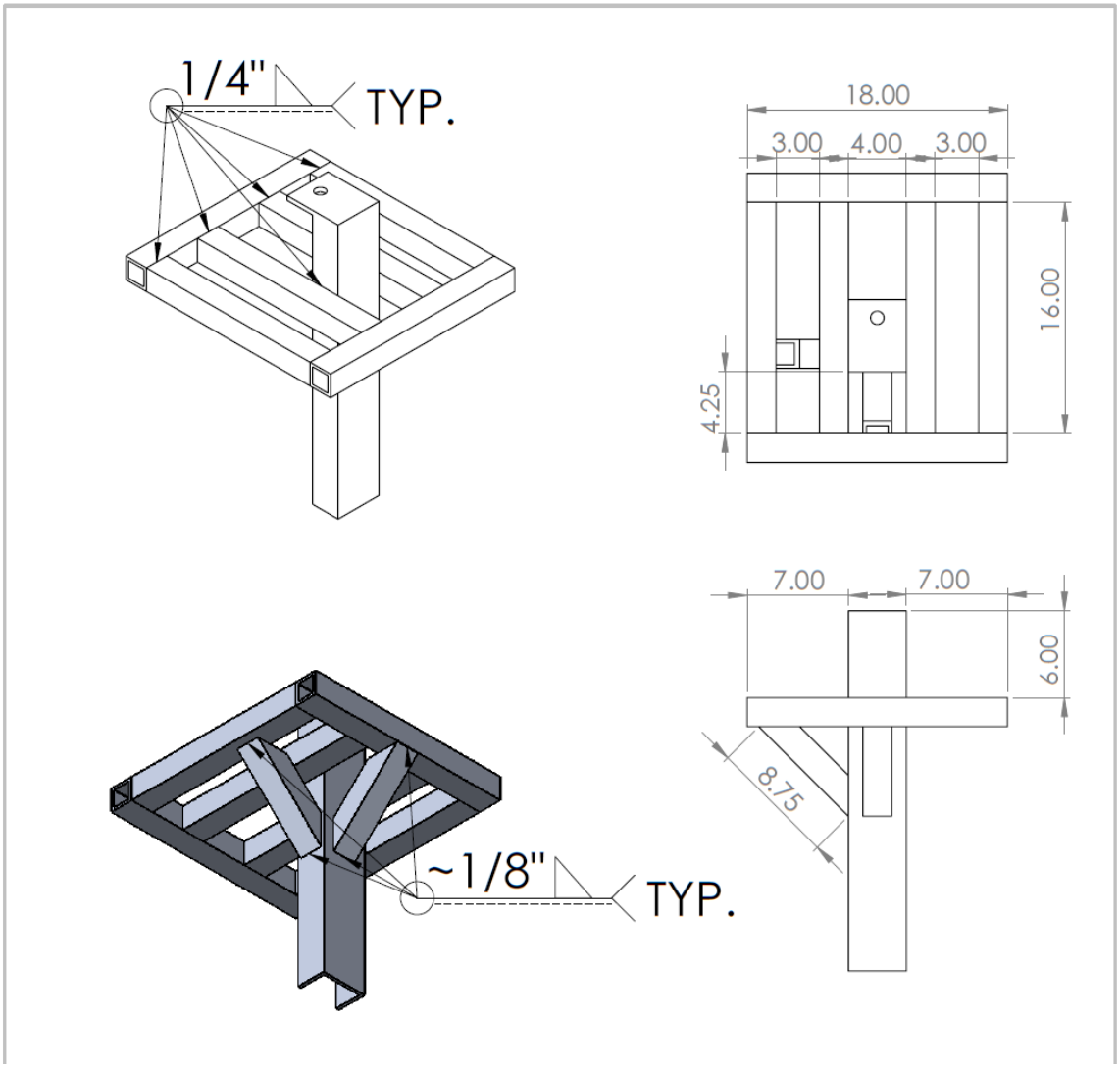

Figure 59:: Y axis carriage.

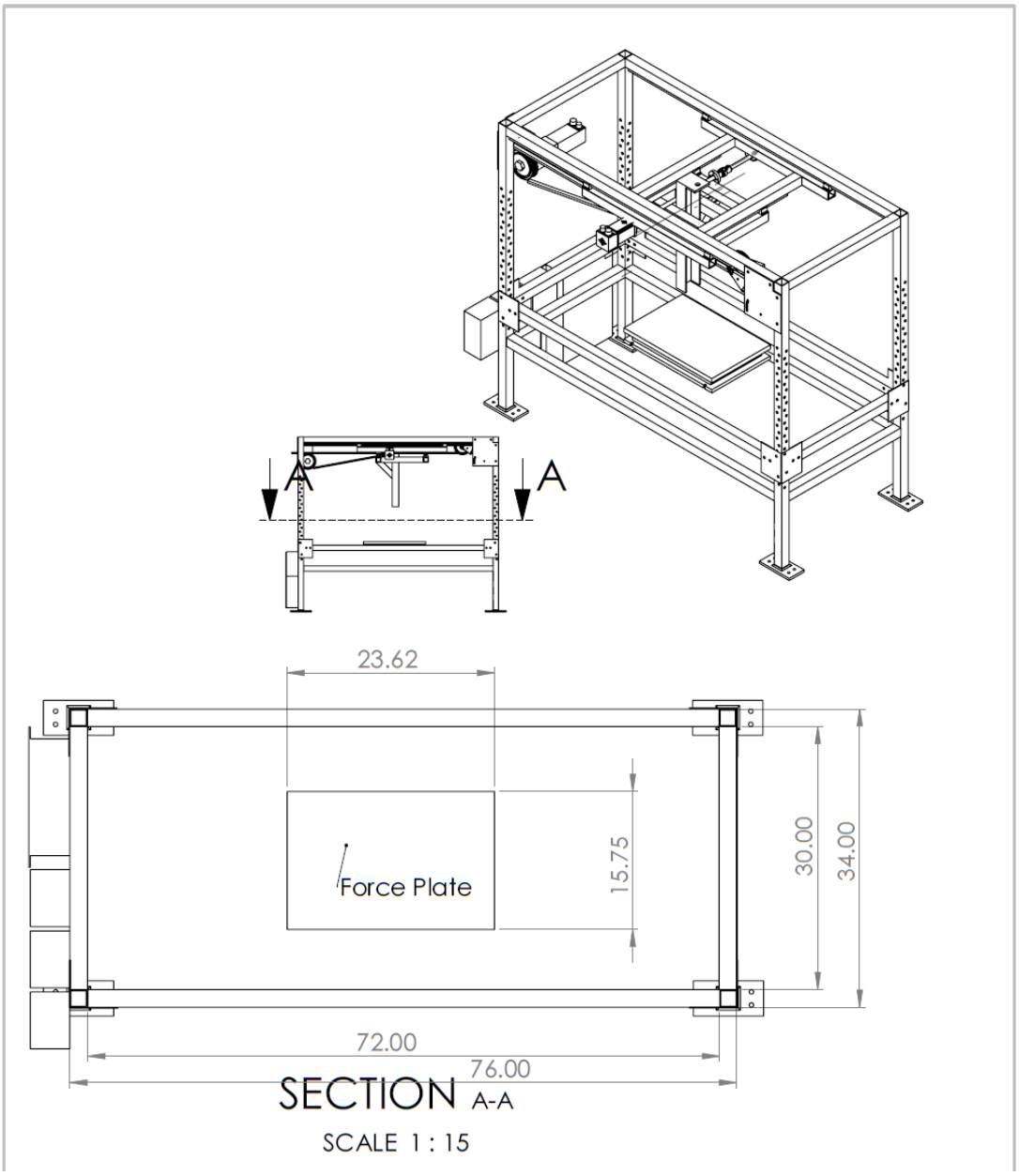

Figure 60:: Layout of the AFS robot.

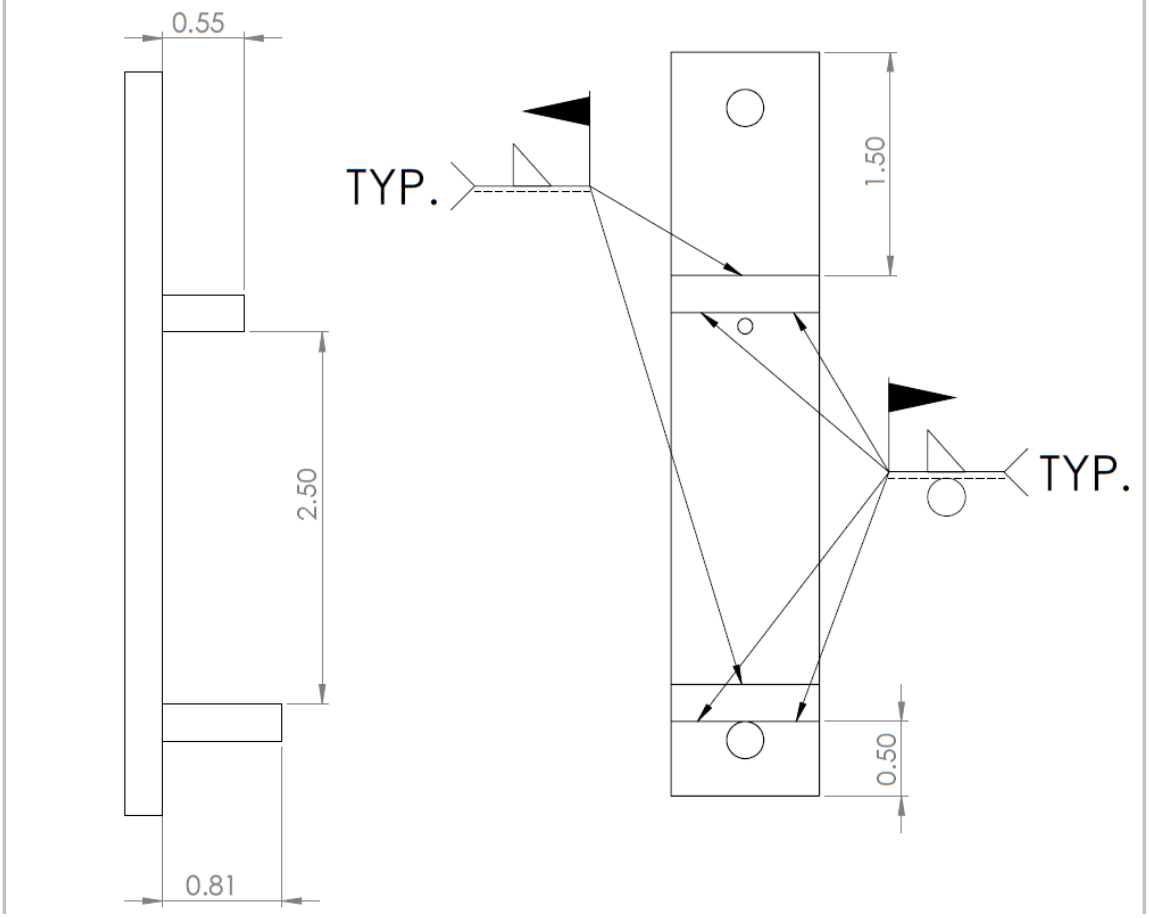

Figure 61:: Linear rails alignment tool.

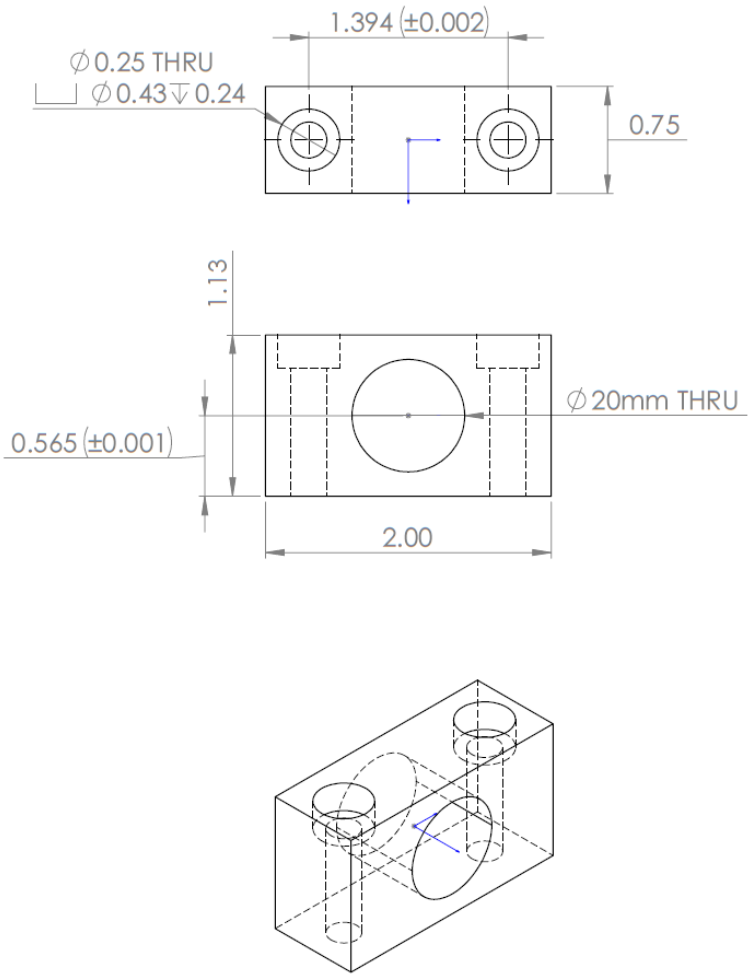

Figure 62:: Bushing mount.

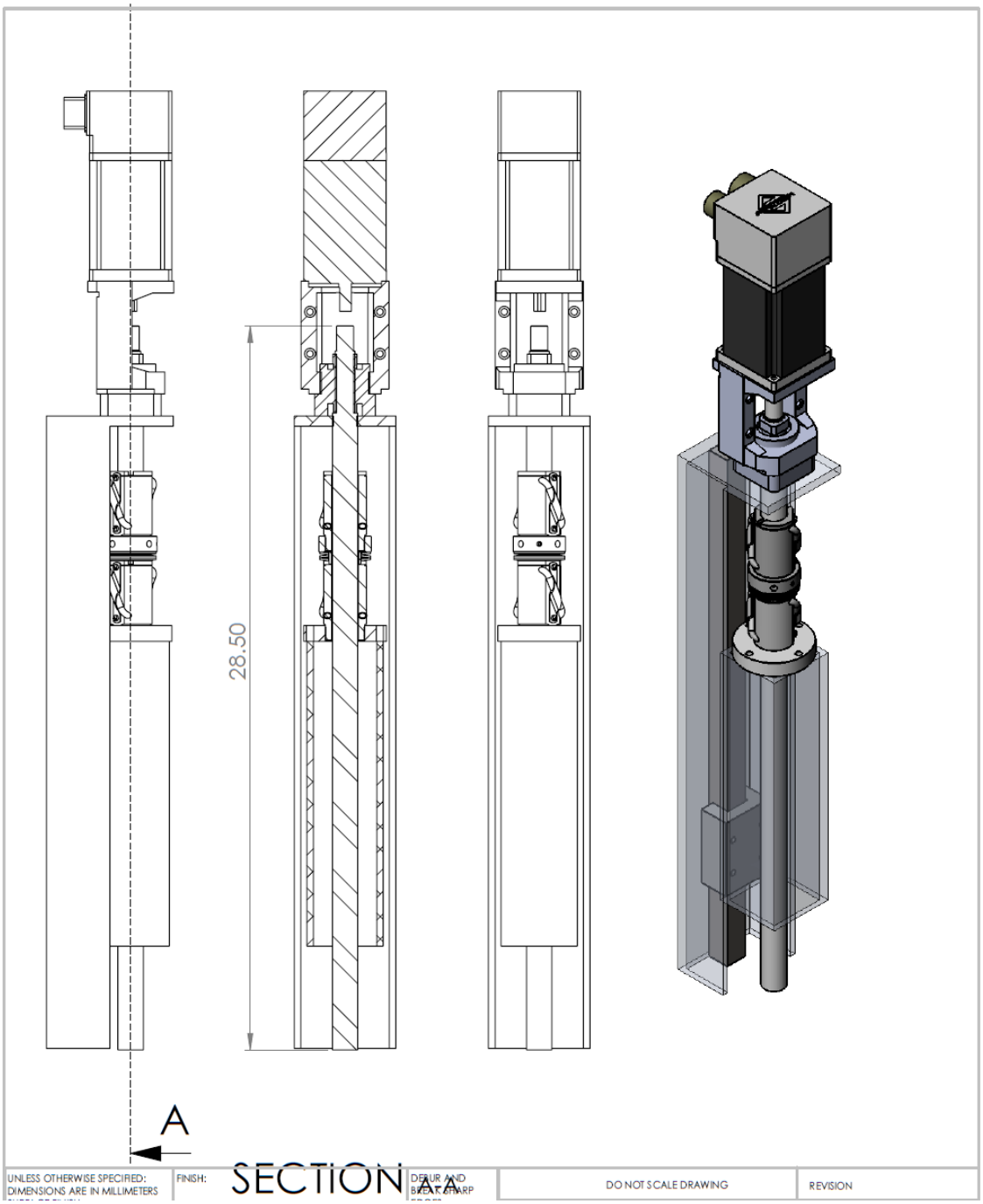

Figure 63:: Z axis technical drawing.

APPENDIX C

MAINTENANCE

- Oil linear rails
- Grease ball screws
- Check cables position for pinch point (data cables)
- Check bolts attaching linear bearings to gantry for loosening

APPENDIX D

SIMULINK AND CONTROL DESK OVERVIEW

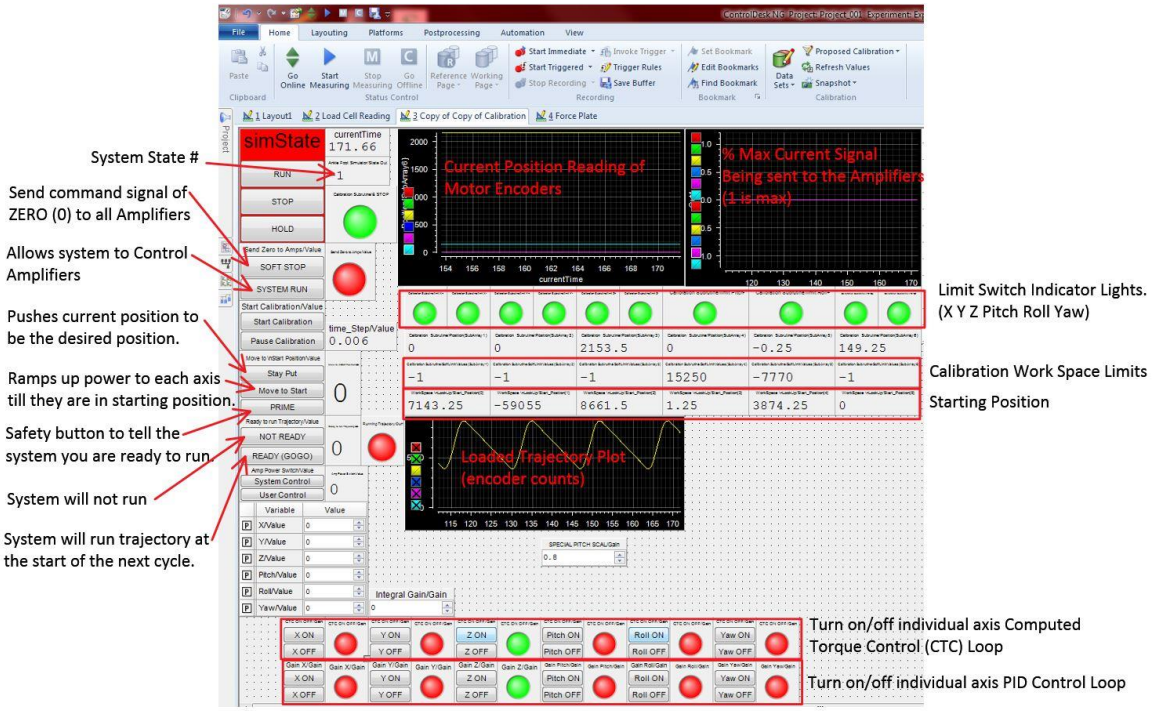

Figure 64:: Control Desk Commented Layout #1.

Figure 65:: Control Desk Commented Layout #2.

REFERENCES

[1] P. s. D. Foundation. (2015). Available: www.pdf.org

[2] P. s. D. C. a. R. Center. (2015). Available: http://pdcenter.neurology.ucsf.edu/

[3] Y. Wang and M. Minor, "Design of a Bladder Based Elastomeric Smart Shoe for Haptic Terrain Display," *(IROS 2014), 2014 IEEE/RSJ International Conference on*, 2014, pp. 1236-1241.

[4] M. C. Hunt, "Gait Modifications on Challenging Terrain: a Study of Persons With Parkinson Disease," University of Utah, 2014.

[5] Jones, "The Human Foot. An Experimental Study Of Its Mechanics, And The Role Of Its Muscles And Ligaments In The Supportopthe Arch,"*AJA.,* 1941.

[6] D. B. Thordarson, "Dynamic Support of the Human Longitudinal Arch," *Clinical Orthopaedics And Related Research,* pp. 165-172, 1995.

[7] N. A. Sharkey and A. J. Hamel, "A Dynamic Cadaver Model of the Stance Phase of Gait: Performance Characteristics and Kinetic Validation," *Clinical Biomechanics,* vol. 13, pp. 420-433, 1998.

[8] P. M. Aubin *et al.,* "Gait Simulation Via a 6-DOF Parallel Robot With Iterative Learning Control," *Biomedical Engineering, IEEE Transactions on,* vol. 55, pp. 1237-1240, 2008.

[9] H. J. Lai *et al,.* "Ankle-Foot Simulator Development for Testing Ankle-Foot Orthoses," *Med. Eng. Phys.,* vol. 32, pp. 623-9, Jul 2010.

[10] T. Natsakis *et al.,*"Inertial Control as Novel Technique for in Vitro Gait Simulations," *JB.* vol. 48, pp. 392-395, 1/21/ 2015.

[11] S. Lohmeier *et al.* "System Design and Control of Anthropomorphic Walking Robot LOLA," *Mechatronics, IEEE/ASME Transactions on,* vol.

14, pp. 658-666, 2009.

[12] T. Otani *et al.*, "New Shank Mechanism for Humanoid Robot Mimicking Human-Like Walking in Horizontal and Frontal Plane," in *Robotics and Automation (ICRA), 2013 IEEE International Conference on*, 2013, pp. 667-672.

[13] K. Kaneko *et al.*, "Humanoid Robot HRP-4 - Humanoid Robotics Platform with Lightweight and Slim Body," in *Intelligent Robots and Systems (IROS), 2011 IEEE/RSJ International Conference on*, 2011, pp. 4400-4407.

[14] D. Gouaillier *et al.*, "Mechatronic Design of NAO Humanoid," in *Robotics and Automation, 2009. ICRA '09. IEEE International Conference on*, 2009, pp. 769-774.

[15] M. E. Rosheim, *Robot Wrist Actuators* Wiley-Interscience, 1989.

[16] A. Roy *et al.*, "Measurement of Passive Ankle Stiffness in Subjects With Chronic Hemiparesis Using a Novel Ankle Robot," *JN,* vol. 105, pp. 2132-2149, 02/23